NEW TRITIUM MONITOR DESIGN BASED ON PLASMA SOURCE ION IMPLANTATION TECHNIQUE

Rafat Mohammad Nassar

A Thesis Submitted for the Degree of PhD
at the
University of St Andrews

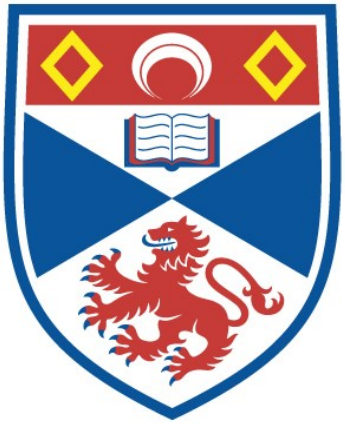

1997

Full metadata for this item is available in
St Andrews Research Repository
at:
http://research-repository.st-andrews.ac.uk/

Please use this identifier to cite or link to this item:
http://hdl.handle.net/10023/13373

This item is protected by original copyright

A New Tritium Monitor Design Based on Plasma Source Ion Implantation Technique

By
Rafat Mohammad Nassar
B.Sc. (Jeddah, Saudi Arabia), M.Sc. (Ames, Iowa, USA)

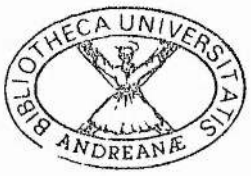

A thesis Submitted in Accordance with the Regulation for the
Degree of Doctor of Philosophy at the
University of St. Andrews,
1996

ProQuest Number: 10167422

All rights reserved

INFORMATION TO ALL USERS
The quality of this reproduction is dependent upon the quality of the copy submitted.

In the unlikely event that the author did not send a complete manuscript
and there are missing pages, these will be noted. Also, if material had to be removed,
a note will indicate the deletion.

ProQuest 10167422

Published by ProQuest LLC (2017). Copyright of the Dissertation is held by the Author.

All rights reserved.
This work is protected against unauthorized copying under Title 17, United States Code
Microform Edition © ProQuest LLC.

ProQuest LLC.
789 East Eisenhower Parkway
P.O. Box 1346
Ann Arbor, MI 48106 – 1346

THESIS ORGANIZATION

Declaration

I, Rafat Mohammad Nassar hereby declare that this thesis has been composed by myself, that it is a record of my own work, and that it has not been accepted in partial or complete fulfillment of any other degree or professional qualification.

Rafat M.Nassar

November, 1996

Acknowledgments

IN THE NAME OF ALLAH, THE MOST MERCIFUL, THE MOST GRACIOUS, ALL PRAISE BE TO HIM AND PEACE BE UPON HIS MESSENGERS.

I wish to acknowledge the support and guidance of my supervisor Dr. David Watt, during the course of this project. Also, I would like to thank all those who have contributed directly and indirectly to the completion of this work, in particular my colleagues in the Department for their constructive discussions, and the staff of the mechanical and electrical workshops in the Department of Physics and Astronomy for their assistance in the construction of the different parts of the developed device.

Additional appreciation is extended for the moral support given by my colleagues at the Energy Research Laboratory, of the Research Institute of the King Fahd University of Petroleum and Minerals, Dhahran, Saudi Arabia.

Finally, I would like to dedicate this work to my parents, my wife and my children for their love, patience and understanding over the years.

Certificate

I hereby certify that the candidate, Rafat M. Nassar, has fulfilled the conditions of the Resolution and Regulations of the University of St. Andrews appropriate to the Degree of Ph.D.

Signature of Supervisor Date

Abstract

Tritium is an important isotope of hydrogen. The availability of tritium in our environment is manifest through both natural and artificial sources. Consequently, the requirement for tritium handling and usage will continue to increase in the future. An important future contributor is nuclear fusion power plants and facilities. Essential safety regulations and procedures require effective monitoring and measurements of tritium concentrations in workplaces. The unique characteristics of tritium impose an important role on the criteria for its detection and measurement. As tritium decays by the emission of soft β particles, maximum 18 keV, it cannot be readily detected by commonly used detectors. Specially built monitors are required. Additional complications occur due to the presence of other radioactive isotopes or ambient radiation fields and because of the high diffusivity of tritium. When it is in oxidized form it is 25000 times more hazardous biologically than when in elemental form. Therefore, contamination of the monitor is expected and compound specific monitors are important.

A summary is given of the various well known methods of detecting tritium-in-air. This covers the direct as well as the indirect measuring techniques, although each has been continually improved and further developed, nevertheless, each has its own limitations. Ionization chambers cannot discriminate against airborne β emitters. Proportional counters have a narrow operating range, 3-4 decades, and have poor performance in relatively high humid environments and require a dry counting gas. Liquid scintillation counters are sensitive, but inspection of the sample is slow and they produce chemical liquid waste.

A new way to improve the sensitivity of detecting tritium with plastic scintillators has been developed. The technique is based on a non-line-of-sight implantation of tritium ions into a 20 μm plastic scintillator using a plasma source ion implantation (PSII) technique. This type of source is different, superior to the line-of-sight implantation and requires no additional beam handling. It is capable of implanting ion species in a broad beam configuration into the entire surface of a target. The technique requires a special ion source with special characteristics of the type obtained from a surfatron plasma source. This ion source has a large high ion density plasma with minimum contamination and produces ions of low temperature. It was constructed to ionize the sampled air and to produce a plasma over a wide range of pressure, 4 - 0.1 mTorr.

A plasma source ion implantation cell was designed and constructed using mathematical modeling with personal computer, to optimize the essential variables of the design and to estimate the implantation rate under different operation conditions. Also, a high voltage pulse modulator was designed and constructed to produce a series of 10 μsec pulses (up to 2 MHz) with a maximum magnitude of -60 kV. The developed device was capable of ionizing air samples and implanting the resulting ions into a plastic scintillator. Two different methods to enhance the collection and deposition of the tritium ions, have been proposed and assessed. A movable prototype device for monitoring environmental tritium in air has been designed and constructed. Although this prototype was not fully tested, the primary calculations have shown that measurable concentrations of tritium ions can be collected from an air sample, with tritium activity ranging from 0.3 Bq/cm^3 down to 0.03 mBq/cm^3, in a short time, to the order of seconds, on-line. This sensitivity fulfills the requirement for environmental monitoring.

Table of contents

List of Figures and Plates

List of Tables

List of Abbreviations

ALI	*Annual Limit of Intake*
CFFTP	*Canadian Fusion Fuel Technology Project*
DAC	*Derived Air Concentration*
EBq	*Exa Bq = 10^{18} Bq*
HT	*Tritium gas*
HTO	*Tritiated water*
HWR	*Heavy Water Reactor*
IAEA	*International Atomic Energy Agency*
IC	*Ionization Chamber*
ICRP	*International Commission on Radiological Protection*
LSC	*Liquid Scintillation Counter*
LWR	*Light Water Reactor*
NCRP	*National Council on Radiation Protection*
PBq	*Peta Bq = 10^{15} Bq*
PC	*Proportional Counter*
PII	*Plasma Ion Implantation*
PIII	*Plasma Immersion Ion Implantation*
PS	*Plastic Scintillator*
PSII	*Plasma Source Ion Implantation*
RF	*Radio Frequency*
STP	*Standard Temperature and Pressure*
SW	*Surface Wave*
TR	*Tritium Ratio*
TU	*Tritium Unit*
UNSCEAR	*United Nations Scientific Committee on the Effects of Atomic Radiation*

CHAPTER 1

INTRODUCTION

Chapter 1

Introduction

The aim of workplace tritium monitoring is multifold: to provide exposure control, protection for workers, to obtain confirmatory data that the work place is safe, and to warn workers whenever a sudden increase in tritium concentration occurs (Nickerson 1982). Hence, diverse tritium detectors, or monitors have been developed. The need to develop new detectors is stimulated by the increasing requirements in tritium detection and monitoring, and by the ever improving engineering technologies that have been available (Wood and Workman 1992), (see chapter 2). During the past 40 years there has been a continuous expansion in tritium technology creating the need for associated monitoring technology to ensure safety. This has been quite evident through five conferences on "Tritium Technology in Fission, Fusion, and Isotopic Applications" held over the last sixteen years (1980; 1985; 1988; 1991 and 1995) in North America and Europe.

Various characteristics of tritium can be utilized to facilitate its detection. For example by identifying its characteristic β^- decay; detection of the daughter nuclide, ^3He; detection of the actual tritium atom directly or the products from nuclear reaction with deuterium, e.g. by the $T(d,n)^4He$ reaction.

A range of devices are available for detection of tritium β^- particles. Typical examples are Liquid Scintillator Detectors, Ion Chambers, Proportional Counters (Knoll 1979), Avalanche Semiconductors Detectors (McGann et al. 1988; Surette and Wood 1993),

and ionization surface activity monitor (Kherani and Shmayda 1995). For high concentrations of tritium it is possible to measure the heat production rate which can be related to the total activity of the sample (Hans et al. 1992; Mason and Vassallo 1992). Another technique used is to detect daughter ^{3}He from the decay of tritium, using mass spectrometry (NCRP 1976). Mass spectrometry may also be used for direct atom collection. This technique is called accelerator mass spectroscopy. It is an ultra sensitive method for detecting tritium atoms (GlaGola et al. 1984; Songsheng et al. 1984). Finally the nuclear fusion reaction, $T(d,n)^{4}He$ is utilized for tritium measurement by detection of the 5 MeV alpha particle (Zhao et al. 1986).

The most common procedure to measure tritium concentrations in tritiated water vapor samples collected from air is liquid scintillation counting (LSC). This is mainly because of its accuracy, reproducibility, sensitivity, rapidness and capability of handling large volume samples(10-50 ml). The lower detection limit for LSC for a condensed, frozen, or desiccant collected samples was in the range of 0.4-4 Bq/m^3 with a counting time of hours (NCRP 1976). Nowadays, the detection limit is about 2-20 mBq/m^3 for the counting time of ~24 hours (Wood et al. 1993). On the contrary, a number of modifications have been made to plastic scintillation detection techniques in order to facilitate direct measurement of tritium in air (see Chapter 2). None have gained widespread acceptance, largely because of the low sensitivity and difficult reproducibility. For the plastic scintillator technique the lower detection limit remained the same, about 5-50 kBq/m^3 (NCRP 1976; Wood et al. 1993). This is slightly higher than the detection limit of ionization chambers. The detection limit of which is in the range of 1-20 kBq/m^3 (Wood et al. 1993). Although plastic scintillators can be used for on-line concentration measurements, they are less sensitive when compared to LSCs. In

LSC the sample is mixed with the scintillant liquid. Therefore most, if not all of the scintillator molecules, are within the range of tritium β^- particles. Thus, the energy of tritium β^- particles is fully spent in the scintillator and not outside it. Therefore, more energy can be provided for the production of scintillations. For plastic scintillators this is not the case. For a dry air sample, only β^- particles emitted towards and close, to the surface of the plastic scintillator within or less than the average range of the β^- particles, will be measured or detected. Other β^- particles will suffer energy loss prior to reaching the surface, suffer back scattering from the detector surface, or will be emitted away from the plastic scintillator surface. In the presence of water vapor the range of tritium β^- particles will be shorter, thus altering the sensitivity of the detector. In order to improve the sensitivity of plastic scintillator detectors, all of the tritium atoms in the sample must be collected. To do this they must be brought into the close proximity of the scintillator molecules inside the plastic scintillator.

It was felt that by introducing a new technique, which utilizes the achievement in the field of plasma ion implantation, the sensitivity of plastic scintillation detectors for measurement of tritium concentrations in air can be improved.

Objectives

The purpose of this work is to develop a new device to detect low concentrations of tritium, HT, in air with optimum sensitivity. This device incorporates the method of Plasma Source Ion Implantation (PSII), developed recently by Conrad et. al. 1987, for collecting ions and using plastic scintillators to detect the tritium. A description will be given of the design, construction, and preliminary optimization testing of the device.

Assumptions

In the laboratory's atmosphere tritium can be found in different chemical forms. Tritium can be found in elemental form, HT, water vapor form, HTO, and hydrocarbon forms. The work is aimed at detecting the elemental form of tritium present in the laboratory.

Approach and Presentation

This work starts by identifying tritium sources and their characteristics in order to identify the difficulties associated with the detection. Then a literature review of the different tritium monitoring techniques used nowadays are elaborated upon. Special emphases are given to ionization chambers, proportional counters and scintillator detectors. This is followed by a summary emphasizing the need for a sensitive, and free from interferences on-line detector. An over view of the developed monitor, the idea, the expectations and requirement are then discussed. In chapter three, the theoretical principles of the plasma source ion implantation technique are given. A literature review on the technique, physics, application and mathematical model are introduced. Then the principles for operating the surfatron plasma source are elaborated. Chapter four describes the designed monitor and its components. The details of component design and operation limitations are given. The results of the modeling calculations are presented accordingly. Finally in chapter five the conclusion, future work, and recommendations are given.

Chapter 2

Tritium characteristics and monitoring

Chapter 2

Tritium characteristics and monitoring

Introduction

Consideration is given in this chapter to sources of tritium, their characteristics, and typical problems. Some of the associated monitoring aspects are discussed. Most of the monitoring requirements can be subdivided into the monitoring of air, gases, liquids and surfaces. Of these, only the monitoring of tritium in air and gases will be discussed. The only exception is measurement of tritium-in-water concentrations using plastic scintillators. Emphasis will be placed on the more common methods for monitoring and on the interferences that can occur with the various tritium monitors. The discussion will cover the direct and indirect principle of air monitoring and its practical aspects.

The fact that different chemical forms of tritium-in-air occur in the workplace, e.g. as gaseous (HT), and water vapor (HTO), has definite implications on whether or not to use discriminating monitors, that are capable of distinguishing between HTO and HT. A conservative judgment, by assuming all tritium present is HTO, can be useful in solving this argument. But, in some situations it may lead to an overestimation of the real hazards. Discriminating monitors facilitate continuous determination of actual hazards present. An overview of the developed on-line monitor is finally discussed.

Tritium sources, characteristics and problems

Sources of Tritium

Tritium, the radioactive isotope of hydrogen, was discovered by Alvarez and Cornog in 1939. Ever since, there has been an expansion in its usage and utilization. Tritium is a prominent element that is linked to heavy water reactors and used as a radiotracer in biological studies, and it has growing use in radioluminescent lights. Also, most important is its significant potential for use as a fusion fuel.

Tritium occurs naturally and can be produced artificially. The naturally occurring tritium is produced predominantly in the upper atmosphere by its interaction with cosmic ray particles, high energy protons and neutrons as follows (Kaufman and Libby 1954):

$$^{14}N + n \text{ -------> } ^{3}H + ^{12}C$$
$$^{14}N + p \text{ -------> } ^{3}H + \text{other products}$$
$$^{16}O + n \text{ -------> } ^{3}H + ^{14}N$$
$$^{16}O + p \text{ -------> } ^{3}H + \text{other products}$$

In 1990 the world inventory of natural tritium was 1.0-1.3 EBq (UNSCEAR 1982). The production rate is 74 PBq/y. A very minor fraction of the natural tritium is produced in the earth's crust from the neutron capture reactions as follows (Kaufman and Libby 1954):

$$^{6}Li + n \text{ -------> } ^{3}H + ^{4}He$$
$$^{238}U + n \text{-----> } ^{3}H + \text{other products}$$

Artificially, tritium is produced during normal operation of nuclear power stations, nuclear fuel reprocessing plants and tritium production plants. In general, tritium is produced by ternary fission and by neutron activation reactions. Table 1 lists the most

important nuclides for tritium production in conventional nuclear reactors by ternary fission.

Table 1: Ternary fission yields of tritium (Lasser 1989).

Nuclides	Range of fission yield (10^{-4} ^{3}H atoms/fission)
^{235}U	0.8 - 1.32
^{238}U	0.68 - 0.91
^{239}Pu	1.34 - 1.8

The nuclear activation reactions responsible for the production of tritium in reactors are listed in Table 2.

Table 2: Neutron activation reactions for tritium formation (Lasser 1989).

Reactions	σ (10^{-28} cm^2)
$^{2}D + n \rightarrow {}^{3}H + \gamma$	3.16×10^{-4}
$^{10}B + n \rightarrow {}^{7}Li + {}^{4}\alpha$	3060
$^{10}B + n \rightarrow {}^{3}H + 2\,{}^{4}\alpha$	1.27
$^{6}Li + n \rightarrow {}^{3}H + {}^{4}\alpha$	693
$^{7}Li + n \rightarrow {}^{3}H + {}^{4}\alpha + n$	5.16×10^{-2}

In light Water Reactors, "LWR", tritium is produced mainly in the fuel elements by ternary fission. In Heavy Water Reactors, "HWR", the major source is the activation of moderator and the coolant, the heavy water D_2O by neutrons. A small fraction of tritium produced in the fuel element will escape into the coolant. In 1984 the global production of tritium from ternary fission and from neutron activation was estimated to

be 105 PBq and 5.5 PBq, respectively (Peterson and Baker 1985). In 1987 the world annual production rate is estimated to increase further to a total of 0.59 EBq, 0.22 EBq from ternary fission and 0.37 EBq from neutron activation (UNSCEAR 1988). The estimated tritium activity that is released into the environment is 0.023 EBq. Tritium is released during reactor fuel reprocessing as is the case with the Sellafield fuel reprocessing plant. From the latter, the annual amount of tritium released into the environment was estimated to be similar to that of a HWR (Okada and Momoshima 1993). Most of the released tritium is in the form of hydrogen gas, tritiated water, and / or hydrocarbons.

The atmospheric tests of nuclear bombs, started in 1945 and intensified during the periods of 1957-1958 and 1961-1963, are the main contributors to the inventory of tritium present in the atmosphere today (Brown 1984). Tritium is produced in fission and fusion explosions. The estimated total amount of tritium produced in fission and fusion explosions are 7025 TBq/Mton TNT equivalent and 2.6×10^5 - 1.8×10^6 TBq/Mton TNT equivalent respectively (Lasser 1989). The total amount of tritium injected in the atmosphere until the cessation of nuclear tests in 1963 was 185-240 times the natural tritium, 240 EBq by fusion bombs and 0.0056 EBq by fission bombs (UNSCEAR 1982). The chemical form of the released tritium from atmospheric tests is mostly HTO.

Tritium is the fuel of the future nuclear fusion reactors. It is expected that about 10 kg of tritium will have to be handled (Lasser 1989). This amount is about three times the total amount of natural tritium on earth. The IAEA, 1990, stated that a Tokamak power plant of 1.2 GW(e) would have several kilograms of the tritium inventory on the site and that partitions of the facility would make it vulnerable to release only a fraction of the tritium inventory under accident conditions.

Tritium is used for self-luminous light sources. In the USA, the amount of tritium used for this purpose was about 400 PBq in 1978, equivalent to tritium produced by the LWRs of the USA (Okada and Momoshima 1993).

Tritium is used as a tracer in hydrology, oceanology, meteorology, cosmic ray physics, medicine and environmental science. The contamination of the earth's atmosphere provided the opportunities to use tritium in the form of gas, oxide, or tritiated methane as tracers in the study of the kinetics of hydrogen, water, and methane in the environment (Okada and Momoshima 1993).

Tritium world production is increasing steadily. The activity associated with use or production of tritium are a potential cause for tritium release or leak in the environment. The concentration of the released tritium in the immediate environment of the nuclear or release site decreases with increasing distance. Consequently very sensitive monitoring techniques are required to monitor any sudden releases.

Tritium characteristics

Tritium is the radioactive isotope of hydrogen. It has an atomic number of 1 and an atomic weight of 3. It has a half life of 4540 days or 12.43 $\pm$ 0.05 years and a corresponding decay probability of 1.7671×10^{-9} per sec (Taylor 1994). Being a pure beta, β^- emitter it decays according to the process;

$$^{3}_{1}H \longrightarrow {}^{3}_{2}He + \beta^-$$

The kinetic energy spectrum of tritium β^- decay is shown in Figure 1.

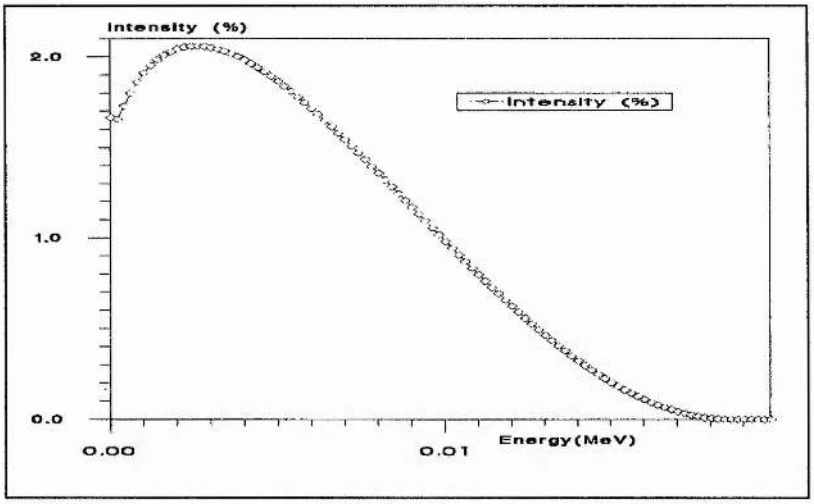

Figure 1. The kinetic energy spectrum of tritium β^- decay.

The maximum energy carried by the emitted β^- is 18.5 keV, while the mean energy is ~ 5.64 keV. The most probable β^- energy is in the range of 2-3 keV. The estimated range of β^- particles in dry air and in water is shown in Figure 2 (Kherani and Shmayda 1992).

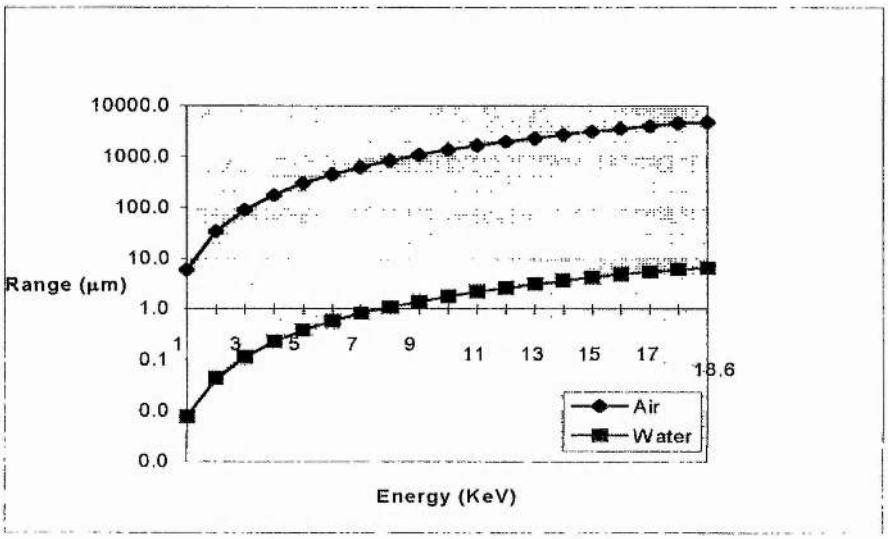

Figure 2. Estimated range of tritium β^- particles in dry air and in water.

Tritium concentrations are measured in units of Bq per unit volume or mass. Another unit called the Tritium Ratio "TR" or Tritium Unit "TU" is in use (NCRP 1976). This

unit relates the ratio of tritium to that of hydrogen in a given sample. A TR value of 1 equals the ratio of one tritium atom per 10^{18} hydrogen atoms. Samples of different composition might have a TR of the same value but with different specific activity.

Interactions of tritium with solids

Tritium has physical properties which are almost the same as those of hydrogen. Also, chemically, tritium behaves like hydrogen so that reactions that occur with hydrogen also occur with tritium. In tritium interactions with materials deviations occur from those of hydrogen because: the tritium mass is three times that of hydrogen; the emission of the β^- particles; and the formation of helium-3. The mass difference will affect the rate of the reaction and the other differences will cause differences in tritium interactions with materials (Shmayda 1984).

Tritium interacts and dissolves to some extent in all materials. When tritium molecules strike a surface of a given material, a fraction will stick, dissociate into atoms, subsequently dissolve into and diffuse through the bulk. The manner of tritium dissolution, being atomic or molecular, will determine the nature of the reactions at the surface and the extent of tritium solubility in the bulk of the material. The rate of occurrence of these processes depends upon other factors, such as, composition of the gas phase and the surface and on the characteristics and properties of the surfaces and the bulk. The material that follows was adapted from (Kherani and Shmayda 1992). A schematic in Figure 3 illustrates some of these processes. When tritium molecules impinge on the surface a fraction of it will be attached to the available adsorption sites. They will dissociate into atoms and then dissolve into and diffuse through the bulk to appear on the down stream surface.

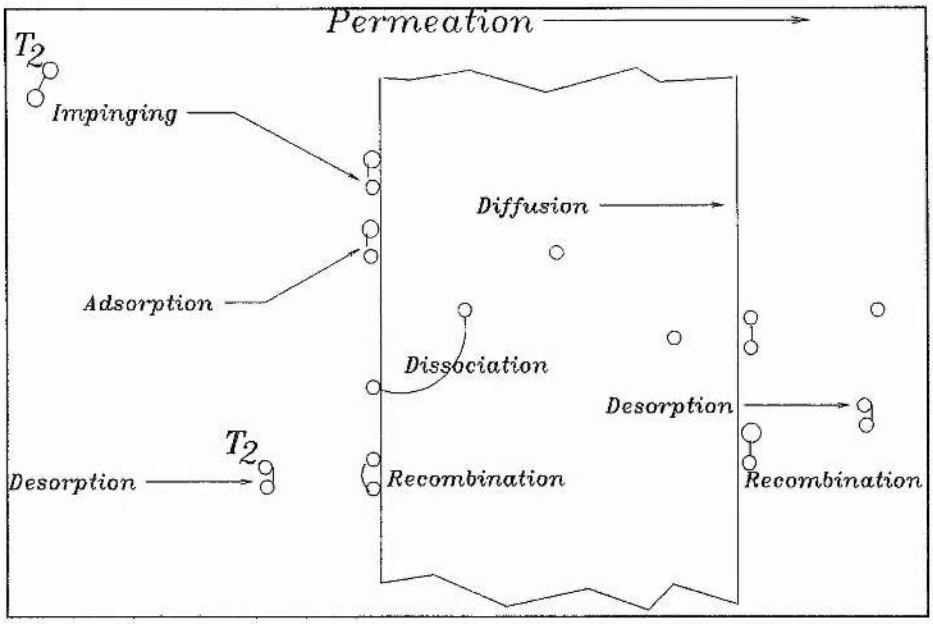

Figure 3. Schematics of tritium permeation into solids.

The molecule tends to associate with other atoms and / or impurity molecular ions available on the surface and subsequently desorb in the gas phase, resulting in what is known as memory effect. Tritium will diffuse and permeate more rapidly through materials that dissolve tritium molecularly than those that dissolve it atomically.

The equilibrium concentration of hydrogen in solids is proportional to the pressure, P. For the case of atomic dissolution (Kherani and Shmayda 1992):

$$C_H = S_H \cdot P^{1/2} \qquad (\#/cm^3)$$

eq. 1

and for the case of molecular dissolution (Kherani and Shmayda 1992):

$$C_{H2} = S_{H2} \cdot P \qquad (\#/cm^3)$$

eq. 2

S_H and S_{H2} are the proportionality constants to the atomic and molecular solubilities respectively. These relations are only valid at low concentrations.

The ease with which a hydrogen particle can traverse a given medium is measured by diffusion. Under steady state conditions, Fick's first law gives the permeation of hydrogen through a solid. The hydrogen flux in a one-dimension case is (Kherani and Shmayda 1992):

$$J = - D \, . \, dc / dx \qquad \textit{eq. 3}$$

D is the diffusion coefficient (cm^2/sec) and dc/dx is the concentration gradient across the solid.

For a given slab of a given material the steady state atomic permeation flux can be expressed by (Kherani and Shmayda 1992):

$$J = D \, . \, S \, . \, (P_u^{1/2} - P_d^{1/2}) / l$$

$$J = J_o \, . \, (P_u^{1/2} - P_d^{1/2}) / l \qquad (mole/sec.cm^2) \qquad \textit{eq. 4}$$

where, P_u ,and P_d are the pressure upstream and downstream of the material with the bulk thickness of l. J_o is the permeability coefficient of the material ((cm^2/sec) . (cm^3 H_2 at STP/ cm^3 of metal . $mb^{1/2}$)). The steady state permeability is a function of the bulk properties D and S_H and the gradient of the driving force across the material.

Once tritium is in the solid, the effect of its radioactivity depends on the nature of the material, the atomic arrangement, the ease with which the lattice can be disrupted by radiation, and the ability of the disrupted lattice to reconstitute itself. Depending on the quantity of tritium dissolved, temperature and the load stress, different materials differ in their response. Glasses tend to be brittle and potentially fracture. Ceramics in comparison dissolve and permeate smaller quantities of tritium and therefore, their properties degrade more slowly. Organic substances tend to dissolve much larger quantities of tritium. Thus, the β^- radiation dose will be significantly greater and therefore, the effect which results in producing ionization and excitations will lead to the rupture of the chemical bonds thus forming reactive intermediates. The latter may, subsequently react to alter the chemical composition and ultimately the physical properties of the given organic material (Kherani and Shmayda 1992).

Metals can be classified into two groups with regard to their interaction with tritium, hydriding and non-hydriding. For the first group hydrogen isotopes are dissolved in the metal exothermically and form a strong bond with it. The metals of this group usually have high solubilities. Titanium, for example, can be charged to an atomic ratio of H/Ti of 2. Such hydride forming metals are used for the purpose of tritium storage and scavenging (cleaning). The second group, the non-hydriding group, dissolves hydrogen isotopes endothermically. The solubility of hydrogen isotopes with this group is much lower than with the former group on the average by a factor of 1000 (Kherani and Shmayda 1992).

Tritium in the body

Tritium β^- particles have a range in water (tissue) of 6 μm. This is less than the thickness of basal skin cells below the surface of the skin (~ 70 μm). Tritium is

therefore not considered a hazard as long as it is outside the body. This implies that the most commonly used monitors such as TLDs, film badges, or pocket ionization chambers are ineffective for detection of tritium in the body. Once inside the body, tritium is a radiation hazard. The pathways are inhalation, ingestion and absorption through the skin directly from air and/or from surfaces (Ballance et al. 1992; Wong et al. 1988). In air, tritium can be found in gaseous form (HT), as tritiated water vapor (HTO), as tritiated hydrocarbon and/or as tritiated hydrides. Tritiated water vapor, HTO, is 25000 times more toxic than is tritium gas, HT. This is because HTO is much more easily taken into the body than is HT.

A harmless HT concentration can change into the more toxic HTO by oxidation or by an exchange reaction with H_2O in air. The two reactions can take place in the laboratory. The rates of the reactions may increase, especially in the presence of metallic surfaces (Housiadas and Douglas 1995; Okada and Momoshima 1993). Hence by knowing the HT concentrations and the different reactions rates, one can forecast the potential hazards imposed by the HTO.

The cells and the body as a whole, consist of water and hydrocarbons. In the body HTO is highly mobile and becomes uniformly distributed in body water. The biological half-life for tritiated water in the body water is 8-10 days (Johnson and Myers 1984). Therefore, bioassay of urine, blood, or water vapor from expired air by the use of liquid scintillation counting is the means to monitor tritium in the body. Only 1.6% of the inhaled HT gas is absorbed into the body water. HT has a biological half life of one hour (Nickerson 1982).

The intake of tritium atoms, into the body, in any calendar year must be limited so that the committed effective doses do not exceed the annual average limit on effective dose

for stochastic effect of 20 mSv. The annual limit of intake (ALI) for tritium is the annual average limit on effective dose for stochastic effect of 20 mSv divided by the committed effective dose per Bq intake of the tritium nuclide. The derived air concentration (DAC) which, if breathed at a rate of 20 l/min for 2000 h/yr (one working year), would result in the ALI by inhalation. It is simply equal to ALI divided by the volume breathed over the working hours of the year. The Derived Air Concentration (DAC) values for HTO and HT are shown along with some of the basic tritium data (ICRP 1991) in Table 3.

Table 3: ALI (Bq) and DAC (Bq/m^3) based on 40 h/ wk, of tritium.

	ICRP-61, 1991 limits
ALI (T_2O)	$1x10^9$ Bq
DAC (T_2O)	300 kBq/m^3 300 Bq/L 0.3 Bq/cm^3
DAC HT	$8x10^9$ Bq/m^3 $8x10^3$ Bq/cm^3
MPC in drinking water for public	$8.5x10^4$ Bq/l = 85 (Bq/ cm^3)

Tritium detection problems

The energy of the tritium decay β^- particle is in fact the lowest of the known β^- emitters. Consequently, detection and / or measurement of tritium concentrations in a sample can be complicated by the presence of other radionuclides, or in the presence of a gamma field. Also, the weak signals that are generated in detectors by the very weak tritium β^- particles are subject to interference from electrical noise.

Tritium β^- particles have a very short range which varies in different materials. These two facts have considerable consequences for the detection of tritium. The maximum range of the 18.6 keV β^- particle is 0.5 cm in air and 6 μm in water (tissue). In water, for example, not all of the tritium β^- particles will have a maximum range of 6 μm, only 0.05% of the emitted β^- particle have energies above 17 keV. Therefore, most of the tritium β^- particles will have the range of ~ 1 μm. The effect of these variations has great consequences on the efficiency of detecting tritium β^- particles. If the plastic scintillator surface is at a distance greater than 1 μm, only β^- particles that have a longer range will reach the detector and induce scintillations. Others, simply are lost, resulting in suppressed sensitivity. Also, the chemical form of the tritiated sample has a considerable effect on the efficiency of the detection. Since tritium β^- particles have different ranges in different materials, the efficiency for detecting tritiated samples of different chemical form will be variable. A plastic scintillator detector, for example, could detect tritium β^- particles emitted in air from a distance of 0.4 cm. The same detector cannot detect the same β^- particles if the sampled air is humid or if the tritium β^- particles are emitted from a water sample.

Principle and practical aspects of air monitoring

For protection of workers and the environment, large quantities of tritium must be doubly or even triply contained. Each containment level requires a special type of monitor. For the primary containment, process monitors provide the necessary information for control. These monitors are of small size and are capable of detecting very high concentrations. In the secondary containment, such as glove boxes, monitors are needed to detect any increase in tritium concentration, or the presence of an

abnormal situation. In the third containment, the working environment, monitors are needed for radiological protection.

Monitoring of general areas, where non-radiation workers and the general public may be present, can be divided into two types:- compliance monitoring, and control monitoring. The former requires high sensitivity and accuracy. It may involve simple field sampling followed by laboratory analysis. The latter requires fast response time, and usually consists of on-line continuous readout instrumentation.

Detectors used for compliance monitoring should be capable of measuring down to at least DAC (HTO) value i.e., 0.3 Bq/cm^3. Meanwhile, detectors for environmental monitoring should be capable of measuring down to the 10-100 mBq/m^3 range.

Tritium-in-air sampling and measurement techniques

All of the well established techniques that are utilized to detect tritium are based on the detection of the emitted β^- particles. The low energy and the short range of the β^- particles have important consequences on measuring techniques to determine the tritium concentration. The sample must be in close proximity, or inside the detector, in order to detect the weak β^- rays. Accurate tritium measurement is subject to interference from radioactive gases, ambient radiation, aerosols and ions. Therefore the monitor must be specifically designed to avoid such interferences (Budnitz 1975; McElroy 1984; Wood 1993).

The different needs for monitoring tritium concentrations in the environment and in the workplace have resulted in the development of different detectors. Hence, tritium detection equipment can be differentiated according to the monitoring range as in Table 4.

Table 4: Monitoring ranges and applications[a].

	Monitored medium and/or purpose	Equipment	Typical concentrations	Remarks
1	Environmental	samplers *	low 10-100 mBq/m^3	air
2	Radiation protection	samplers + monitors	down to fraction of DAC for HTO (0.3 Bq/cc)	must discriminate against other forms of radiation and radionuclides
3	Process	monitors	up to pure tritium	must operate under pressure and/or vacuum

* Monitoring equipment that requires sample collectors.
[a] Adopted from (Wood 1993).

There are two common approaches to detect tritium in air. The first one is by discrete sample measurement, or indirect measurement. The second approach is a real time measurement where the sampled air is led into the detector at a constant flow rate and the tritium concentration is measured (Budnitz 1975).

Indirect measurement.

Indirect measurements operate in two steps. First, samples are collected from the monitored area. Secondly, the tritium content is measured.

Sampling

Obtaining a truly representative sample is a major concern in any sampling program. Factors to be considered are: the environmental conditions (e.g. wind, and concentration gradient in water). Sample size depends on the purpose of the measurement. For routine monitoring a few milliliters is usually sufficient, whereas, for low level measurements, 20 ml to 500 ml may be required. A constant volume sample taken at regular intervals from an effluent, which has a reasonably constant flow rate will yield a representative sample (NCRP 1976).

Active air-sampling

The basic sampling system for HTO consists of a filter, a pump, a sample collector, and a flow-measuring device (Hofstetter and Wilson 1991). Air is drawn through the collector for a given period of time at a monitored flow rate to determine the total volume of air sampled. The total amount of HTO recovered is divided by the total volume sampled to determine the average HTO in air concentration. Other radioactive gases have limited solubility in water. Their concentration can be reduced by purging the collected water with clean air.

Collectors can be cold traps, gas-washing bottles (bubblers), or solid desiccants (Budnitz 1975). Cold traps are usually made of glass, through which sample air flows. The traps are cooled well below 0 C^{o} in order to condense air water vapor, usually with liquid nitrogen. Bubblers are bottles filled with a collecting liquid, usually tritium-free water. Solid desiccants can be silica gel or a molecular sieve. The use of bubblers instead of cold traps or solid desiccants will dilute the sample resulting in raising the lower detection limit.

Passive sampling

Passive HTO sampling is analogous to active sampling with one exception, the pump is replaced by natural diffusion (Stephenson 1984). The collectors can be cold traps, tritium free water or solid desiccants. Standard scintillation vials make good sample collectors, to which a small a mount of water or other absorbent is added. The vial lid should have a stainless steel insert with an orifice in the center (Wood et al. 1993). These vials should be placed in the field for a measured period of time in order to allow HTO to diffuse into it (Wood and Workman 1992). The sampling time depends on the

sampling rate and the amount of absorbent in the vial. The effective sampling rate is determined by the size of the opening in the sampler lid (Otlet et al. 1992).

Following sampling, the vials are prepared for liquid scintillation counting. The average tritium concentration in the air is the activity of tritium found in the vial divided by the volume of air sampled.

The specific activity of the condensate is determined using knowledge of the absolute humidity and isotopic fraction factor of condensation (Fukui 1993).

HT sampling

When the sampling of HT is required, the sampled air passes through an HTO trap. Then, the sampled air passes through an oxidizer with an appropriate catalyst, wherein HT will be oxidized to HTO, which in turn is collected by a desiccant or a bubbler (Mason and Ostlund 1978).

For environmental HT sampling, a desiccant (molecular sieve or silica gel) coated with palladium is often used (Brown and Workman 1986) (Mason and Ostlund 1978). The latter acts as both an oxidizer and collector.

Sample preparation

HTO samples require minimum preparation, water recovery and in some cases purification (NCRP 1976). But if HT or other tritiated compounds are to be measured, the compound has to be converted to water for analysis. Furthermore, precautions must be taken to prevent sample losses or dilution. HTO diffuses through plastic. Consequently, plastic containers should not be used to store samples for a long time. However, if long term storage is required, the samples must be stored in glass, or even metal containers.

Measurements of tritium

Typical amounts of water required from the sample for analysis is 5-10 ml, assuming enrichment is not needed. Otherwise, larger samples are required. The collected samples are usually analyzed by Liquid Scintillator Counters (LSC) (McElroy 1984; NCRP 1976).

Liquid Scintillation

The samples are mixed with a cocktail of scintillation chemicals contained in a vial. The typical volume ratio is 10 ± 5 :1 of cocktail to water, and for low level counting special cocktails are used in which the ratio may be 1:1. The usual volume of the scintillator/sample mixture $\cong$ 20 cm^3. The absorption of the beta radiation in this cocktail causes the scintillator to emit photons of light. These photons can be detected sensitively by a pair of photomultiplier tubes, which are run in coincidence mode, in order to distinguish the photon pulses from photomultiplier tube noise. The intensity of these photons is proportional to the amount of activity present in the sample.

The LSC has a typical detection limit in the order of 200 kBq/m^3 for a 1 ml water sample counted for 10 minutes. However, the detection limit for an air sample is much better. For a sample collected by a bubbler or a passive sampler, a detection limit in the range of 40-400 Bq/m^3 and for a measurement time of 10 min was achieved. While for a condensed or desiccant collected sample that is counted for 10 min a lower detection limit of 0.4-40 Bq/m^3 was achieved. A longer counting time (24h) would result in a lower limit of detection, 2-20 mBq/m^3. For tritium-in-air the detection limit depends on the amount of vapor collected and the specific activity of that water vapor. Recent progress in electronics and chemistry has led to the development of better LSCs with a detection limit of 650 Bq/m^3 for an 8 ml water sample counted for 500 min (Wood et al. 1993).

On line measurement.

Ionization chamber (IC)

Of the various methods used to measure the tritium concentration in air, ion chamber (IC) based monitors tend to dominate. Also, for process monitoring IC's are most common. The sensitivity required for environmental monitoring of tritium in air is in the range of 10-100 mBq/m^3. This is well below the Derived Air Concentration (DAC) value. The sensitivity of ionization chambers is not yet sufficient to permit direct measurement. However, the most common real-time method for measuring tritium in air is accomplished with an ion chamber (Budnitz 1975; Wood et al. 1993). The device is simple and economical to operate. It requires an electrically polarized chamber, a very sensitive and stable electrometer with associated electronics, and a system that draws the monitored gas or air inside the IC. This is because tritium beta rays cannot penetrate the walls of the IC. The very low number of ion pairs produced per tritium β^- emitted inside the chamber means that the IC must be operated in the integrated current mode. Therefore, ion pairs produced outside must be prevented from entering the chamber by the use of particle filter and ion traps. Otherwise, interference can arise. In the integral charge current mode the current produced is proportional to the tritium activity present. Typically the ionization current due to tritium in air is about 0.025 fA/Bq, a tritium air concentration of 40 kBq/m^3 will produce 1 fA current in a 1 L IC (McElroy et al. 1985). Different calibration factors should be used if tritium is monitored in gases other than air. Impurities in the carrier gas can affect the value of this calibration factor (Rodrigo et al. 1992). The practical lower limit of tritium concentration measurable by a small IC in the field is 40 kBq/m^3.

A common concern in radiation protection monitoring is how best to compensate for background radiation. ICs are not specific to tritium. They respond to other airborne

radionuclides such as N^{13} , N^{16} and Ar^{41} as well as ambient gamma radiation (Davey and Faught 1986). The IC will produce a current which is proportional to the gamma dose rate. This current is the same as that produced by the more radiologically hazardous tritium concentration. To reduce the response to gamma radiation, heavy shielding is not a satisfactory solution. Two techniques have been used: the gamma compensation technique and the source modulation technique. Compensation is required in most environmental monitoring where gamma fields are present. To do this a second sealed and identical IC is used to compensate for background fields (Cowper and Osborne 1968). Then the signal due solely to tritium is equal to the difference in ionization current produced by the two chambers. Various geometric arrangements of the two chambers are used. The best arrangement is for the IC's to occupy the same place at the same time, which is not possible. Therefore, the compensation is never perfect because of perturbation of the real gamma field. Common arrangements to overcome this problem are to have two chambers mounted base to base, two chambers mounted side to side, or to use concentric chambers with the same volume. Another but less attractive method is to rotate the chambers or alternate the sampled air and the dry air between the two chambers (Jalbert and Hiebert 1971). The best result that can be achieved with simple compensation arrangements is about 95% (McElroy 1984). Another approach for gamma ray discrimination in tritium assay based on a statistical analysis is proposed by Purghel and Vylcov (Purghel and Vylcov 1995).

In some applications it is necessary to discriminate between tritium and other beta-emitting or alpha-emitting gases. Introduction of selective membranes to the ion chamber monitor have helped to reduce the effect of background counts resulting from alpha radiation (Jalbert 1985; Yamamoto et al. 1988)

ICs are sensitive to vibration, and cannot tolerate prolonged periods of exposure in high humidity conditions. Surface contamination of an IC with tritium becomes a problem if a wide range of tritium concentrations is to be measured. Different techniques have been adopted to overcome this (Wood et al. 1993), such as, using two ionization chambers that have identical inner surface area but different volumes and when operated in differential mode, the current resulting from the contamination buildup will cancel each other out (Wood et al. 1993).

For process monitoring, where gas composition, flow rate, and pressure may vary for different applications, ICs are preferred to proportional counters because they are more suitable for close systems. They do not need counting gas, and can be easily calibrated for each application. In process monitoring, there is no special need for background gamma compensation as high tritium concentrations are involved.

Proportional Counters (PC)

The PCs are similar in principle to ICs but differ in design, the amount of bias voltage applied, and the requirement for a particular counting gas (Knoll 1979). In PC the sampled air is mixed with a counting gas, such as argon-methane, before filling the detector. The counting gas is needed to minimize influence on the gain of the detector. The ratio of the counting gas to air sample must be constant, and the sampled-air flow rate should be constant as well. Proportionally enhanced signals are obtained by amplification of the ion pairs in the strong electric fields surrounding the anode. This is sufficient to produce a detectable charge pulse. The number of pulses of appropriate energy is proportional to the tritium concentration inside the counter.

There are two types of PCs with respect to the utilization of the counting gas: the open window type (Pixley and Stussi 1987), where the sampled air is mixed with the counting

gas prior to the introduction into the detector; and the thin window type which permit passage of the external tritium beta rays. The window, 0.1 μm thick is highly susceptible to physical damage.

Another type of PC is the air proportional counter. The monitor offers high detection efficiency and needs no special counting gas (Aoyama 1990; Aoyama and Watanabe 1985; Aoyama and Watanabe 1989). The detector is a multi-wire PC with short anode-cathode distance thereby maintaining a stronger electric field near the cathode.

PC advantages over IC's are high sensitivity, and good gamma discrimination. Pulse shape and pulse height discriminations are used to separate tritium signals from those of noble gases and /or external gamma fields (NCRP 1976). To discriminate against other radiation an anti-coincident technique was applied (Aoyama et al. 1987). The detection limit of commercial instruments using 1.3 L PI and methane counting gas is in the order of 3 Bq / L for a one minute counting time, and 0.4 Bq / L for 1 hour counting time. A detection lower limit of 0.2 Bq/L is achievable in several minutes response time (Aoyama 1990)

Scintillators

The most convenient and practical procedure, nowadays, for measuring tritium activity in water is liquid scintillation counting of single samples. Different approaches have been used to utilize plastic scintillators to measure tritium concentrations in air and water samples, none have found widespread acceptance. Some of these approaches involve direct measurement of air samples. The difficulties are in reproducibility and attaining good sensitivity. Other techniques, aimed at collecting water vapor by different means for measuring tritium concentrations exist but these face the problem of low sensitivity

and degradation of the plastic scintillator by contamination, decolouring and memory effects.

Plastic scintillator and anthracene were used by Moghissi (Moghissi et al. 1969), and Osborne (Osborne 1970). The aim in developing their detector cells was to enlarge the ratio of scintillator surface area to sample volume. The higher the value of the ratio the better is the sensitivity. The two detector cells showed a good sensitivity. The first, gave 10 counts/min. per 40 kBq/ml, and the latter gave 24 counts/min. per 40 kBq/ml. These two designs were intended to measure tritium concentrations in liquid samples. The main problem with these designs is that the counting efficiency degrades with usage. The development of sedimentations, bacterial growth and discoloring is responsible for losses in light collection, and hence, decrease in detection efficiency. Cleaning can help sometimes but not always. When used to measure tritium concentration in an air sample, the Osborne scintillation detector cell gave a better sensitivity of 150 counts/min per 0.04 Bq/cm^3. Accordingly the minimum detectable activities were in the range of 0.004 - 0.04 Bq/cm^3 (NCRP 1976). When measuring air samples of the same tritium concentration but of different chemical forms, the response of the detector to tritiated water vapor was higher than that of tritium gas. This was because of water adsorption on the scintillation surface. Also, it was found that the detector response is sensitive to the relative humidity of the air. The higher the humidity the lower the counting rate. The attenuation that the tritium beta particles are subjected to in water samples reduces the number which actually reach the scintillator. This is not the case with tritium in air samples. Therefore, the use of plastic scintillator for direct tritium in air measurement had limited success, and hence limited usefulness for ambient air monitoring. The influence of external gamma radiation did not affect the ability of a very thin scintillator

layer (few microns) to detect 0.04 kBq/L tritium concentration (Moghissi et al. 1969). However, a 10 cm thick lead shield was needed for the case of cubic cells (Osborne 1970).

Another approach for direct plastic scintillators was to allow water collected from ambient air to flow through a cell filled with plastic scintillator powder (Singh and Kadwani 1974). The packed powder had a water vapor holding capacity of 6 ml, proportional to its volume. The efficiency of tritium counting was found to be inversely proportional to the square root of the particle size of the scintillator. The efficiency of the detector increases with the decrease in powder size. This decrease in the powder size is actually an increase in the total surface area offered by the plastic scintillator (PS). The detector recorded 2500 counts/sec per 1 MPC with a single PMT. The counting efficiency was 2.5 %. The cell did not show any background build-up over long periods of operation and had a low gamma response. Glass tubing filled with anthracene crystals embedded in a clear plastic flow cell are commercially available

Another approach was to collect the HTO vapor as ice and measure the tritium concentration in the ice with a scintillator connected to a PMT. A portable monitor that utilized the cooling effect to condense HTO only, and then measures the tritium concentration, was developed by Mihai (Mihai et al. 1984). This monitor consists of a thin plastic scintillator film deposited onto a thin reflective aluminized Mylar sheet which is connected to the cold side of a thermoelectric element. The scintillator is mounted opposite to the cathode of the PM tube. When the sampled air flows above the cooled scintillator, only the HTO condenses onto it and the emitted β^- rays are counted. The detection limits were not reported.

Other methods involve dissolving the airborne HTO in a water flow and then measuring the tritium in a flow cell filled with plastic scintillator (Osborne 1975); a 40 Bq/L can be detected. An alternative method involves the continuous collection of the volatile tritium compound in a stream of liquid scintillator which subsequently flows through a counting cell. Ethylene glycol was used as the tritium absorbent (Kato 1979). Tritium from the atmosphere is adsorbed into it, then it is mixed in a liquid scintillator and measured by liquid scintillator counter (LSC). The detectable concentration of tritium in air was found to be 0.004 Bq/ml. Silica gel was used as an absorber for HTO in air. Instead of recovering water from the desiccant and complicating the procedure, the desiccant is mixed with distilled water and liquid scintillator chemicals then the tritium concentration is measured by the LSC (Mclain and Lee 1987).

A disadvantage of all the condensed flow cell methods is that the sensitivity in terms of concentration in air is dependent upon the humidity of air (NCRP 1976). This is specially important when measuring an uncontrolled environment. The advantage of collecting tritiated samples into a desiccant and then mixing it with the liquid scintillator is that a more concentrated sample is obtained than when collecting the sample into water.

A plastic scintillator sponge-like detector was developed by Singh, (Singh et al. 1985). The sponge which weighs 1 gram was made out of 5 μm thick plastic scintillator films, and shaped in the form of a disc of .8 cm thick and 2.4 cm radius. The total surface area offered by the scintillator was in the range of .03 m^2. This sponge scintillator is placed inside a cell made of prespex. Counting is carried out in the coincidence mode. The detector has sufficient sensitivity to measure tritium concentrations in water in practical situations. Indeed, the monitor was used to scan water samples from the heavy water

facility at Rajastan Atomic Power station in India. The monitor alarm was set at 400 kBq/L. The life of the detector was prolonged to several weeks by the use of suitable filters. Only 6 cm thick lead shielding was used to reduce the background to 0.2 cps. The memory effect of the cell was cleared after purging with 500 ml of inactive water.

Inorganic scintillator, $CaF_2(Eu)$, has been used successfully as a monitor for tritium in natural gas with a single photo-multiplier tube, but with poor sensitivity (NCRP 1976). Also, a thin $CaF_2(Eu)$ scintillator which is optically coupled between two low-noise photo-multiplier tubes was investigated to measure tritium concentration in nitrogen gas (Chiles 1987). Here, it was found that the area of the scintillator is the only parameter that can be increased to improve the sensitivity. A very large area of 2 m^2 is required to measure tritium concentrations as low as .004 Bq/ml.

Compound Specific Measuring

When measuring tritium in air, tritiated chemical compounds are present and must be measured also. The dose consequences of a particular concentration are dependent on the chemical form of tritium. When considering the dose from exposing the lungs, HTO is 25000 times more hazardous than HT (ICRP 1979). However, a significant dose can rise from the HT that is dissolved in the blood where it is oxidized to HTO. Therefore, a more appropriate relative hazard of HT to HTO is 10000 (McElroy and Johnson 1988). Several schemes have been employed to separate HT from HTO (Jalbert 1985). The most simple method is to use a dryer as follows. First monitor the total tritium concentration, HT and HTO, with a detector. Then route the exhaust through a dryer which would contain HTO only; the dried air can be routed into a second detector to determine the HT concentration. This technique is applicable when HTO dominates the radiological hazards. A second technique implies the use of semipermeable membranes

to separate HTO from HT. The detector can be an ionization chamber (Davey and Faught 1986; McElroy et al. 1982; Yamamoto et al. 1988), or a proportional counter (Beach and Hoots 1980).

In the review of the need for a species specific tritium monitor, R. McElroy and J. Johnson concluded their evaluation with the following Table 5.

Table 5: The need for a real time species specific tritium monitor (McElroy and Johnson 1988).

Dose estimation	Not required
Release monitoring	
Control	Desirable but not required
Compliance	Not required
Work place monitoring	
Area monitoring	Desirable but not required
Low level surveys	Not required
Maintenance	Desirable
Accident assessment	Desirable

This judgment is legitimized by having an unbiased estimate of a situation rather than having only a measure of the worst case.

Summary

For an immediate detection of tritium-in-air concentration, the on-line ionization chamber and proportional counters are widely used, plastic scintillation based monitors are not. The ionization chambers are limited by the difficulty for measuring low concentration of < 40 kBq/m^3 for a 1-2 liter chamber. Also, it cannot discriminate against γ-radiation, unless compensated design is used. Furthermore, ionization chambers cannot discriminate against β emitter gases, which are common air activated products expected in fusion facilities and 14 MeV neutron generation facility. The transition ionization produced can reach 8-80 mBq/m^3. This can be mistaken for ~ 10-100 DAC of HTO of tritium. On the other hand large ionization chambers which are built for high sensitivity would interpret an ambient level of 20 Bq/m^3 of α emitter, radon Rn^{222}, to be about 20 kBq/m^3 of tritium. Proportional counters have an order of magnitude higher sensitivity than ionization chamber, but have a narrow operating range of 3-4 decades; and they consume around 15 l/h of counting gas. Liquid scintillation counters based tritium assay are time-consuming and in an emergency, will not be fast enough to allow for prompt response. Table 6 compares the different major tritium-in-air detection techniques. This highlights the need for an on-line monitor that can combine the high sensitivity, wide range of operation and rapidness.

Plastic scintillator detectors, unlike other detectors and despite their shortcomings are capable of detecting tritium down to fractions of DAC value (300 kBq/m^3). The lower limit of detection is in the range of 4-40 kBq/m^3. This limit is around that of ionization chamber. Hence, plastic scintillators have been used for radiation protection purpose in some laboratories. The counting geometry of this detector (position of the source with

respect to the detector), unlike the others, is external i.e. the sample is placed outside the detector. This simply indicates that the full capability of this detector has not yet been fully explored. If the source arrangement with respect to the detector is made to be internal the detector sensitivity would be enhanced. Plastic scintillator would have an edge over the other techniques, this would combine the sensitivity and real-time rapidness.

Table 6: Comparison between the different major tritium-in-air detection techniques.

Monitoring technique	LSC1	LSC2	LSC3	Ionization Chamber	Proportional Counter	Plastic Scintillator
Typical lower limit of detection	40-400 Bq/m^3	0.3-3 Bq/m^3	2-20 mBq/m^3	40 kBq/m^3	3 kBq/m3	4-40 kBq/m^3
HTO	Yes	Yes	Yes	Yes	Yes	Yes
HT	Not direct	Not direct	Not direct	Yes	Yes	Yes
Sampling technique (time)	-Bubbler (5 min) -Passive sampler (5 min)	-Condensation (2 min.) -Desiccant (4 h)	-Condensation (2 min.) -Desiccant (4 h)	On Line	On Line	On Line
Measuring time	10 min.	10 min.	24 h	On Line	On Line	On Line
Interferences	γ fields & PMT random noise	γ fields & PMT random noise	γ fields & PMT random noise	-Airborne isotopes $\beta + \alpha$ -γ fields	-Airborne isotopes -γ fields	-γ fields for big cells.
Correction methods	-Shielding -Coincidence counting tech	-Shielding -Coincidence counting tech	-Shielding -Coincidence counting tech	-γ compensation	-Discrimination by -Pulse shape -Pulse height & anticoincidence discrimination	-Shielding
Short comes	Liquid scintillation wastes	Liquid scinti. cocktails wastes	Liquid scinti. cocktails wastes	-Vibration sensitive -Contamination potential	-Needs counting gas. -Delicate	-Humidity sensitive -Efficiency degrades
Counting geometry	Internal source counting	Internal source counting	Internal source counting	Internal source counting	Internal source counting	External source counting
Usage	-Rad. protection -Envi. monitoring	-Rad. protection -Envi. monitoring	-Rad. protection -Envi. monitoring	-Rad. protection	-Rad. Protection	-Rad. protection

Overview of the proposed 'on-line' monitor

Introduction

The main objective of this investigation was to develop a sensitive on-line tritium movable, if not portable, monitor relying on and utilizing the present achievement in engineering and the well defined techniques. Two methods were considered. The first is based on the detection of α particles produced by the T(d,α)n reaction. The second is based on the detection of the scintillation induced in a plastic scintillator by β^- particle emitted from tritium atoms.

The first method

The T(d,α)n reaction is a well studied reaction (Brolley and al 1960). It is utilized to produce high energy neutrons which are used for activation analysis (Nagowala et al. 1973; Soete et al. 1973). The utilization of D-T reaction to detect tritium has been demonstrated by Zhao (Zhao et al. 1986). Also, the reaction has been used for profiling tritium in solids (Caterini 1986; Sawicki 1988). The produced α particles will be detected by a surface barrier Si detector. The yield rate of α particles production in the reaction as a function of the incident particle energy can be described by:

$$Y(E) = n \,.\, \phi \,.\, \sigma(E) \qquad \textit{eq. 5}$$

Where,

- n = the number of target atoms per cm^2,
- ϕ = the number of incident particles per unit time (beam current), and
- $\sigma(E)$ = is the reaction cross section as a function of incident particle energy.

For a tritiated sample an with activity of 1 Bq/ cm^3 there is only one β^- emission per second. However, there are $5.6x10^8$ tritium atoms. If we assume that the efficiency of separating tritium from the sample, and the efficiency of accelerating the atoms to the target are Fs and Fa, respectively, then the number of atoms available for the reaction is

F_s x F_a x $5.6x10^8$ atoms. Now if we assume that the number of deuterons in a target is $1x10^{20}$ per cm^3 (CRC 1987), and the cross section of the reaction for 150 keV beam is only 2 barn, then the yield of the reaction is:

$$Y = N_1 . N_2 . \sigma$$
$$Y = F_s . F_a . 5.6x10^{8} x\ 1x10^{20} . 2\ x10^{-24}$$
$$= 1.12x10^{5} . F_s . F_a \ reactions$$

The yield of the reaction is directly proportional to the number of deuterium and tritium atoms and the cross section of the reaction. The maximum cross section for the reaction as a function of the incident deuterium energy is 5 barns (Brolley and al 1960) at 100 keV. The yield of the T(d,α)n reaction depends, amongst other things, on ion beam characteristics. Different beam intensities will give different yields. Atomic beam have a higher yield for energies less than 250 keV than molecular beams (CRC 1987). The yield resulting from beams with energies less than 100 keV varies greatly with a small change in the energy of the incident particles. Therefore, it is very important to have a stable beam with the optimum energy of 120 keV.

The alpha yield of the reaction is isotropic and is peaking forward (Caterini 1986). The energy carried by the α particles varies with the energy of the incident beam, and emission angle. The energy varies between 2 and 5.81 MeV. However, for α particles emitted at an angle of 80° with respect to the incident beam, the variation in the energy,

of the α particles, is independent of the energy of the incident beam. Also, the reaction yields fast neutrons with energies around 14 MeV.

This method was put aside because of two main factors, i) the cost, and ii) the production of 14 MeV neutrons. A 120 kV high voltage power supply is required, the price of which was high, > 4000 pounds sterling. Also, such a power source would be large and heavy to move around. The production of 14 MeV neutrons would require shielding adding to the size and weight of the overall monitor. Despite the potential of a very good sensitivity that this technique may have, the above mentioned factors were enough to bring the investigation of this technique to a halt.

The second method

This method would develop a detector based on a plastic scintillator. The developed detector would be an internal source detector, where the sample is introduced inside the plastic scintillator. By so doing the device will hopefully achieve the low detection limit of the internal LSC technique, i.e. 400 Bq/m^3, with a very short response time.

In the following section the proposed conditions of use are described along with an analysis of the design criteria and requirements.

General description

Liquid Scintillation Counters (LSC) have a low detection limit which is far better than that of Plastic Scintillator (PS) counters. One of the reasons is that in the case of LSC, the samples are dissolved as part of the scintillator solution. Therefore, all of the β^- particles emitted by the tritiated sample are initially released inside the scintillation cocktail. This situation is unique to LSC. For plastic scintillators this is not the case because the tritium β^- particles enter the scintillator from outside. Consequently they must pass through some medium, air or water, a protective covering and/or light

reflector before reaching the surface of the scintillator material. The β^- particle energy loss that may occur in these intervening materials can significantly affect the detection efficiency.

For low level LSC counting of tritium, the ratio of the sample to scintillator solution is usually decreased in order to increase the sensitivity of the cocktail solution. The sensitivity in turn increases when the β^- particle's energy is best utilized by the scintillator molecules. This of course is accomplished by using the most efficient solid scintillator that can fulfil the operating conditions required.

The total number of β^- particles emitted from a tritiated air sample, which reach the detecting plastic scintillator foil, can be estimated by assuming: that all disintegrations carry the spectral mean energy of 5.7 KeV. Only 1/6 of the emitted β^- particles will be directed towards the surface of the plastic scintillator and the energy deposited at the surface decreases linearly with distance from 5.7 keV at 0 cm to 0 keV at a distance equal to the range of a 5.7 keV β^- particle in dry air, approximately 0.035 cm. Therefore, the total number of β^- particles reaching the surface of the plastic scintillator is:

$$1/6 \times (0.035\ (cm)\ .\ 1\ (cm^2)) \times 1\ (Bq/cm^3) = 0.0058\ Bq$$

or, only 0.6 % of the emitted β^- particles is available for the plastic scintillator to detect. The total number of tritium atoms available within the above volume can be calculated, knowing $\lambda = 1.7671 \times 10^{-9}\ sec^{-1}$, as follows:

$$N = (1\ (Bq/cm^3) / \lambda\ (sec^{-1})) \times (Range\ (cm) \times 1\ (cm^2))$$

$$= 5.6 \times 10^8\ (\#/cm^3) \times (0.035\ (cm) \times 1(cm^2)) = 2 \times 10^7\ atoms$$

of these only $2 \times 10^7 / 6 = 3.3 \times 10^6$ atoms are directing their β^- particles towards the plastic scintillator.

The PS detector cells developed by Osborne (Osborne 1970), and by Singh (Singh et al. 1995) to measure tritium concentration in air illustrates the effect of this geometry factor. The former cell contained 60 square plates of PS, each is 5 x 5 cm^2 and 0.0125 cm thick and the total surface area is 3000 cm^2. The plates are mounted vertically and are 0.075 cm apart. The latter cell is made out of 4 PS films full of holes, the thickness of each film is 5 μm and the total surface area is 1200 cm^2. Table 7 compares the two cells used to monitor air samples. It is evident that the more efficient cell, utilized its surface area better. Although the Osborne cell offered a larger scintillation surface area for detection and has higher concentration of tritium atoms within the volume (0.005 cm x 1 cm^2), it failed to utilize this surface area efficiently as in the case of the Singh cell. From Table 7 one can notice that the Singh cell utilized a much smaller volume of PS to achieve a high sensitivity. The averaged air layer thickness was 50 μm allowing a large fraction of the emitted β^- particles, with energies less than 5.7 keV, to deposit a larger fraction of its energy within the PS bulk. Also, the sample to PS sheet geometry is such that the probability of the emitted β^- particles to reach the PS is at least 2 out of 6, see Figure 4.

While in the case of the Osborne et al model, the air layer thickness is 313 μm, only β^- particles with energies greater than approximately 4 keV will pass through 313/2 μm and reach the PS. Therefore, a large fraction of the emitted β^- particles will not be utilized.

Also, from the geometry of the Osborne design only 1/6 of the emitted β particles will reach the surface of the plastic scintillator. Therefore, the effective number of tritium atoms available, for the plastic scintillator, over 1 cm^2 is $1.04 \times 10^5 / 6 = 1.73 \times 10^4$ atom. Whereas for Singh's cell the number is larger 2.26×10^4 atom. Therefore, the Singh cell was able to detect a minimum of 4.2×10^{-5} Bq/cm^2, or 2.3×10^4 tritium atoms/cm^2 (row 'i' in table 7) at ~65 % efficiency in comparison of 1.4×10^{-3} Bq/cm^2, or 6.5×10^5 tritium atoms/cm^2 at ~60 % efficiency for the other cell.

Table 7: Comparison between two plastic scintillator detectors used for monitoring tritium concentration in air.

	Comparison points	**Osborne 1970**	**Singh 1995**
	Detection mode	Coincidence	Coincidence
a	Flowcell volume (cm^3)	112.575	6.3
b	PS volume (cm^3)	18.75	0.3
c	PS thickness (cm)	.0125	.0005
d	PS Surface area [(b/c) . 2] (cm^2)	3000	1200
e	Averaged sample layer thickness over the PS [(a-b)/d] (cm)	.0313	.0050
f	Tritium concentration (Bq/ cm^3)	0.037	0.008
g	Total activity in the cell (Bq)	3.472	0.048
h	The total # of tritium atoms in the cell	1.96×10^9	2.7×10^7
i	# of tritium atoms *over* cm^2 of the PS (#/cm^2).	6.5×10^5	2.26×10^4
j	# of atoms *within 50 μm over* the PS (#/cm^2).	1.04×10^5	2.26×10^4
k	sample to PS sheet geometry	one sided	surrounded
l	Resulted CPM / cell	150	2
m	Resulted CPS	2.5	0.033
n	Efficiency (CPS/DPS)	60%	66%

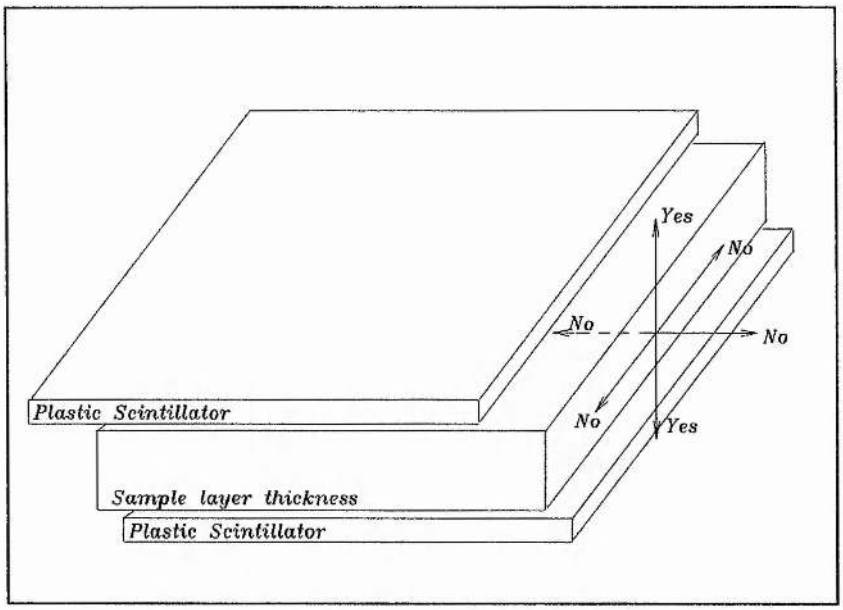

Figure 4. The geometry in which β^- particles are emitted.

In order to utilize the bulk of the plastic scintillator, the total number of tritium atoms available in the sample, and all of the energy carried by β^- particles emitted from tritium atoms must be implanted inside the plastic scintillator at a depth ≥ the maximum range of the β^- particles in plastic scintillator (this range is ~ 6μm). The deposition of multiples of $2x10^7$ ions in the plastic scintillator may take a few seconds. Then when the β^- particles are emitted they are totally absorbed inside the plastic scintillator. This would make the plastic scintillator comparable with the liquid scintillator technique.

Design requirements for an on-line tritium monitor

The on-line tritium monitor is designed to have a sensitivity around 400 Bq/m^3 for tritium in air. In principle the method first ionizes the air sample in a plasma source, implant tritium atoms present in the sample into a plastic scintillator and count the resulting scintillations efficiently. The major components proposed to accomplish these tasks are an ion (plasma) source, implantation unit, a thin scintillator target, and scintillation counting assembly.

The plasma source is required to efficiently ionize air samples which include trace amount of tritium. The implantation unit is designed to extract most of the ions produced in the ion source, accelerate, implant and selectively accumulate the tritons in the plastic scintillator target. Nearly all of the β^- particles emitted in the decay of the tritium atoms will be absorbed inside the plastic scintillator target. The scintillations produced inside the plastic scintillator target by the β^- rays will be detected by the photomultiplier tube, then processed and registered by the connected electronics

Sample characteristics

The monitor was developed to detect elemental tritium concentrations in air samples. An air sample consists of a mixture of gases. Table 8 shows the typical air gas composition. Beside these gases an air sample may contain water vapor at different concentrations depending on the ambient temperature and conditions.

Table 8: Typical air composition at sea level (CRC 1964-1965).

Gas	Atomic mass	no. density at STP (#/cm^3)	Volume Percentage (%)	Content (ppm) by volume.
Nitrogen	14.0067	$1.9896*10^{19}$	78.1	
Oxygen	15.9994	$5.324*10^{18}$	20.9	
Carbon dioxide	44.0098	$7.643*10^{15}$	0.03	
Argon	39.948	$2.369*10^{17}$	0.93	
Krypton	83.80	$2.7*10^{11}$		$1.14 \pm .01$
Xenon	131.30	$2.1*10^{9}$		$.087 \pm .001$
Helium	4.0026	$1.241*10^{9}$		$5.24 \pm .004$
Hydrogen	1.0079	$1.18*10^{11}$		.5

An air sample containing the derived air concentration (DAC) value of 0.3 Bq/cm^3 would have 1.68 x10^8 cm^{-3} tritium atoms mixed in 2.55 x10^{19} atoms/cm^3 of different air gases. It is expected that the monitor would be used in a workplace where different types of radiations and or radioactive isotopes are present. The monitor should show minimum response, if not zero response, to the presence of other types of radiations. Also the monitor is expected to at least achieve the sensitivity of liquid scintillation counting. Only tritium atoms are desired to be implanted into the plastic scintillator, other atoms are unwanted. The major requirements for the developed monitor are to collect the maximum number of tritium atoms present in an air sample and to assay the amount by selectively counting the tritium β^- decays.

Material requirements

Based on tritium characteristics with regard to interaction with matter all parts of the developed monitor that would come in contact with tritiated air samples are selected to minimize tritium absorption in order to avoid or minimize memory effect after exposure.

Plasma source

The plasma source should be easy to operate, be stable, and be able to produce high-density, and highly excited plasmas with no or minimum contamination, in a reproducible discharge over a wide range of operational conditions such as pressure and gas composition, and it should be of low-cost.

Implantation unit

Ion implantation can be achieved by a variety of techniques. The selected one has to fulfil certain important requirements. These are: high efficiency of ion collection, high efficiency of ion deposition inside the plastic scintillator over a wide region, minimal sputtering, simplicity of the design, small volume, ease of operation, and low cost.

The plastic scintillator target / detector

A solid scintillator is required which has a relatively high sensitivity of detection for tritium β^- particles; is of low atomic number and can be formed into very thin microfoils. For practical reasons the cost of the detector should be relatively low.

Anthracene and NE 102 plastic scintillators has the desired properties and have long been used to detect tritium in real time. As mentioned in page 36 above a sensitivity of 40 kBq/m^3 has been achieved. Table 9 gives a comparison of some solid scintillators. They are relatively insensitive to gamma radiation as there is very low photo-electron absorption because of their low atomic number (Z).

Table 9: Comparison of various solid scintillators.

Scintillator	Type	Density	Refractive Index	Light output, % Anthracene	Decay con. main component (nsec)	Wave length Maximum int. of emission (nm)
Anthracene	Crystal	1.25	1.62	100	30	447
Stilbene	Crystal	1.16	1.626	50	4.5	410
NE 102	Plastic	1.032	1.581	65	2.4	423

Also, a thin layer of a few microns of these organic scintillators can be made which is the desired thickness. It would stop all of the tritium β^- particles but would pass gamma rays with almost negligible attenuation, therefore giving rise to a pulse that can be related to the tritium β^- particles alone. Anthracene and NE 102 plastic scintillators are sensitive to alpha particles. Consequently pulse height analysis is required to facilitate the discrimination against alphas. The relative pulse height of an alpha interaction is much smaller than that of β^- interaction, for equal energy deposition. However, as most

alpha energies range from 5.3 to 8.8 MeV with ranges ~ 30 μm the light output is in practice much greater than for the low-energy tritium β^- particles and therefore some form of pulse discrimination is necessary (Knoll 1979).

Organic scintillators can suffer from memory effects when detecting tritium. This is because tritium can migrate easily into the plastic scintillator and can be a problem when a solid scintillator is used for a long period of time to detect tritium β^- particles. Consequently it may be necessary to change the detector periodically. For short time exposure periods, the memory effect is not likely to be a problem.

Tritium separation

In order to introduce more tritium ions, which are collected from an air sample, into the plastic scintillator without adding to the risk of introducing impurities, which have a quenching effect on the scintillation output, tritium ions alone have to be implanted into the plastic scintillator. The heavy particles can be separated by coating the plastic scintillator with a suitable thickness of an absorber to prevent all accelerated ions except that of tritium from reaching the plastic scintillator. The absorber foil should have a low Z number and should act as a barrier to prevent or minimize tritium mobility from the deposition side of the microfilm to the other; and to serve as a light reflector.

Light guide

The implantation of the solid scintillator will take place under vacuum using very high negative voltage pulses (~60kV). Therefore, it is impractical to couple the solid scintillator directly to the photomultiblier tube (PMT). A light guide of sufficient length is required to transmit the light from the scintillator to the PMT. The light guide should be coupled to the scintillator using an optical coupling fluid of matching refractive index. Also, the light guide should have a relatively high index of refraction to minimize the

critical angle for total internal reflection. Ideally light guide surface should be highly polished and surrounded by a reflective wrapping to reflect back the escaping light.

A prespex light guide with no reflective covering, so as to prevent any possible short circuit is required.

Scintillation detection

Ideally, measurements of low levels of tritium in the phosphor require the use of two photomultiplier tubes each viewing the sample but operated to sum coincidences. This is to reduce the random high background noise that is thermally generated in a photomultiplier tube. This noise consists of relatively low voltage pulses which are similar to the pulses driven from low energy tritium β^- particles.

Chapter 3

Theory

Chapter 3

Theory

The theoretical principles of operation for the major components are elaborated in this chapter.

Plasma Source Ion Implantation (PSII)

Introduction

Plasma Source Ion Implantation is the only technique capable of fulfilling the above mentioned design requirements (see chapter 2). Plasma source ion implantation (PSII) and plasma immersion ion implantation (PIII) are cost-effective, non-line of sight ion implantation methods which have been developed in recent years (Conrad 1987). Both techniques are classifications of plasma ion implantation (PII) for modifying the surface of metals, ceramics and polymers (Hahn and Lee 1992). The typical plasma density for PSII is in the range of $\sim 10^9$ cm^{-3}, while for PIII it is $\sim 10^{10}$ cm^{-3}. The latter requires a high voltage of shorter pulse duration. PSII places the target inside the plasma source itself, eliminating the need for ion beam extraction, manipulation or focusing and hence, minimizing ion losses. High voltage negative pulses applied to the target attract positive ions in the plasma which eventually strike all parts of the target at normal, or below 30° off-normal, incidence which is the optimal angle for ion implantation (Wang et al. 1993b; Wang et al. 1994b). PSII is capable of implanting various ionized atomic and molecular species into the entire surface of a target, resulting in distributing the implanted ions over a wider region. The instantaneous current density is large when it is compared to that of conventional implantation.

In the PSII process a series of negative high-voltage pulses are applied to a target that is immersed in a plasma (see Figure 5). Electrons are repelled from the surroundings of the target region leaving behind a bare cloud of ions which form a non-neutral region called the plasma or ion matrix sheath. The size of the ion matrix sheath is several Debye lengths, λ_D, $(=((\varepsilon_0.k.T_e)/(n_0.e^2))^{1/2}$, where ε_0 is the free space permitivity, k is Boltzmann's constant, T_e is the electron temperature, n_0 is the neutral plasma density, and e is the electron charge = 1.6×10^{-19} C) = $69.02\ .\ (T_e/n_0)^{1/2}$ (cm) (Hastie 1993). The resulting electric field accelerates the ions to a high energy toward the target where they are implanted.

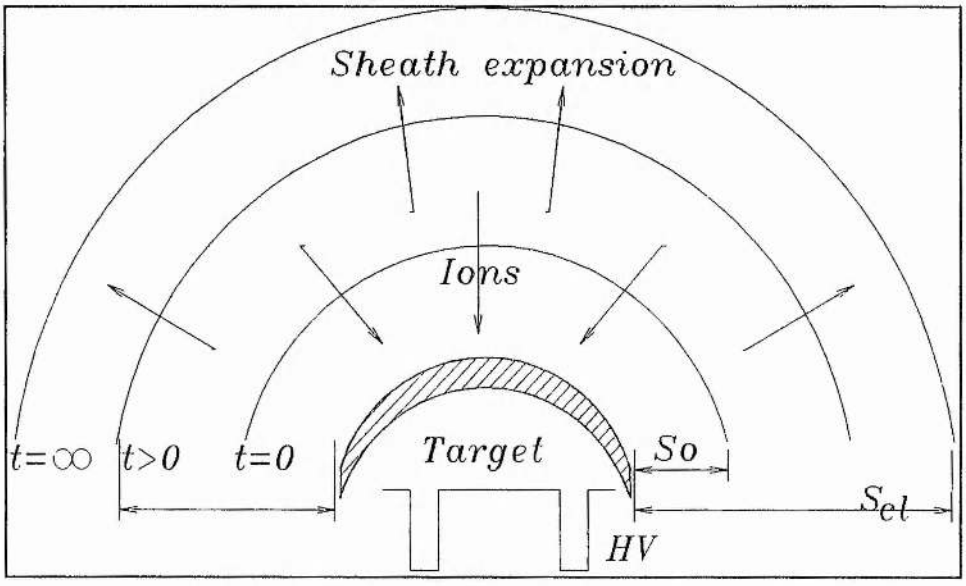

Figure 5. Schematic representation of a transient plasma sheath after applying the negative HV pulse. 1) at t=0, an ion matrix sheath is formed almost instantly. 2) at t>0, the sheath edge expands into the plasma. 3) at t= ∞, a Child-Langmuir sheath limit is reached.

The behavior of the sheath evolution can be clarified by knowing the time scale that governs the response of the plasma sheath. At t = 0 the electrode (target) is at zero potential. Then, when the negative high voltage pulse is applied and at a time scale of

$1/\omega_{pe}$ (in the range of ~ nsec) electrons are repelled from the target region while ion motion is negligible. Here, ω_{pe} is the electron plasma frequency (Anders 1990)

$$\omega_{pe}^{-1} = ((\varepsilon_0 \, . \, m_e) / (e^2 \, . \, n_e))^{1/2} \qquad \textit{eq. 6}$$

$$= 1/(56.4 \, (n_e)^{1/2}) \qquad \textit{(sec)}, \qquad \textit{eq. 7}$$

where, m_e, e, and n_e are the electron's mass, charge and number density respectively. Hence, a region of nearly uniform positive space charge is established. This region establishes a potential profile described by the ion-matrix model. Subsequently, on a time scale of $1/\omega_{pi}$ (in the range of ~ μsec) ions within the sheath are accelerated toward the target, eventually, decreasing ion density in the sheath. Here, ω_{pi} is the ion plasma frequency (Anders 1990)

$$\omega_{pi}^{-1} = ((\varepsilon_0 \, . \, m_i) / (e^2 \, . \, n_i))^{1/2} \qquad \textit{(sec)}, \qquad \textit{eq. 8}$$

where, m_i, e, and n_i are ion's mass, charge and number density respectively. Next, and in a time scale of several times of $1/\omega_{pi}$, the decreasing ion density causes the sheath edge to expand in order to maintain the sheath potential. This will expose new ions which are finally extracted and implanted into the target. Ultimately, on a larger time scale, the ion and electron density profile relax when the sheath reaches its orbit limit or the Child-Langmuir steady-state.

The propagating sheath was described by the Child-Langmuir law quasi-statically. Lieberman, using the same law has described sheath evolution for collision-less plasma in planar geometry (Lieberman 1989). Scheuer et al modified Lieberman's model and extended it to include planar, cylindrical, and spherical geometries (Scheuer et al. 1990). Different versions of models based on the Child-Langmuir law have also been set up for different plasma conditions and different voltage pulse shapes (Conrad 1987; Qin and Chan 1992; Stewart and Lieberman 1991; Vahedi et al. 1991; Wang et al. 1993a). Conrad, et al developed an analytical expression for the potential profile and sheath thickness of the transient ion-matrix sheath which forms when the high voltage negative step potential is applied. Vahedi, et al applied the model for the case in which ion motion in the sheath can be assumed to be highly collisional. They described the sheath expansion, ion velocity distribution and ion flux at the target as functions of time for both planar and spherical geometries. The above mentioned Sheuer et al model was extended for voltage pulses with finite rise and fall times. Qin, et al developed a collisional model that describes the evolution of the sheath in the ECR plasma source. Wang, et al developed a model describing the temporal evolution of the sheath (i.e. the sheath expansion velocity and the position of the sheath edge as a function of time) in planar geometry. Their model covers the whole range from collision free to collision dominated sheaths.

Theory

Analytical description

The ion sheath evolution can be described analytically. The sheath thickness of the transient ion matrix that is formed as the large negative step potential is applied, for planar geometry, is:

$$S_0 = ((2\ \varepsilon_0 .\ V) /(e .\ n_0))^{1/2} \qquad (cm) \qquad \textit{eq. 9}$$

where, ε_0 is free space permitivity, V is the magnitude of the negative potential, *e* is electron charge and n_0 is the plasma density (Conrad 1987).

The subsequent evolution of the ion sheath according to a quasi-static Child law is based on assumptions that deal with ion velocity at the sheath edge and the electrostatic field structure during the ion motion across the sheath. These assumptions are (Lieberman 1989):

1) The ion flow is collision-less therefore only sheath expansion at low pressure is covered.

2) The electron motion is instantaneous.

3) The applied negative high voltage pulse is very large compared to electron energy hence, $\lambda_D << S_0$. The sheath edge S_0 is abrupt.

4) During and after the matrix sheath implantation a quasi-static Child law sheath forms and the current demanded by the sheath is supplied by the uncovered ions supplied by the moving sheath edge.

5) During the motion of an ion across the sheath the electric field is frozen at its initial value, independent of time except for the change in field due to the velocity of the moving sheath.

The Child-Langmuir current density J is

$$J = ((4\,\varepsilon_0)/9)\,.\,((2\,e/m_i)^{1/2})\,.\,(V^{3/2})/S^2 \qquad \textit{eq. 10}$$

where e and m_i are the charge and the mass of the ion, V is the absolute value of the applied high negative voltage, and S is the location of the sheath edge relative to the target. The target ion current due to sheath edge movement is

$$J = e\,.\,n\,.\,dS/dt \qquad \textit{eq. 11}$$

Here, n is the plasma density. The sheath expanding velocity can be found by combining equations eq. 10 and eq. 11

$$dS/dt = ((4\,\varepsilon_0)/(9\,n))\,.\,((2/e\,.\,m_i)^{1/2})\,.\,(V^{3/2})/S^2 \qquad \textit{eq. 12}$$

The evolution of the sheath for the case of collisional plasma where ion motion is highly collisional (ion-neutral mean free path λ_i << S the sheath thickness) can be described by the collisional model developed by Qin (Qin et al. 1991). This model assumes that collisional sheath evolution obeys the sheath ion current law derived by Lieberman (Lieberman 1989). The current density J,

$$J = ((500 / (243\ \pi)) ^{1/2} .\ \varepsilon_0 ((2\ e\ .\ \lambda_i / m_i) ^{1/2} .\ (V ^{3/2} / S ^{5/2}))$$

eq. 13

where λ_i is the ion-neutral mean free path. From equations eq. 11 and eq. 13 the sheath expansion velocity is

$$dS/dt = ((500 / (243\ \pi)) ^{1/2} .\ (\varepsilon_0 / n) .\ ((2\ \lambda_i) / (e.\ m_i)) ^{1/2} .\ (V ^{3/2} / S ^{5/2}))$$

eq. 14

A collisional sheath evolution model, that covers the whole range from collision-free to collision dominated sheath, based on the quasi-static law was developed by D., Wang, et al (Wang et al. 1993). Here, the current density J is

$$J = \{((4\varepsilon_0) / 9) .\ ((2\ e) / m_i)^{1/2}\}.\{V ^{3/2} /(S ^{2}.(1+((12\ \pi) / 125) .\ (S/\lambda_i)) ^{1/2})\}$$

eq. 15

and from equation eq. 11 and eq. 15 the sheath expansion velocity is

$$dS/dt =\{((4\varepsilon_0) / (9n)).(2 /(e.\ m_i)) ^{½}\}.\{V ^{3/2} /(S ^{2}.(1+((12\pi) / 125).(S/\lambda_i)) ^{1/2})\}$$

eq. 16

Now the extent of the sheath evolution during the negative high voltage pulse can be obtained by solving equation eq. 16 numerically. The initial conditions are t = 0 and $S=S_0$. The final condition is that when $t = t_{pulse}$. A typical curve for the position of the sheath edge as a function of time is shown in Figure 6.

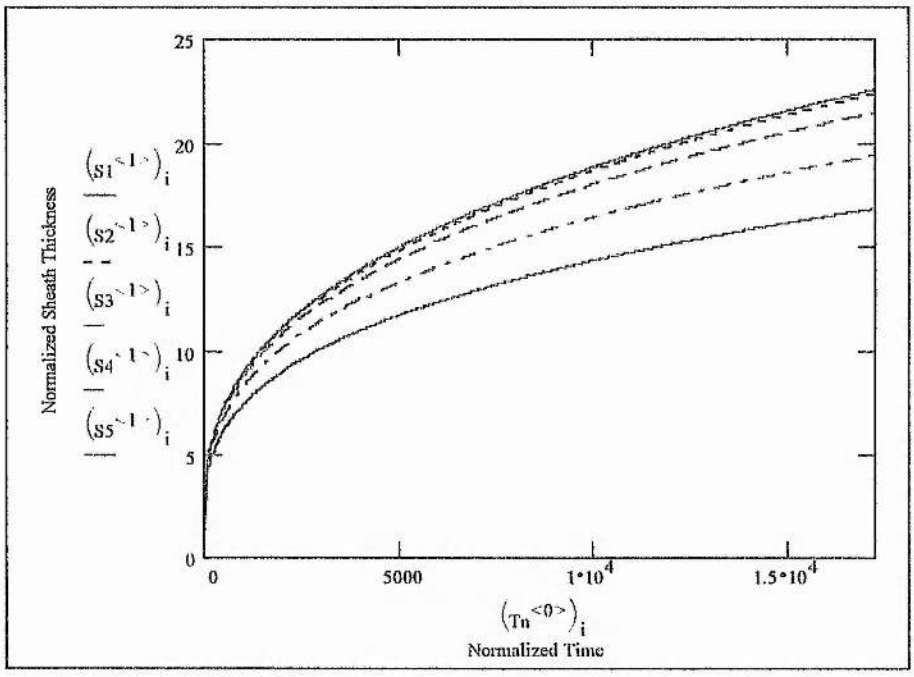

Figure 6. The position of the sheath as a function of time in planar geometry. Amplitude of negative pulse is V = 60 KV at different gas pressures $S1^{<1>}$ for 0.12 mTorr, $S2^{<1>}$ for .42 mTorr, $S3^{<1>}$ for 1.9 mTorr, $S4^{<1>}$ for 10 mTorr, and $S5^{<1>}$ for 210 mTorr.

It is quite evident from Figure 6 that the increase of the pressure will reduce the extent of the sheath propagation and reduces the velocity of sheath edge expansion. This is a result of ion energy losses caused by ion-neutral collisions, which reduces the ion current implanted into the target and in turn causes the drop of the sheath expansion velocity (Wang et al. 1993a; Wang et al. 1994a; Wang et al. 1994b).

Ion current dose calculation

The dose to the target can be approximately determined by calculating the volume of the plasma within the final sheath extent reached during the high voltage pulse and assuming that all ions in this volume are implanted into the target (Shamim et al. 1991a). The average ion current to the target per pulse is I_i (A) (Scheuer et al. 1990; Uhm and Lee 1991a; Uhm and Lee 1991b):

$$I_i = \{(e \,.\, A \,.\, n_i) / (t_{pulse})\} \,.\, S_f$$

eq. 17

where $e = 1.6 \times 10^{-19}$ (C), A (cm^2) is the target area, n_i (cm^{-3}) is the plasma density, t_{pulse} (sec) is the pulse duration and S_f (cm) is the final sheath extent calculated from eq. 16. For a given target, the delivered dose can be increased by maximizing the plasma density and the magnitude of negative pulse potential. The latter will result in an increase in the sheath volume.

The time required to deliver a given dose ϕ (atoms/cm^2) to the target is (Chen et al. 1993):

$$t = (e \,.\, A \,.\, \phi) / (t_{pulse} \,.\, f \,.\, n \,.\, I_i)$$

eq. 18

where f (Hz) is the pulse repetition rate, n is the average number of atoms per ion and I_i is calculated from equation 17. The average ion current, I_{ave}, can be calculated by

$$I_{ave} = I_i \,.\, t_{pulse} \,.\, f$$

eq. 19

At the onset of the high voltage pulse the current to the cathodic target is expected to rise rapidly and then decay to a steady decay of ~ 5 % of the initial current spike (Collins and Tendys 1994; Franklyn and Nothnagel 1994; Goebel 1994; Matossian 1994; Shamim et al. 1991b; Wood 1993). This spike current is due to the combined effect of the plasma sheath capacitance, stray-circuit capacitance, the implanted ions, and the secondary electrons produced as a result of the incident ions.

The expected net current is

$$I_n = I_i + I_e = I_i (1 + \gamma) \qquad \textit{eq. 20}$$

I_i is the collected ion current, I_e is the emitted electron current and γ is the secondary electron emission coefficient (Goebel 1994). When designing the high voltage power modulator precaution measures need to be taken to reduce the effect of the current spike. When ions are collected by a pulse, more ions are diffused into the depleted region. At sufficiently high frequency pulses, ion repopulation cannot replenish the depleted region around the target fast enough (Wood 1993), hence the amount of the collected ions tends to decrease with each consecutive pulse. Wood predicted that ions with temperatures consistent with those found in an electron-cyclotron resonance discharge require more time to fill in the depleted region than that for ions with lower temperature. Therefore, for maximum implantation current a plasma source capable of producing a large plasma with density in the range of 10^9-10^{12} cm^{-3} with low electron temperature that ranges from 2-10 eV and lower ion temperatures are needed.

The prediction of the dose and the energy of implantation is critically dependent on the ratio of ion species (Tang et al. 1993). If, for example, there are 30 % N^+ and 70 % N_2^+ in a nitrogen plasma the average number of atoms produced per ion equals 1.7 (0.3 X 1 + 0.7 X 2 = 1.7). When the target is biased at 60 kV, after implantation each implanted N_2^+ is converted into two nitrogen atoms with 30 keV energy while each implanted N^+ is converted into one nitrogen atom with 60 keV. Therefore, the composition of the depth-profile will vary. The higher the ratio of molecular ions to atomic ions produced

in the plasma source the higher the number of atoms implanted, but the shallower the deposition depth, and visa versa.

The ion energy distribution function, IEDF, which describes the energy range and distribution when hitting the surface of the target substrate, is a critical parameter for the choice of plasma source for a particular material processing application (Johnson 1993). In PSII, the energy of ions bombarding the target is not monoenergetic. The IEDF depends on the target charging voltage, temporal pulse shape and on the ion-neutral collision in the boundary layer (Speth et al. 1994; Wang et al. 1994a; Wang et al. 1993b; Wang et al. 1994b). These phenomena, however, do not have a significant effect on the ion implanted dose. The ion-neutral collision is governed by the pressure of the neutral gas. As the pressure increases the energy loss of ions in the sheath by collision increases, and the IEDF will cover the whole range of the energy spectrum. The effect of charge exchange collisions can be reduced by operating the PSII system at a gas pressure of $\leq$ 0.1 mTorr (Wang et al. 1993a). The temporal pulse shaping effect is evident if an exponential shut off pulse is used, which tends to produce ions with low energies.

Target charging phenomena can have a significant effect, depending on the target thickness and on the ion impact energy if the target is not metallic (Emmert 1994). When bombarding a dielectric material (plastic scintilator) for a long time a space-charge potential may build up on the target surface. This may cancel or reduce the negative biased voltage thereby preventing ions from falling into the target with the desired energy. Therefore, the propagation of the expanding ion sheath and consequently the energy of the implantation into the plastic scintillator is affected. The voltage at the plastic scintillator-plasma interface is given by

$$V = V_o(t) - (E \cdot d / \kappa) + (\sigma / \varepsilon_o)(d / \kappa)$$

eq. 21

$V_o(t)$ is the absolute value of the potential applied to the target, σ is the surface charge density implanted in a given pulse. E is the electric field in the plasma at the surface of the plastic scintillator, ε_o is the dielectric permitivity of free space, d is the thickness of the plastic scintillator and κ is the dielectric constant of the plastic scintillator material (Emmert 1994).

$$E = - (4/3) (9 j / 4 \varepsilon_o)^{(2/3)} (m S / (2e))^{1/3}$$

eq. 22

$$\sigma = n_o e (S(t) - S_o)$$

eq. 23

Combining equations eq.10 eq. 21, eq. 22 and eq. 23 yields (Emmert 1994).

$$V = (V_o(t) - (n_o e d (S-S_o) / (\varepsilon_o \cdot \kappa))) / (1 + (4 d / 3 S \cdot \kappa))$$

eq. 24

By combining eq. 24 into eq. 16, an equation that contains allowance for the target charging effect and which describes the sheath-evolution expansion velocity for a collision free and collision dominated sheath is developed as

$$dS/dt = (4\,\varepsilon_o/(9\,n_o)) \,.\, (2/(e\,.\,m_i))^{1/2} \,.$$
$$\{1/(S^2 .\, (1+((12\,\pi)/125) \,.\, (S/\lambda_i))^{1/2})\} \,.$$
$$\{(V_o(t) - (n_o .\, e \,.\, d\,(S-S_o)/(\varepsilon_o .\, k)))/(1 + (4\,d/3\,S \,.\, k))\}^{3/2}$$

eq. 25

The effect of the characteristics of the HV pulse

The high voltage pulse characteristics have a significant effect on the implantation process and ion current to the target. These characteristics are the shape of the pulse, the width of the peak (on-time), the repetition rate and the magnitude of the negative HV pulse. The pulse is required to be as square as possible to achieve the maximum acceleration of ions (Malaczynski et al. 1993). This is very important since pulses with slow rise and fall time would produce slow ions, therefore, sputtering of the target rather than ion implantation will take place. Sputtering would reduce the density of the deposited ions. Nevertheless, the falling tail effect is minimal since most of the available ions are consumed (collected) during the pulse peak time (Malaczynski et al. 1993). While a pulse with a linear shut off or a very fast rise and fall time would reduce the pulse shape effect on ion impact energy (Speth et al. 1994).

The width of the applied negative pulse is defined by the plasma ion density, chamber dimension and target size. The width of the peak should be, in general, large enough to allow for the collection of all ions and short enough for the developed sheath not to reach the walls of the chamber (Deb et al. 1994). Therefore, proper selection of the pulse width would minimize the pulse tail effect on implantation (Malaczynski et al. 1993).

In the case where the plasma consists of a mixture of different gases the model developed by K. Thomas et al for a two-fluid plasma, where ions are assumed to be cold and collisionless, will help in defining the width of the pulse. The results of the model

predict that the lighter ions, tritium ions being among the lightest, present in a sample will be accelerated more rapidly towards the target than the other more massive ions and it will enrich the initial portion of the total current density that reaches the target (Thomas et al. 1994). Therefore, the pulse peak should be long enough to acquire an ion current with the highest percentages of tritium ions, and it should be short enough not to collect current with low tritium ion content. Since ions are accelerated across the sheath on a time scale equal to the inverse of plasma the frequency, $\omega p_i^{-1} = ((\varepsilon_o \, . \, M_i) / (e^2 \, . \, n))^{1/2}$, lighter ions present in a cold collisionless plasma, consisting of nitrogen and tritium ions, will be accelerated in an estimated time scale of $\omega p_{Ti}^{-1} \equiv \omega p_{Ni}^{-1} (M_{Ti} / M_{Ni})^{1/2}$., where the subscripts Ni and Ti resemble nitrogen and tritium ions respectively. For the ions of tritium this is equivalent to $1/2 \, \omega p_{Ni}^{-1}$.

The maximum repetition rate of the applied negative high voltage pulse is determined by the volume of the depleted sheath and the rate of refill of this volume (Deb et al. 1994). These in turn are functions of ion density, modulator current, pulse width and the rate at which plasma ions can refill the depleted volume. Furthermore, a higher repetition rate will implant a larger dosage of ions in a shorter time. However, the repetition rate must allow the depleted region around the target to be repopulated. The time to fill in the depleted region increases with higher ion temperature (Wood 1993).

The HV negative pulse magnitude has an effect on the implantation process. For relatively low magnitude pulses sputtering of the target increases.

In general, the amplitude of the PSII HV negative pulses is commonly in the range of a few kV to ten's of kV. The pulse duration is in the range of 1 to 10 μsec. The rise time is a few nanoseconds.

Different large plasma source generators have been used by different authors to conduct PSII experiments. Table 10 lists the different plasma source generators used along with the different parameters of these experiments.

Table 10: PII experiments and the plasma generators used.

#	Plasma source	Chamber volume (*l*)	Working pressure	Negative H.V. (kV)	Pulse duration (μsec)	Repetition rate (Hz)	Ions	Substrate	Reference
1	Microwave plasma	206	40-45 (mTorr)	10-20	20	0.1-30	N_2	304 L Stainless steel	(Smith et al. 1994)
2	Microwave multipolar bucket (2.45 GHz - 600 W)	30.5	50 (mTorr)	1-10	20	500	Boron	Silicon	(Qin and Chan 1994b)
3	DC plasma source		1 (mTorr)	2-5	20	0.5-1 k	Boron	Silicon	(Sheng et al. 1994)
4	RF inductive generation (.4 MHz - 500 W)	151	< 1 (mTorr)	10	4	20-30 k	O_2^+ , N_2	Silicon	(Tuszewski et al. 1994)
5	a- Filament discharge (6 A current). b- Townsend discharge	15	2 (Pa)	≤ 35	20	100	O , N	Al	(Gunzel et al. 1994)

#	Plasma source	Chamber volume (l)	Working pressure	Negative H.V. (kV)	Pulse duration (μsec)	Repetition rate (Hz)	Ions	Substrate	Reference
6	Glow discharge plasma (Pulses at low pressure)		0.5 (mTorr)	50		60	N	Al and Al alloy 7075	(Walter 1994)
7	RF glow discharge	415	10^{-3} (mbar)	50	50-100				(Collins and Tendys 1994)
8	= =	=	0.2 (Pa)	45	50		N	AISI 316 (austenitic stainless steel)	(Samandi et al. 1994)
9	Filament source		0.2 (mTorr)	30	40		O_2^+	Silicon	(Zhang et al. 1994)
10		32	1-10 (mTorr)	25	15-50	50-100 k	N_2^+	Stainless steel	(Franklyn and Nothnagel 1994)
11	Thermo-filament source	38.5	0.1 (mTorr)	25	10		Ar	Copper and stainless steel	(Shamim et al. 1991a)
12	Thermoionic source	2715	0.05 (mTorr)	50-100	10	200	85% N_2^+, 15% N^+	Silicon	(Vajo et al. 1994)

#	Plasma source	Chamber volume (l)	Working pressure	Negative H.V. (kV)	Pulse duration (μsec)	Repetition rate (Hz)	Ions	Substrate	Reference
13	Ring-cusp hot filament	1000	0.1 (mTorr)	up to 150	10-20		N_2^+, N^+		(Malaczynski et al. 1993)
14	ECR source		1-3 (mTorr)	2-14		1000-5000		Si	(Jones et al. 1994)

Numerical description

The evolution of the ion sheath can be described by solving the nonlinear partial differential equations of ion and electron motion across the sheath numerically. The numerical solutions were found to be consistent with the analytical quasi-static model for the case of collision-less plasma (Lieberman 1989; Stewart and Lieberman 1991; Thomas et al. 1994).

The sheath evolution can be described using the fluid dynamic model. This model requires the use of a computer code to solve numerically the fluid equations. A number of simplifying assumptions are usually made:

1) The ion and electron thermal motions are neglected. The applied voltage is much greater than the plasma electron temperature.

2) The ion motion is collision-less.

Thus the equation of continuity is:

$$dn_i / dt + d(n_i . u_i) / dx = 0 \qquad \textit{eq. 26}$$

and the equation of motion is:

$$d^2x / dt^2 = du_i / dt = - (e / M) (d\phi (x,t) / dx) \qquad \textit{eq. 27}$$

3) Electrons follow the Boltzmann distribution:

$$n_e(x,t) = n_o \exp(e\phi(x,t)/T_e) \qquad \textit{eq. 28}$$

And, the Poisson equation is obeyed

$$d^2\phi/dx^2 = (-e/\varepsilon_o)(n_i - n_e) \qquad \textit{eq. 29}$$

where M is the ion mass, $n_i(x)$, x, $u_i(x)$ are the ion density, position and velocity in the sheath. n_o, u_o are plasma density and ion velocity at the sheath-plasma boundary. ϕ is the sheath potential, T_e is electron temperature and e is the electron charge.

Surfatron

Introduction

The designed tritium monitor employs the plasma source ion implantation (PSII) technique for collecting tritium ions. The PSII technique requires a large plasma with density in the range of 10^9-10^{12} cm^{-3} with low electron temperature that ranges from 2-10 eV and low ion temperatures. The PSII does not require any kind of beam extraction whatsoever. Any known ion source can be used for plasma ion immersion implantation (Malaczynski et al. 1993). Plasma is usually generated by RF or glow discharges or by thermoionic emission from a hot filament (Uhm and Lee 1991b). However, when a plasma with minimum contamination levels is needed, elctrodeless plasma sources are used. When higher ion density is required, microwave generated plasmas are the better alternative (Qin and Chan 1994a).

From among the vast number of ion sources and plasma producing techniques reported in the literature (Brown 1989; Valyi 1979), the Surfatron, Surface Wave (SW) launcher,

was selected as the best option for the purpose. The Surfatron is one of the family of high frequency (HF) field wave launchers that can generate plasma (Moisan et al. 1979). The advantages of the SW produced plasmas are, in general, that of the typical RF and microwave plasma. The most important operation requirement is that there be no electrodes inside the plasma chamber to avoid corrosion, that there be minimal contamination of the construction materials or air sample and finally the production of low temperature ions, less than those found in electron-cyclotron resonance discharges (Wood 1993). The SW produced plasma has distinct advantages. The plasma is perfectly reproducible for given discharge conditions and it can be achieved over a broad range of frequencies (200 kHz-10 GHz), at different pressures (0.1 m Torr-7.6 k Torr) in tubes of various diameters (0.5-150 mm). Also, it is highly stable in response to changes in gas composition, wave frequency or power value. It can be produced in long columns or large volumes. Also microwave power sources at high frequencies, such as magnetrons, are readily available and relatively cheap. In a nutshell, the Surfatron launcher is simple, compact, cheap, easy to operate, and an efficient surface-wave (SW) launcher which can sustain a very stable and perfectly reproducible long plasma. It was therefore the source of choice. It was developed in the seventies by M. Moisan et al (Moisan et al. 1974; Moisan et al. 1975; Moisan et al. 1979). The HF surface-wave can propagate along the interface between a positive-column plasma and the surrounding dielectric along which the wave energy is concentrated (Trivelpiece and Gould 1959). Different investigations aiming at defining the characteristics and properties of the plasma column developed by the SW were carried out by Zakrzewski, Z., et al, 1977 & 1983, Gloude, V., et al 1980, Ferreira, C., 1981, 1983, & 1986 and Margot-Chaker, J., 1989. Many reviews on the properties and applications of the plasmas produced by the SW can be found (Moisan et al. 1982; Moisan and Zakrzewski 1986; Rahman and

Solntzev 1995a; Rahman and Solntzev 1995b). The nature of the wave sustaining such a plasma is well described by its dispersion and attenuation characteristic. Stable, reproducible and quiescent plasmas are produced. The surfatron does not affect the plasma parameters, such as electron and excited atoms densities, average electron energy and the shape of the electron energy distribution. However it determines the efficiency of the power transfer from the power generator to the plasma and it imposes the wave propagation mode. The properties of the discharge depends on the amount of power absorbed per unit length, the pressure and composition of the gas, the dimension of the discharge tube, the tube wall materials, the wave mode and the frequency. The parameters of the produced plasma are easily controlled by changing the power or frequency of operation of the UHF.

SW plasmas have different application in the fields of ion sources, hydrogen fluoride laser, elemental analyses by optical emission spectroscopy, small plasma-jet, spectral lamps, and He-Ne laser (Moisan and Zakrzewski 1986). Several articles on the different applications of SW sustained plasmas can be found (Pomathiod et al. 1988)(Beneking and Anderer 1992; Francou et al. 1995).

This section starts by describing the surfatron then elaborates on the theory of high frequency discharges under surface waves.

Description

A surfatron (see Figure 7) is a small, simple and easy to operate device which is capable of launching surface waves along a dielectric tube (Moisan et al. 1974; Moisan et al. 1975; Moisan et al. 1979). It is constructed from two parts: the UHF coaxial structure that shapes and orientates the electrical field; and the coupler that adapts the system impedance to that of the UHF generator to increase power transfer.

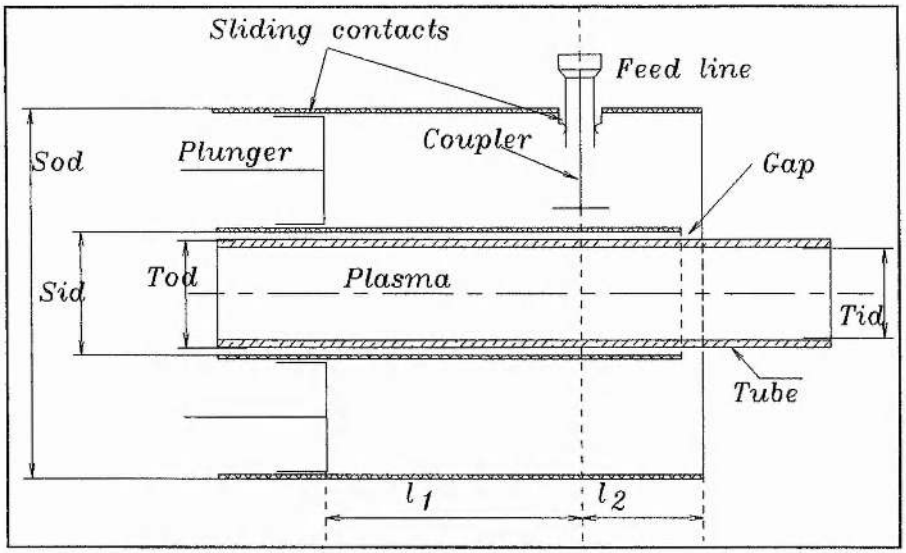

Figure 7. The surfatron. The double coaxial metal structure is shown with S_{od} and S_{id} being the structure outer and inner diameters respectively. T_{id} and T_{od} are the dielectric tube inner and outer diameters respectively.

The UHF coaxial structure is made of two metal cylinders forming a section of a coaxial line terminated by a short circuit at one end and by a circular gap at the other. A dielectric tube is placed axially inside the central cylinder. This UHF coaxial structure has the required symmetry and shape to allow the UHF electric field to extend through the gap to excite the azimuthal symmetric surface-wave required to sustain the plasma column in the dielectric tube. The HF field is parallel to the axis at the gap and near the dielectric tube.

The coupler is made of a semi-rigid coaxial cable. The cable is placed radially in the UHF structure and is extended outside the structure through a hole in the wall to be connected to the input transmission line. The coupler is electrically connected to the structure wall by a sliding contact. The external conductor of the semi-rigid cable, inside the UHF structure, is partly removed and the cable is terminated by a curved plate which is insulated by a thin insulator plate to prevent breakdown. A capacitance therefore exists between this plate and the inner tube of the UHF structure. The coupler

is not allowed to rotate, although it is allowed to move in the radial direction and also it is allowed to move in the axial direction but for a very small length.

Theory

The physical processes occurring in high frequency discharge.

In any given finite volume of gas there are always some free electrons and ions present. When an electric field is applied across such a volume charged particles are accelerated. Electrons oscillate in the gas volume, while ions because of their relatively large masses can be considered immobile (Nasser 1971). During this oscillation process electrons collide with other particles which will gain some energy at the expense of the field. Electrons are the only medium that is able to effectively absorb energy from the high frequency field and transfer it to the heavy particles and to the environment. The randomization of the electron movement due to collisions leads to the establishment of an electron energy distribution with a mean energy much larger than the energy available from the organized motion in the high frequency field. The fast electrons of the distribution can ionize the gas molecules. As a result new electrons can be produced, others are lost due to processes such as diffusion, volume recombination and attachment (MacDonald 1966). The charged particle balance in the discharge can be determined by assuming that direct ionization from the ground state and diffusion are the predominant processes for particle creation and loss. The physical processes directly related to the maintenance of the diffusion controlled discharge are elastic and inelastic collisions, and diffusion (MacDonald 1966). Assuming the total power loss per electron, θ, is independent of electron density. The total power loss per electron due to collisions can be written as (Moisan and Zakrzewski 1986):

$$\theta / \nu_m = 2m / M < \varepsilon > + \Sigma_i < h_i > e.V_i$$

eq. 30

where, m and M are electron and ion masses, ε is the electron kinetic energy ($\varepsilon = mv^2/2$), ν_m is the collision frequency for momentum transfer. h_i and V_i are respectively the efficiency and threshold potential for excitation to the i^{th} level by collision. The average power loss per electron remains constant along the plasma column, although the wave power can vary substantially along it.

Diffusion of electrons results from the random motion of electrons and causes a net directed flow, the flux of which is opposite to the electron density gradient. The proportionality factor between the flux value and the gradient value is called the diffusion coefficient D. In the most general case, D depends on both the electron energy and the electron density. However, there exist two cases for which the diffusion coefficient does not depend directly on the electron density. The first case corresponds to the low electron density limit where no interaction between charged particles takes place. The diffusion coefficient is called the free electron diffusion coefficient D_e. The other, opposite case, is called ambipolar diffusion. It corresponds to large electron density with the diffusion coefficient, D_a. Here the charged particles interact strongly and a collective diffusion movement of electrons and ions occurs. Free electron diffusion is faster than ambipolar diffusion and consequently the corresponding D_e is much larger than D_a. In the intermediate range of electron density values, the diffusion coefficient is density dependent. Therefore, it varies spatially within any plasma boundary.

The transfer of electromagnetic energy to the plasma

To describe the plasma interaction with the electromagnetic field, it is required to know the complex electron conductivity of the plasma, the value of which depends on the

electron density and collision frequency, ν_m, for momentum transfer (MacDonald 1966; Moisan and Zakrzewski 1986; Nasser 1971). The collision frequency is not constant for all gases. Therefore, by assuming that ν_m represents an effective value of the collision frequency, the transfer of energy to the plasma from the electromagnetic field can be expressed. The power gained, from an electromagnetic field of angular frequency ω and spatially averaged value of field intensity E, and lost in collisions by electrons is

$$P_L=(e^2 .n .E_e^2 .Vp) /(m . \nu_m) \qquad \textit{eq. 31}$$

where,

n = electron density in the active zone,

m = electron mass,

ν_m = effective value of collision frequency

V_p = volume of the active zone

$$E_e^2 = (\nu_m^2 . E^2)/ 2(\omega^2 + \nu_m^2) \qquad \textit{eq. 32}$$

E_e = the effective value for the electric field intensity

ω = field angular frequency

E^2 = is a spatially averaged value of the field intensity.

Figure 8 shows a schematic of energy transfer from the electromagnetic energy to the plasma.

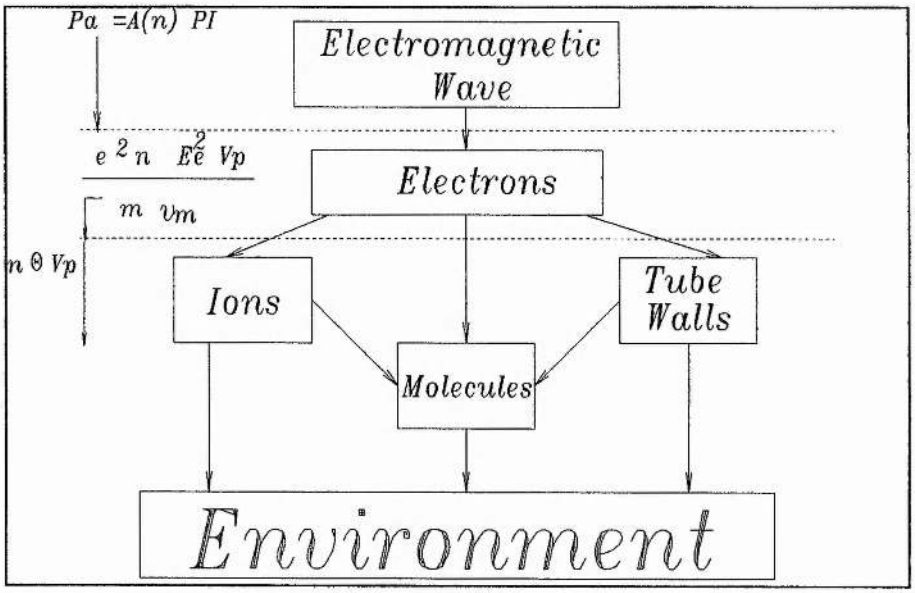

Figure 8. The simplified power flow diagram.

The power absorption coefficient

The power transfer from the HF field to the plasma depends strongly on the kind of the SW launcher used and on the way the plasma is located within it. For a given discharge setup consisting of a plasma, an HF field launcher, and matching circuit the power absorption coefficient A(n) is defined as

$$A(n) = P_A/P_I \qquad \text{eq. 33}$$

where P_A is the total flux of power absorbed by the plasma and P_I is the total flux of power directed inward to a chosen arbitrary surface enclosing the plasma together with the lossless elements of the setup. Under given discharge conditions, A(n) depends only on the average electron density.

Energy balance in a steady-state discharge

For a steady-state discharge, the energy acquired by the electrons from the HF field must equal the energy lost by them due to interactions with heavy particles and tube walls. Thus,

$$A(n) \,.\, P_I = n \,.\, \theta \,.\, V_P \qquad \textit{eq. 34}$$

therefore,

$$n = A(n) \,.\, P_I / \, (\theta \,.\, V_P) \qquad \textit{eq. 35}$$

Hence, the increase in power density absorption will result in an increase in the average electron density value but not in the intensity of the maintenance field. The amount of power transferred to the electrons from the HF field depends on the electrodynamic characteristics of the SW launcher.

The intensity of the electric field within the plasma which sustains the steady-state discharge is called the maintenance field intensity. It does not depend on the electron density. The effective value of the maintenance field intensity (E_e) is determined only by the physical processes occurring within the plasma (charged particle loss mechanism) and not by the amount of the absorbed power or by the launcher characteristics. Thus from the right hand side of equations eq. 31 and eq. 34,

$$(E_e / \nu_m)^2 = (m \,.\, \theta) / (e^2 \,.\, \nu_m) \qquad \textit{eq. 36}$$

The energy balance condition (eq. 34) needs to be stable in order for a steady-state discharge to exist. A stable steady-state discharge can be obtained in a range of electron densities for which the relative changes of A(n) due to density fluctuations are either smaller than the relative changes in density or of opposite sign (Moisan and Zakrzewski 1986; Moisan and Zakrzewski 1991; Zakrzewski 1983).

$$dA(n)/A(n) < dn/n \qquad \textit{eq. 37}$$

The general concept of a traveling wave discharge

For a long cylindrical tube filled with gas, an appropriate launcher will excite an electromagnetic wave that will propagate in the z-direction along the tube. Under the action of the electric field, electrons and ions are created in the gas volume. Also, under the action of diffusion, electrons and ions will reach the walls of the tube and recombine. Electromagnetic wave power will decrease as it propagates along the tube z-axis producing and sustaining the plasma. Dimensionally the length of the active zone of the discharge along the z-axis is much larger than its diameter. Although, the effective collision frequency ν_m for momentum transfer is constant in the plasma volume, the electron density may vary axially. The axial density gradient is small with respect to the radial averaged transverse gradient.

If dA(n) is the fraction of the wave power absorbed in the plasma as the wave travels over a distance dz located between z and z + dz planes. The amount of power absorbed in this slab is dP_A, given by:

$$dP_A = dA(n) \,.\, P(z) \qquad \textit{eq. 38}$$

P(z) is the total flux of the wave power in the z-plane.

The radial inhomogeneity of the plasma has a negligible influence on the propagation of the wave. The phase coefficient $\beta(n)$ ($= 2\,\pi/\,\lambda$, λ = wave length in free space) and the attenuation coefficient $\alpha(n)$ of the wave at each z plane depends only on the local value of the cross-section average electron density, n(z), provided that $dn(z)/n(z) << \beta(n).dz$.

The attenuation coefficient $\alpha(n)$ links the amount of power lost in the plasma upon propagating a distance dz with the total power flux P(z) (Moisan and Zakrzewski 1986). Therefore,

$$dA(n) = 2\ \alpha(n)\ .\ dz \qquad \textit{eq. 39}$$

The attenuation coefficient $\alpha(n)$, of the wave sustaining the plasma, and the electron energy loss 'θ' are the key elements of the discharge. The wave power absorbed at position z along the plasma column is proportional to the electron density at this axial position thus having a local balance of power (Moisan and Zakrzewski 1991),

$$dP_A = 2\ \alpha(n)\ .\ P(z)\ .\ dz \qquad \textit{eq. 40}$$

$$2\ \alpha(n)\ .\ P(z)\ .\ dz = \theta\ .\ n\ .\ S \qquad \textit{eq. 41}$$

where, $S = a^2\ .\ \pi$

Figure 9 shows the flow of power within an elementary axial slab.

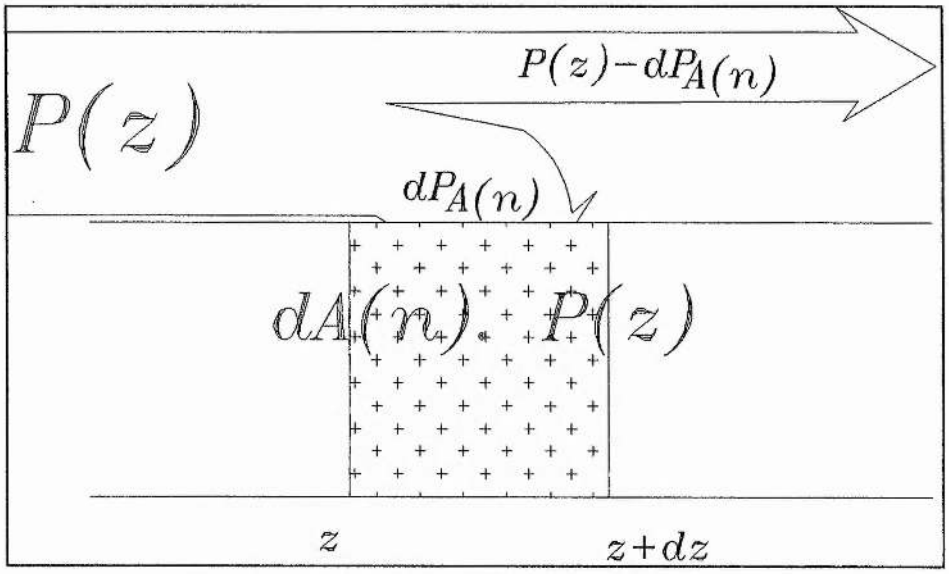

Figure 9. The flow of power within an elementary axial slab of a plasma for a traveling-wave discharge.

The minimum wave power needed to sustain the plasma must exceed the threshold:

$$min\ (P0) = limz \rightarrow l P(z) \qquad \text{eq. 42}$$

l is the axial position where the minimum electron density, n_D, can be found. This power can be estimated using equations eq. 41 and eq. 42:

$$min\ (P_0) = \theta\ .\ n_D\ .\ S/(2\ \alpha(n_D)) \qquad \text{eq. 43}$$

If the plasma is contained in the cylindrical glass tube of the surfatron, the surface wave will travel along the tube obeying the following condition for wave propagation

$$\omega_p^{\,2} \geq \omega^2 (1+ \varepsilon_g) \qquad \textit{eq. 44}$$

where ω_p is the electron plasma frequency

$$\omega_p = (n e^2/(m.\varepsilon_0))^{1/2} \qquad \textit{eq. 45}$$

ω is the angular excitation frequency, $\omega = 2\pi.f$, and ε_g is the relative dielectric constant of the walls of the tube containing the plasma. From eq. 44 and eq. 45 the plasma column ends at the axial position when the electron density drops below the cut-off density, n_c (Beneking and Anderer 1992).

$$n_c = (\varepsilon_0. m . \omega^2 /e^2)(1+\varepsilon_g) \qquad \textit{eq. 46}$$

$$n_D = n_C$$

$$min (P_0) = \theta . n_c . S /(2 \alpha(n_c)) \qquad \textit{eq. 47}$$

Dispersion and attenuation characteristics of the surface wave

The various possible modes of propagation for a surface wave along a cylindrical medium are characterized by the azimuthal wave number m which is an integer number. It enters the field amplitude factor as exp (jmϕ) where j is $\sqrt{(-1)}$ and ϕ is the azimuthal angle. The dispersion and attenuation properties of SW is highly affected by the mode of the SW plasma (Margot-Chaker et al. 1989). The measured surface wave field

of the SW. The measured surface wave field intensity as a function of azimuthal angle ϕ is shown for m = 0 and m = 1 in Figure 10 (Moisan et al. 1982).

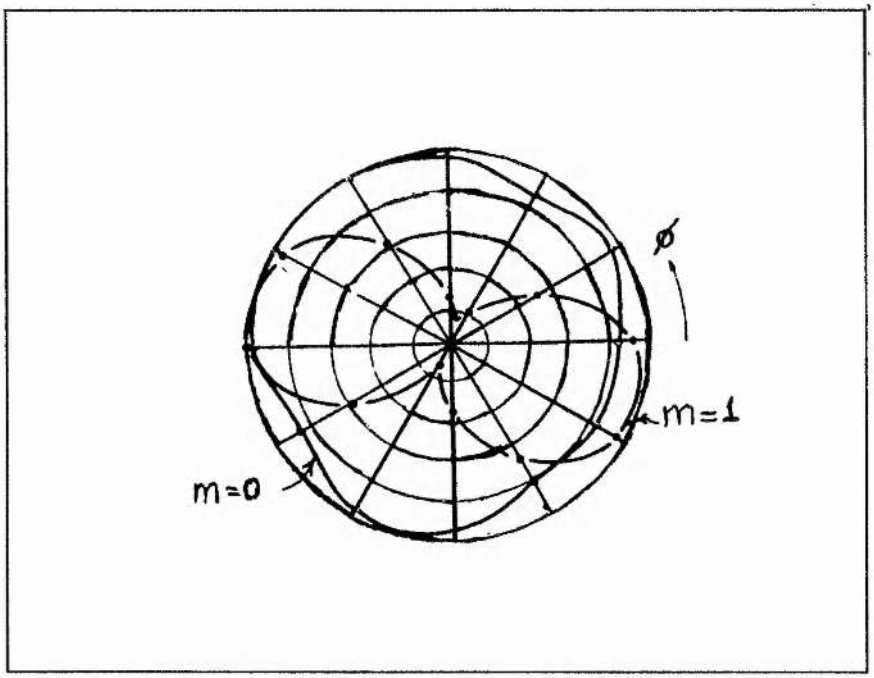

Figure 10. The measured surface wave field intensity as a function of azimuthal angle ϕ for m = 0 and m = 1.

The m =0 mode is more dispersive than the m =1 mode, and has a larger attenuation coefficient. The attenuation coefficient for SW of m =1 mode increases with frequency. Also, for SW discharge in a tube with a large diameter the attenuation coefficient for the m =1 mode approaches the same value as that of the m =0 mode. Moreover, the wave power is almost totally used up as the wave attains the end of the plasma column, for a plasma sustained by m =0 mode or for a large diameter m =1 mode plasma (Margot-Chaker et al. 1989). There is no direct influence of the intrinsic properties of the launcher on the appearance conditions of the m =1 mode plasma. The selection of the m =1 mode can be achieved by applying the scaling law $(f\,a)_{min} \cong$ constant (= 2 Ghz cm),

Controlling of the Surfatron

The functions of the surfatron

The fundamental functions of any SW launcher (including surfatrons) are field launching and impedance matching. The first function provides the appropriate electromagnetic field distribution in the wave excitation region in order to launch a SW in a given mode. The second function is to optimize the power transfer to the plasma. Ideal SW launchers should accept all the power coming from the feed line and fully convert it into SW power flux. It transfers the power coming from a given mode in a wave guide to a given mode in another wave guide.

Launching a surface wave

The initial breakdown of the plasma column starts when the intensity of the HF field at the launching gap is large enough or when it is triggered by the auxiliary source. The field gradient within the gap will drive electrons along the tube axis. When the electron density, n, in the launching area exceeds the minimum possible electron density, n_D, the SW will propagate until, at the axial position where $n = n_D$, it is reflected back. At this reflection position a large axial gradient of electric field is formed. This will cause electrons to be ejected forward forming an ionization front which will produce an additional segment of plasma column thereby allowing the HF wave to propagate further and hence extending the ionization front until a full discharge is taken place. The total length of the discharge depends on the amount of power delivered by the launcher. The larger the power the larger the plasma column. The plasma column produced always exhibits the same general features. Equation, eq. 44, holds near the gap:

$$(\omega_{pe} / \omega) \geq (1 + \varepsilon_g)^{1/2}$$

where ω_{pe} is the plasma angular frequency, ω. The ratio (ω_{pe} / ω) decreases gradually along the axis and away from the launcher until

$$(\omega_{pe} / \omega) \cong (1 + \varepsilon_g)^{1/2} \qquad \textit{eq. 48}$$

This is where the plasma column ends abruptly and the wave ceases to propagate due to the reduction in the cross-section electron density, which will reduce ω_{pe}.

The value of the axial gradient of electron density along the plasma column, for a given tube diameter and a given pressure, increases with wave frequency. Also, for a given wave frequency and plasma diameter, the axial gradient of the electron density increases with the gas pressure (Moisan and Zakrzewski 1986). Furthermore, for a given wave frequency and gas pressure, the electron density gradient increases as the plasma diameter decreases (Rahman and Solntzev 1995a). Finally, increasing the UHF power will increase the length of the plasma column (Moisan et al. 1979).

Efficiency of power transfer

Efficient transfer of HF power to the plasma is essential to increase the plasma volume and plasma density whereas transferring this energy to other parts, results in a loss of energy with possible damage to components. The three possible loss mechanisms are reflection, losses in the dielectric and metallic components of the plasma source, and radiation from non guided waves into the surrounding space. The power flow diagram is shown in Figure 11.

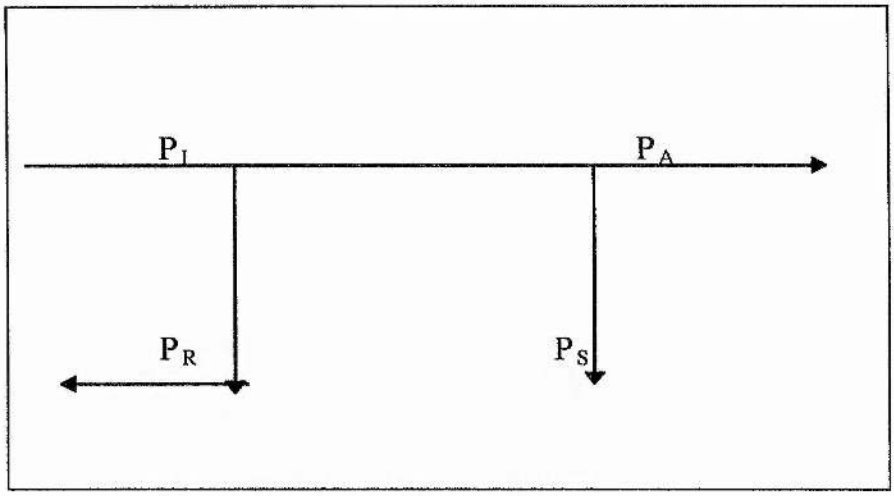

Figure 11. Power flow diagram: P_I, P_R, P_A, and P_S are the incident, reflected, absorbed and radiated powers respectively.

The overall efficiency of power transfer is determined by the coupling and launching efficiencies. The coupling efficiency is

$$\eta_C = (P_I - P_R)/P_I \qquad \textit{eq. 49}$$

while the launching efficiency is

$$\eta_L = P_A/(P_A + P_S) = P_A/(P_I - P_R) \qquad \textit{eq. 50}$$

The overall efficiency is

$$\eta = \eta_C \eta_L = P_A / P_I = (P_I - P_R - P_S)/P_I$$

eq. 51

$$\eta = (P_I - P_R) / P_I$$

eq. 52

These power values can be measured directly using a standard reflectometer technique on the power feeding line (Moisan and Zakrzewski 1991).

Impedance matching in a surfatron plasma source

In order to find the HF characteristics of the plasma source, circuit analysis is used. The equivalent circuit representation of the plasma source directly relates its components to the electromagnetic energy dissipation or storage processes. Optimizing the power transfer can be achieved by minimizing the reflected power at the launcher. This can be accomplished by a network that consists either of intrinsic tuning by means incorporated into the launcher, or of physically separated tuning elements.

Impedance matching for minimum reflection

The reflection coefficient, Γ_L, is the quantity that characterizes the impedance mismatch of the transmission line and the wave reflection level. It is given by:

$$\Gamma_L = (Z_L - Z_0)/ (Z_L + Z_0)$$

eq. 53

$$|\Gamma_L|^2 = P_R/P_I$$

eq. 54

where, Z_L and Z_0 represents the plasma source and feed line impedances respectively.

Considering no radiation to the space and no losses within the surfatron launcher, the overall efficiency is:

$$\eta \cong 1 - |\Gamma_L|^2 \qquad \textit{eq. 55}$$

Impedance matching can be achieved by the termination of the feed line with an impedance equal to its impedance Z_0. The perfect matching conditions are

$$R_L = Z_0 \quad \textit{and} \quad X_L = 0$$

where, R_L and X_L represent the resistance and reactance parts of the plasma source load impedance, Z_L.

Gap impedance

The wave launching aperture of the surfatron is shown in Figure 12. Here the inner coaxial tube (metallic sleeve) of the surfatron surrounds the discharge tube. The thin metallic plate is positioned at a few millimeter from the metallic sleeve and is located perpendicularly to the metallic tube axis.

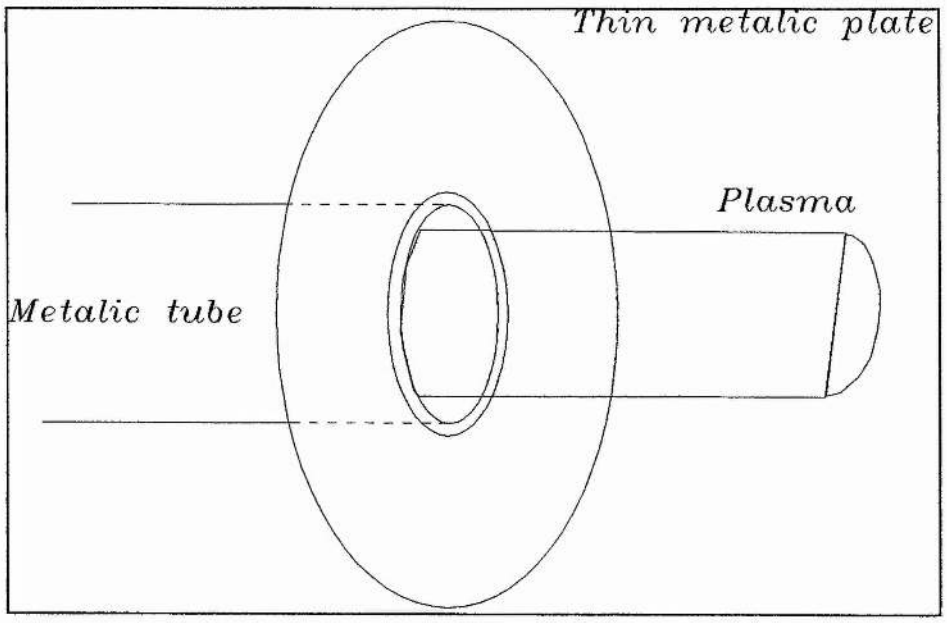

Figure 12. Wave launching aperture.

The surfatron establishes a large electric field in the gap region. This field excites the waves and launches it into the discharge tube in two opposite directions (see Figure 13-a). The waves will carry with it most of the energy that leaves the gap. This power will be used up gradually along the discharge tube to sustain the discharge. In addition reactive energy is stored in the electromagnetic field at and near the gap. Also, a small amount of power is dissipated in the plasma near the gap. The corresponding equivalent circuit (see Figure 13-b) consists of power dissipation elements and energy storage elements.

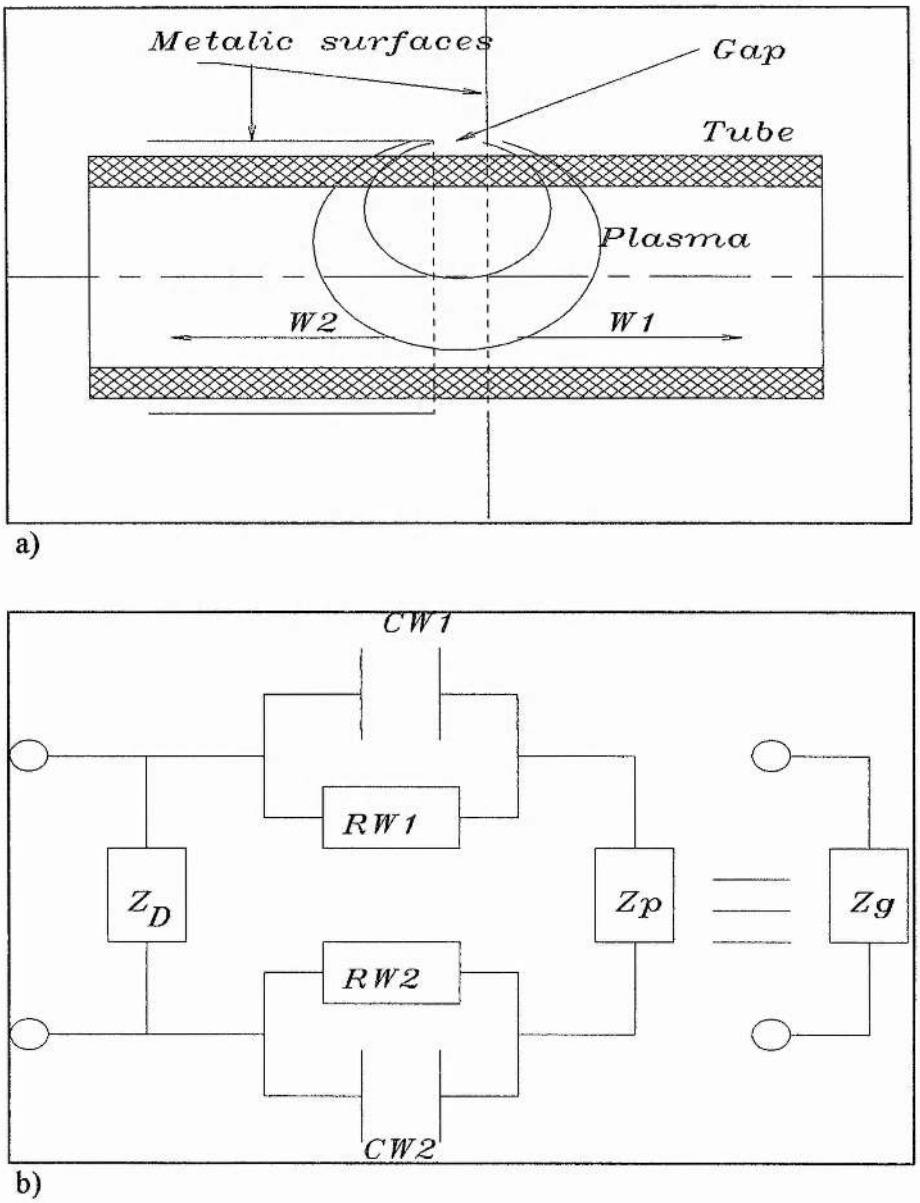

Figure 13. a) Wave launching in the gap region, and b) its corresponding equivalent circuit.

The power carried away by the waves are represented by the characteristic impedance of the plasma column as seen by wave1 and wave2 and are represented by RW1 and RW2. The energy storage associated with wave launching is represented by the capacities CW1 and CW2 for the two waves. The energy storage and dissipation in the gap region are represented by Zp and Z_D. The former impedance is for the plasma and the latter is for the region outside the plasma. The resulting impedance of the gap is Zg and is defined

with respect to a reference plane chosen in the launcher structure. The power losses in the discharge tube walls and within the plasma in the gap region are very small when compared to the wave power flux. Zp and Z_D are considered imaginary, and when the conditions of wave launching in both directions of the gap are the same, simplifications can be made so that RW1 ≅ RW2 = RW and CW1 ≅ CW2 = CW (Moisan and Zakrzewski 1991).

The gap impedance, represented by Zg is given as follows:

$$1/Z_g = Y_g = G_g + j\,B_g \qquad \textit{eq. 56}$$

$$Y_g = \{1/R(1 + (X/R)^2)\} - j\,\{(1/X_D) + (X/R)/(1 + (X/R)^2\} \qquad \textit{eq. 57}$$

where,

$$R = 2\,RW/(1 + \omega^2 + \tau_w^2) \qquad \textit{eq. 58}$$

$$X = Xp - (2\,.\,RW.\,\omega\,.\,\tau_w)\,/\,(1 + \omega^2 + \tau_w^2) \qquad \textit{eq. 59}$$

$$\tau_w = RW\,.\,CW \qquad \textit{eq. 60}$$

ω = wave angular frequency = $2\ \pi\ f$

Plasma source impedance

The equivalent circuit of the surfatron is shown in Figure 14.

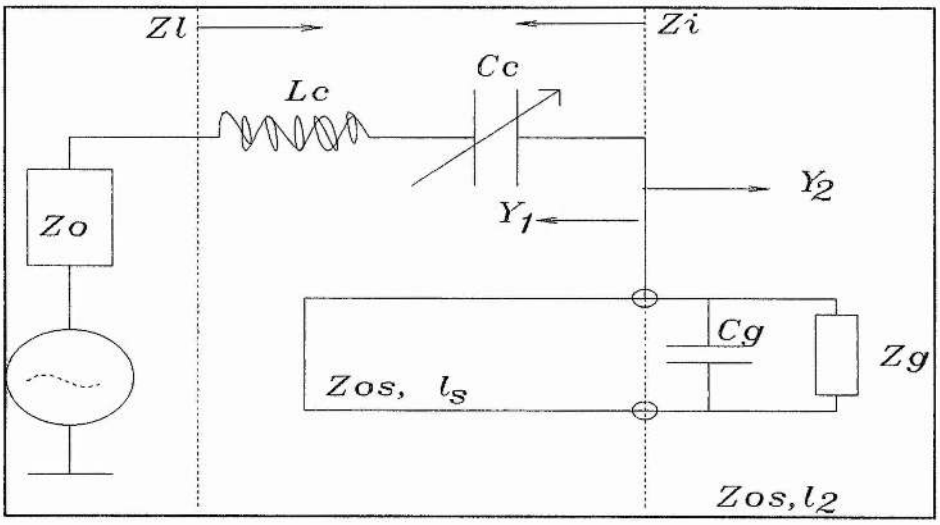

Figure 14. The equivalent circuit for the surfatron.

The input impedance of the surfatron normalized with respect to Z_0 is

$$Z_I/Z_0 \equiv R_I/Z_0 + j\,X_I/Z_0 = \\ = (g_2/(g_2^2 + (b_2-b_1)^2)) + \\ j\{(\omega L_C/Z_0) - (1/(\omega C_0 Z_0)) - ((b_2-b_1)/(g_2^2 + (b_2-b_1)^2)\} \qquad \text{eq. 61}$$

where,

$$b_1 = Z_0 (Z_{0S} \tan (2 \pi l_S/\lambda_0))^{-1} \qquad \textit{eq. 62}$$

$$g_2 = g_g = Z_0 G_g \qquad \textit{eq. 63}$$

$$b_2 = Z_0 (\omega C_b + B_g) \qquad \textit{eq. 64}$$

The impedance matching conditions are $R_L = Z_0$ and $X_L = 0$ therefore,

$$(g_2 - g_2^2) = (b_2 - b_1)^2 \qquad \textit{eq. 65}$$

and

$$\omega (L_C/Z_0) - (1/\omega C_C Z_0) - ((b_2 - b_1)/(g_2^2 + (b_2 - b_1)^2)) = 0 \qquad \textit{eq. 66}$$

Considerations for the design and operation

The performance and flexibility of operation of a given surfatron is governed by the intrinsic properties that can be adjusted. These properties are l_1, l_2, the gap width and the coupler insertion depth Figure 7. The operating frequency (middle frequency) of the surfatron varies with l_1. And it is possible to adjust l_1 to get zero reflected power for a given middle frequency, except at higher frequencies where both m = 0 and m = 1 modes are present. Changing the gap width would vary the middle frequency by a few percent. Changing l_2 would change the bandwidth, which is the band between the lowest and highest frequencies at which the rate of reflected power to incident power (P_r/P_{in}) is lower than a specific value. Finally, changing the insertion depth of the coupler would tune the surfatron for the minimum reflection of incident power.

The total length of the surfatron is the main construction factor that determines the matching operating frequency. The normalized total length to the free space wavelength λ_m of its corresponding operating frequency is approximately a constant (Moisan et al. 1979) lying within the limits:

$$0.1 < (l_1+l_2)/\lambda_m < .2 \qquad \textit{eq. 67}$$

This ratio is affected slightly by increasing the ratio of external to internal diameter of the UHF structure in which case the required total length (l_1+l_2) of the surfatron should be correspondingly reduced.

Chapter 4

Design

Chapter 4

Design

Introduction

In this chapter the actual design of the tritium on-line monitor is developed and described in detail. Decisions made in the course of the development are discussed and justified.

Each component of the monitor has a specific task and was designed, constructed and tested individually to optimize its performance in operation. Then the components were assembled together and tested in stages before the final assembly and test of the complete monitor. For the final test of function and sensitivity of the monitor it was planned to use a standard source of tritium gas of known activity.

Figure 15 shows the block diagram of the different parts of the monitor. Plate 1 and Plate 2 show the different components from different sides. The monitor main components are

1) The plasma source (surfatron),

2) The plasma source ion implantation system, and

3) The scintillation counting assembly.

The developed monitor is intended to function as follows: an air sample to be monitored for tritium is extracted from the environment into an ion source where it is ionized. The PSII system, on application of the negative high voltage pulses, extracts, accelerates and implants the ions into a thin plastic scintillator target, where any implanted tritium

accumulates and results in a build-up of tritium β^- activity. The scintillations produced by the β^- activity are detected by the photomultiplier tube (PMT) which forms an integral part of a conventional scintillation counting assembly. The entire system is operated under vacuum.

The plasma source 'Surfatron'

The surfatron (Figure 16) was designed, with flexibility of operation in mind, to produce a relatively large plasma. This was achieved by constructing the device to operate at different frequencies and with a variable input impedance. The design allowed for (1) the length of the coaxial structure to be varied by means of a moveable plunger, (2) changing the radial and axial position of the coupler and (3) variation of the gap width between the front thin plate and the inner tube of the UHF coaxial structure.

The UHF coaxial structure along with the front plate and plunger are made out of stainless steel. The dimensions are shown in Figure 16. In order to ensure good electrical connections required throughout the surfatron structure, copper EMI shielding foil was used and was placed at the junctions where connections tended to be poor. The technical specifications of this EMI foil is shown in Appendix II. The same material was used to prevent leakage of the UHF signal (power) out from the openings in the surfatron structure. A quartz tube Figure 16 with 2.6 cm inner diameter and 12 cm long was designed in a T shape to enclose the produced plasma and to efficiently utilize the launched surface waves. The quartz tube is fixed into the plasma ion implantation source vacuum chamber from one end and is connected to a leak valve at the other. The air samples are drawn into the monitor through this leak valve. The quartz tube is placed inside the coaxial UHF structures as shown in Figure 16 in a manner which forces

the launched energy-carrying waves to be unidirectional, resulting in maximizing the power available for ionizing the air sample.

A magnetron that produces a 2.45 GHz signal was chosen to supply the necessary RF signal to operate the surfatron which was constructed to operate at this frequency. According to the construction rule presented in chapter 3 eq. 67 the value of l_1 of the UHF structure should be 2.45 cm which is within the limit of the designed surfatron.

However, at 2.45 GHz frequency, and with a 2.6 cm diameter quartz tube, it is expected to have both m = 0 and m = 1 mode surface waves propagating in the plasma column. Therefore, the condition for zero power reflection could not be guaranteed and hence, allowance had to be made for tolerance of a certain percentage of reflected power to be made.

The coupler (see Figure 17) was made out of a semi-rigid coaxial cable RG-204, that is terminated by a 1 cm^2 copper plate. The characteristics of the semi-rigid coaxial RG-402 cable are shown in appendix II. The coupler was placed as shown in Figure 16 and

Figure 17. Only teflon tape separates the square copper plate from the surface of the inner tube of the UHF structure. The thin layer of teflon tape was wrapped around the relevant part of the inner tube so as to prevent a short circuit. The coupler in turn is connected to a semi-rigid coaxial cable (RG-402) which feeds in the microwave signal produced by the magnetron of a microwave oven. The maximum power of this magnetron is 990 watt. The capacitive coupling method was used to extract the microwave signal from the rectangular wave guide of the microwave oven into the coaxial cable (Frenzel 1994). This was achieved by inserting a probe of a quarter wavelength vertically inside the wave guide of the microwave oven at one-quarter wavelength from the end of the waveguide as shown in Figure 17.

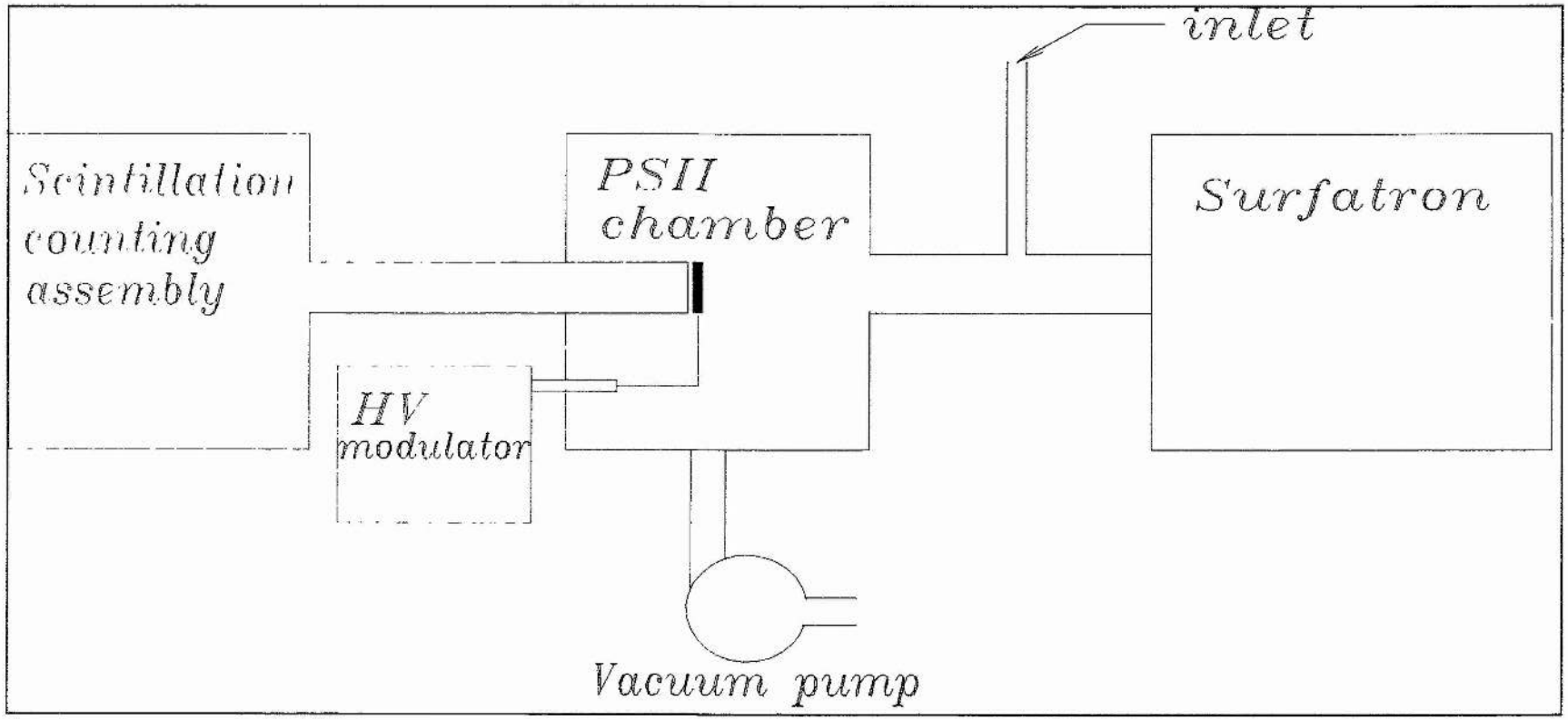

Figure 15. The block diagram of the developed monitor.

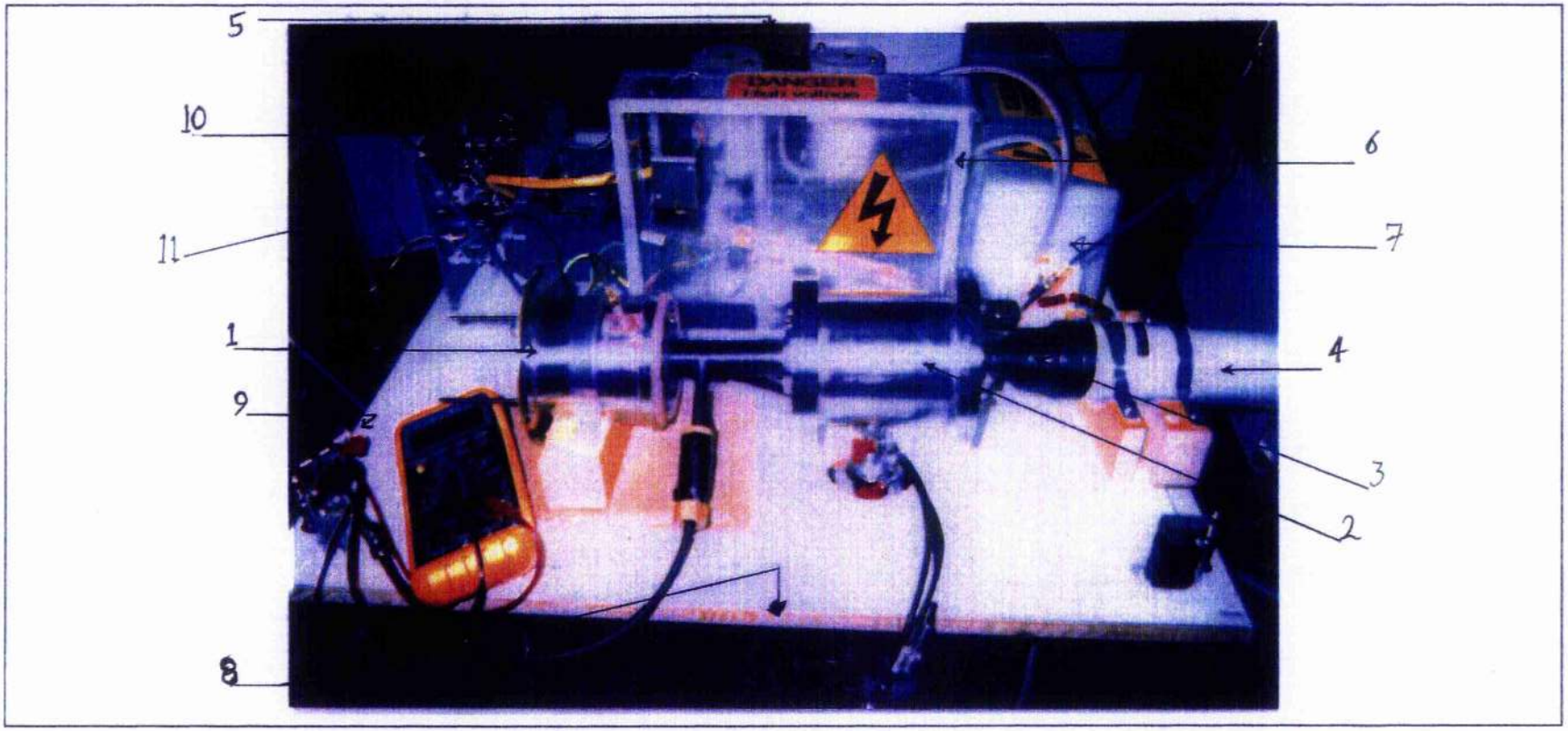

Plate 1: The different components of the developed monitor. 1) the surfatron, 2) the PSII chamber, 3) the light guide, 4) the PMT, 5) the HV transistor switch, 6) the dump relay, 7) HV capacitor, 8) Vacuum pump, 9) the air sample inlet, 10) the microwave and 11) RG-204 cable.

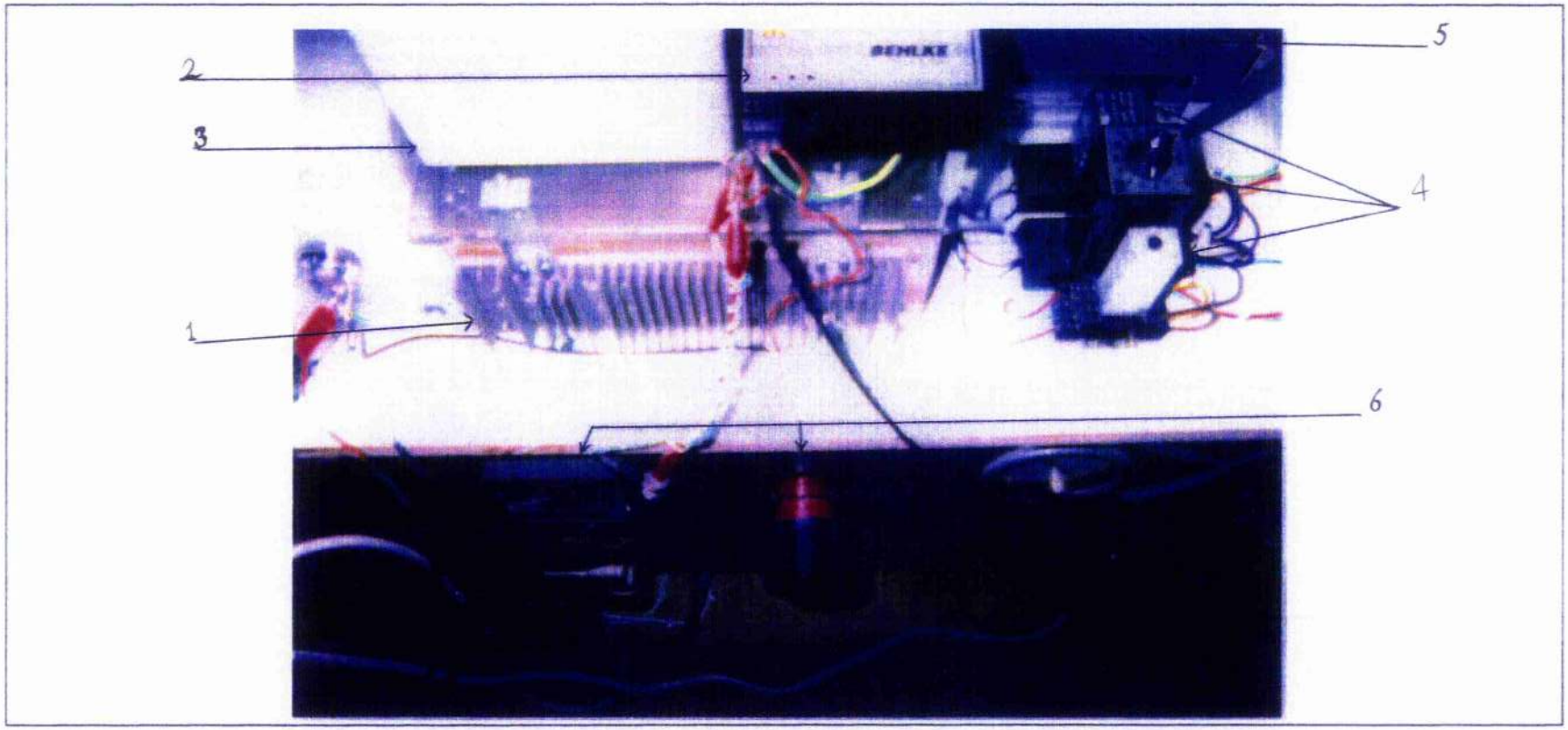

Plate 2: The different components of the developed monitor. 1) The power supply, 2) the control side of the HV transistor switch, 3) the HV capacitor, 4) the delay switches, 5) the signal generator and 6) the vacuum pump control.

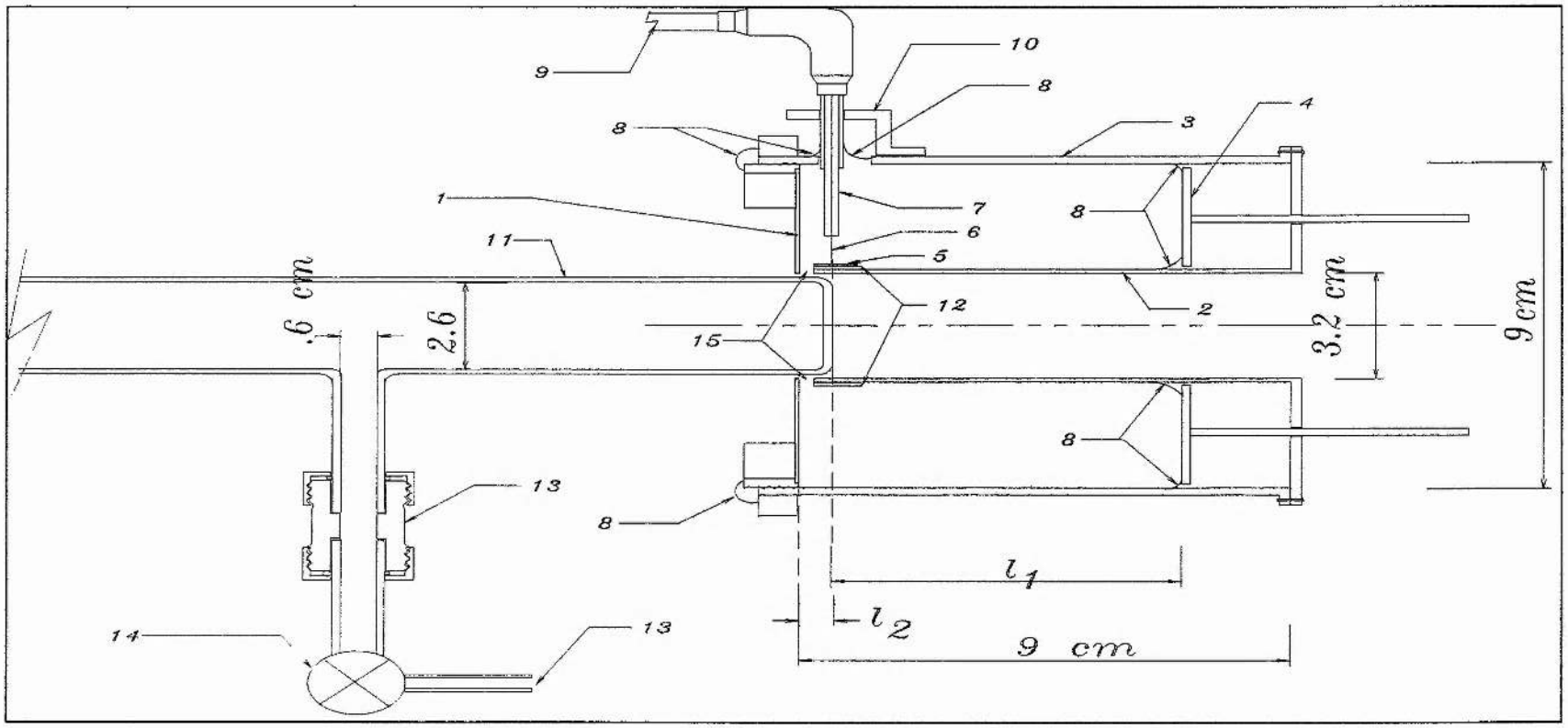

Figure 16. The designed surfatron: 1) Front plate, 2) inner tube, 3) outer tube, 4) the plunger, 5) the coupler copper plate, 6) the bare center of the coaxial cable, 7) the coupler, 8) EMI foil, 9) microwave feed cable 10) coupler holder, 11) the quartz tube, 12) Teflon insulator, 13) Air sample inlet, 14) the leak valve, and 15) gap distance (l_2).

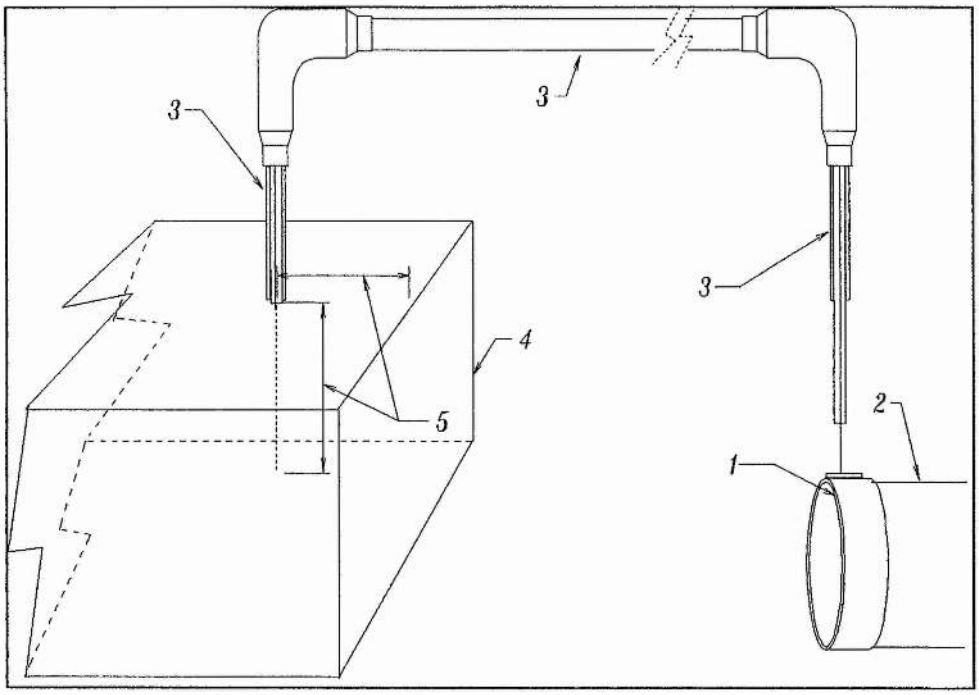

Figure 17. The coaxial feed through coupler connection from the microwave source to the surfatron: 1) Teflon tape, 2) Inner tube of the UHF structure, 3) RG-204 cable, 4) Waveguide, and 5) The length is $\lambda / 4$.

Since it is expected that some power will be reflected from the surfatron back to the magnetron, where it could heat up the connecting cable to a point where the cable junction may blow up, it is essential to reduce the amount of the reflected power. Two ways can be adopted. The first way is by minimizing the microwave power, transmitted through the cable into the surfatron, to a level that is capable of sustaining the desired plasma. This was done by introducing a load inside the microwave oven. The second possibility is to operate the microwave oven for 9-10 seconds then automatically switch it off for 30 seconds before it is re-started. The surfatron was able to produce plasma successfully using both methods concurrently. In order to optimize the operation of the surfatron the size of the plasma was checked for different settings of the plunger distance (l_1) in Figure 16, the gap width, and the coupler position. The optimum values for the

production of the longest plasma was achieved with $l_1 \approx 4.2$ cm, $.2 \leq$ gap width $\leq .4$ cm and with the square plate of the coupler resting on the Teflon which is wrapped around the inner tube of the surfatron. The designed surfatron was able to produce plasma over a wide pressure range starting from 4 Torr down to 0.1 mTorr. The production of the low pressure (0.1 mTorr) plasma was achieved by introducing a ring magnet that was placed around the quartz tube resting on the front plate of the surfatron. Surprisingly the plasma obtained happened to be very position sensitive. Therefore, care must be taken when the plasma is formed that the surfatron is not subjected to any movement. Otherwise, the alignment of the quartz tube inside the surfatron inner tube might change causing a change in the plasma volume.

Plasma Source Ion Implantation system

In order to achieve optimum operation for efficient and maximum ion implantation into the plastic scintillator target, the pressure dependence of the plasma frequency, ion density, final sheath position and the total number of ions available for collection were calculated. Equation 25, in chapter 3, that contains allowance for sheath evolution over the insulator for the full range for collisionless to collisional plasma was used. The calculation were made by 'Mathcad 'software utilizing a personal computer. The written program and the detailed calculation are shown in Appendix III. Two possible cases were considered. Case-I is for plasma source ion implantation into a plastic scintillator target on top of which the cathode was placed. The cathode is a thin, 0.15 μm thick, aluminum microfoil. Case-II is for the PSII into a plastic scintillator target that is placed on top of the cathode. The target position in the two cases is shown in Figure 18.

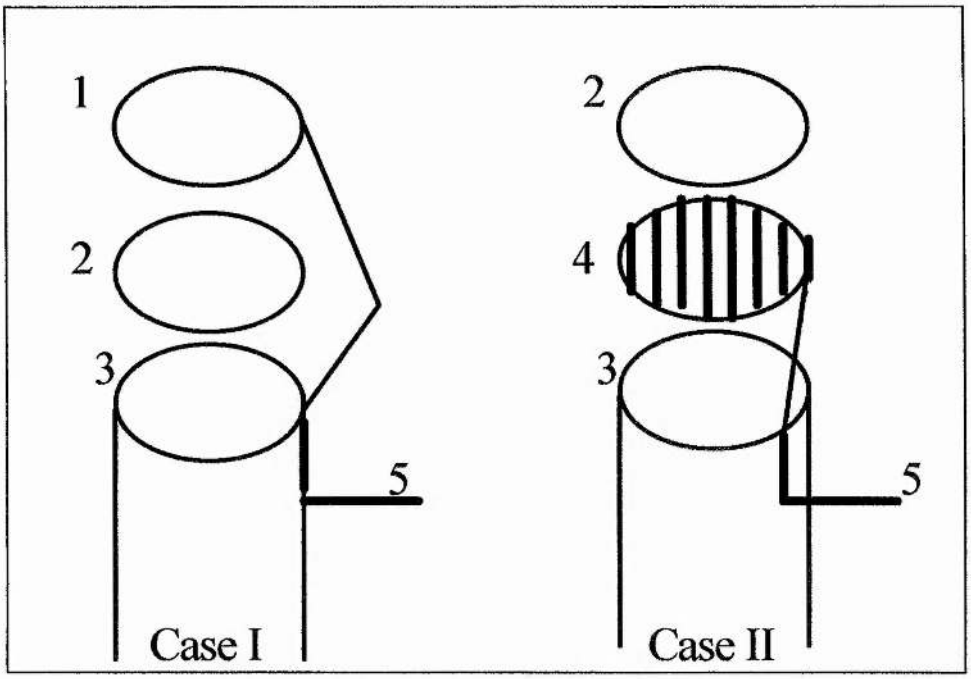

Figure 18. Target and cathode assembly. 1) Al-microfoil cathode, 2) plastic scintillator target, 3) the light guide, 4) striped cathode, and 5) high voltage contacts.

The calculations were made in the following sequence. First, calculations of the number densities at different working pressures were made and then the plasma frequencies at those pressures were calculated. Also, the sheath extent at the commencing of the -60 kV pulse was calculated at each pressure. The numerical calculations of the final sheath extent at the end of different pulses of 0.2, 1, and 10 μsec durations and for the different pressures were conducted. These numerical calculations were made for Case-I and Case-II. The total number of ions available within the sheath volume was calculated at the different pressures for a target of a radius of 1.15 cm and for different pulse durations. Finally, the time durations required to implant certain doses of ions into the plastic scintillator of different radiuses were calculated.

As may be expected ion density number increases exponentially with pressure and so does the plasma frequency. This can be seen in Figure 19.

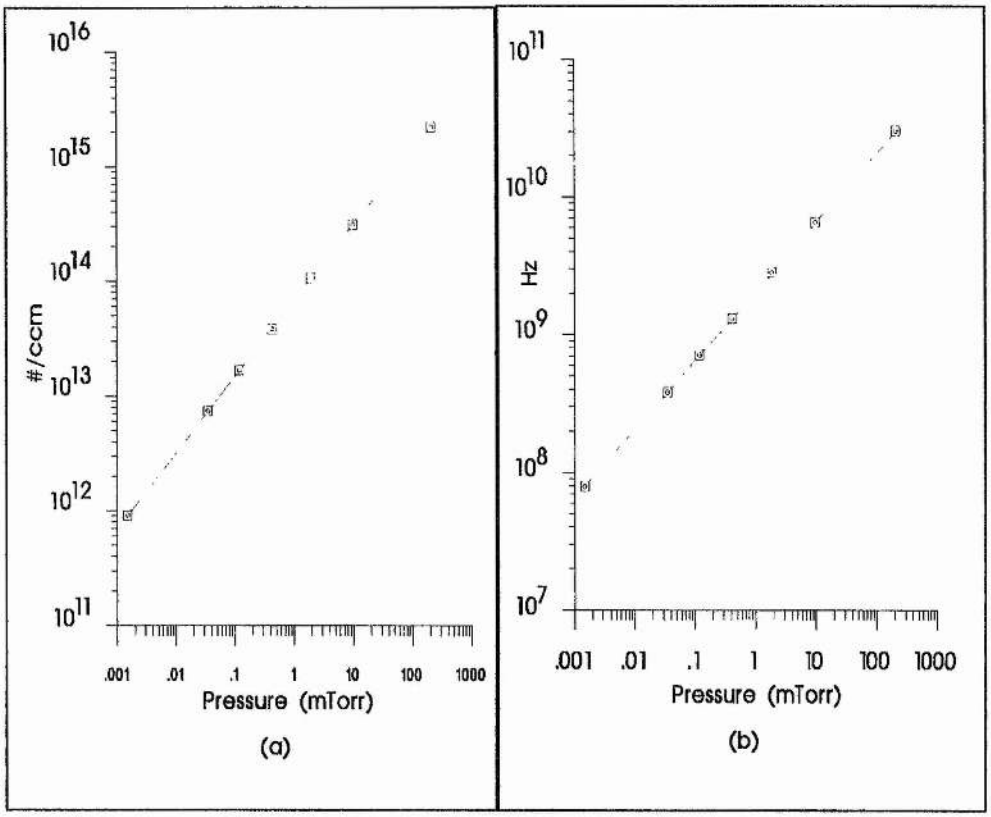

Figure 19. a) The ion density number vs. pressure and b) the ion plasma frequency vs. pressure.

The tritium ion plasma period, ω_{PTi}^{-1}, is compared to that of nitrogen ions, ω_{PNi}^{-1}, and is shown in Figure 20. From the results of the two ion fluid models developed by Thomas et al, lighter ions, in a plasma with mixed light and heavy ions, are responsible for a large portion of the current density reaching the target. This is due to their lower mass and hence more rapid acceleration (Thomas et al. 1994). Consequently for the work in hand, the pulse peak duration at a given pressure should be within the tritium ion plasma period, ω_{Pti}^{-1}, in order to acquire an ion current with the highest percentage of tritium content whilst minimizing the collection of other unwanted heavier ions. In other words, for a pressure $\leq$ .1 mTorr, the pulse duration should be in the range of nanoseconds and should have a rise time of a fraction of this time.

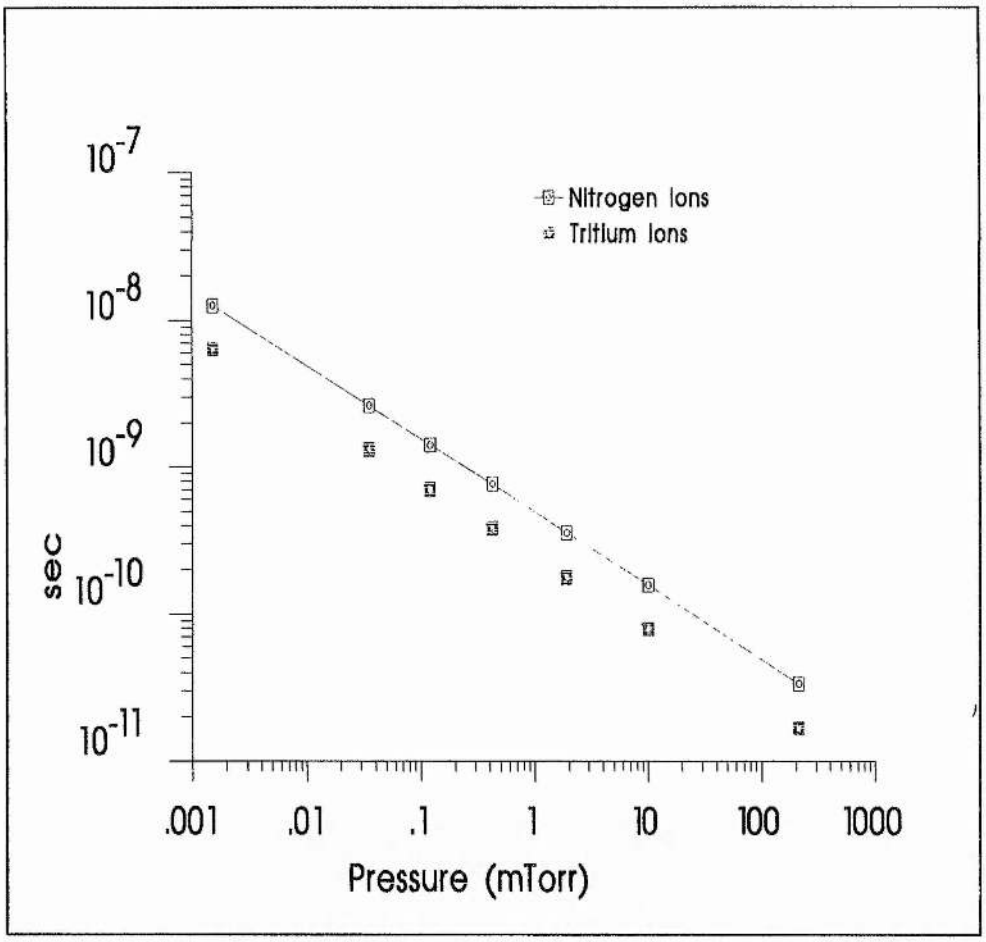

Figure 20. The ion's movement time scale at different working pressures.

The total number of ions collected for such a pulse would be very small but there would be a high percentage of lighter ions. When compared with a μsec pulse the total number of ions collected would be larger but would have a much smaller percentage of the light ions. Therefore, the pulses should be produced with a high frequency in the range of kHz or MHz in order to be able to collect high concentrations. And as far as the author knows, a high voltage pulse modulator with such characteristics is not yet available, and therefore sub μsec pulses were ignored. Figure 21 shows the final sheath thickness for a) Case-I and b) Case-II.

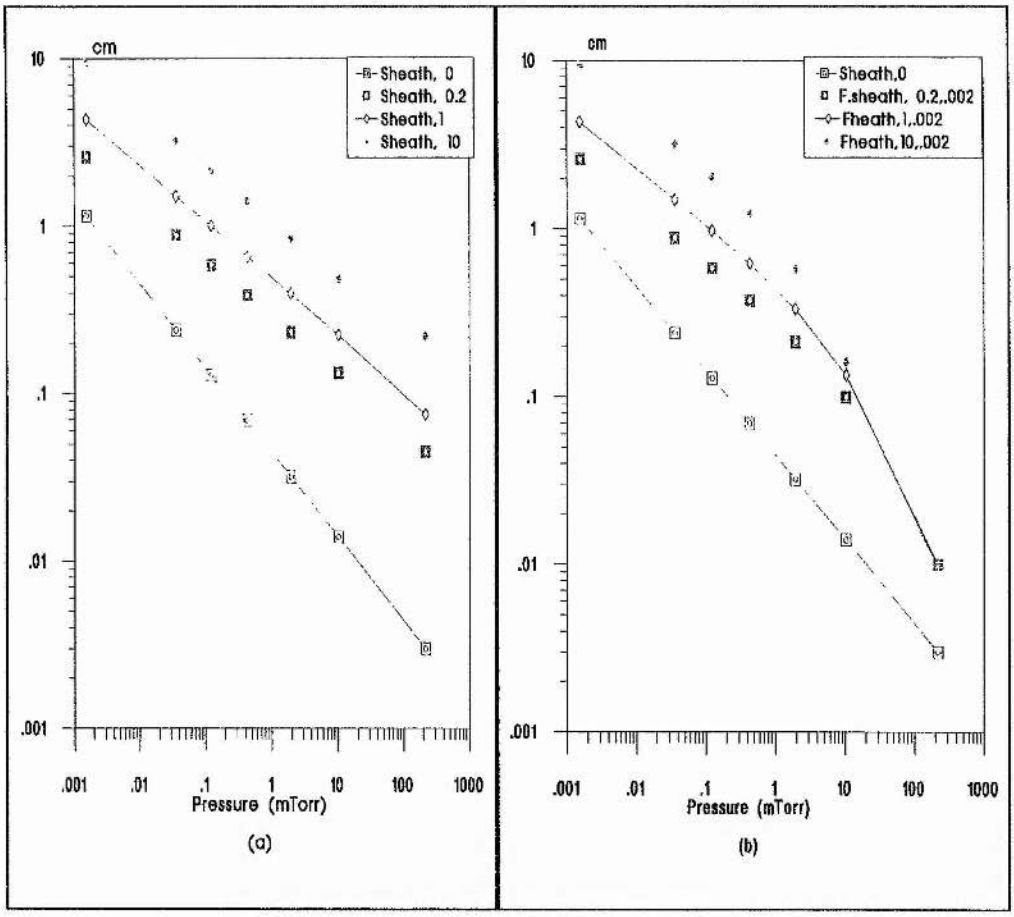

Figure 21. a) The final sheath thickness for Case-I, and b) Case-II. 'Sheath, 0' is the thickness of the sheath at the moment of commencing the high voltage, time = 0 sec. Sheath , 0.2; Sheath , 1 and Sheath, 10 are the final sheath position at the end of pulse durations 0.2, 1, and 10 μsec respectively.

As the pressure increases the final sheath thickness decreases. This is because an enhancement of ion energy loss by collisions with neutrals in the sheath occurs and results in a reduction in ion current to the target. This in turn will cause a drop of sheath expansion velocity, therefore, reducing the sheath thickness.

For Case-II the final sheath thickness decreases further. The reason is explained below. The total number of ions available for collection within the sheath increases exponentially with the increase of pressure and for the two cases discussed (see Figure 22) except at pressures >1 mTorr for Case-II.

The reduction in the sheath thickness for Case-II is a direct result of the reduction of the high voltage at the target due to surface charge accumulation on the plastic scintillator target. This in turn will lower the energy of the incident ions, lower the number of ions available for collection and could cause high sputtering. However, surface charging has a stronger effect on the implantation energy than on implanted dose (Emmert 1994).

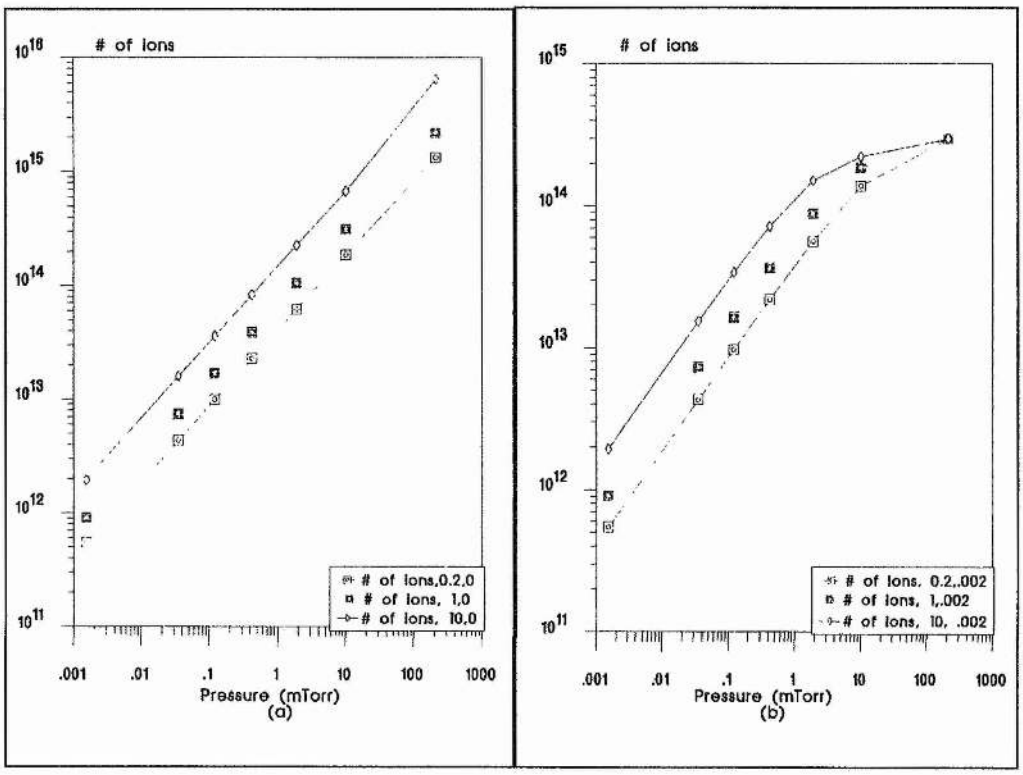

(a) *(b)*

Figure 22. a) The total number of ions available for collection for Case-I, and b) the Case-II. Here, the "# of ions, T_P ,d" is the total number of ions available within a sheath that evolved by a pulse of time T_P (0.2, 1, 10 μsec) where the target is a plastic scintillator of thickness d cm.

From Figure 21 and Figure 22 it is seen that the longer the pulse duration the larger the sheath thickness and consequently the larger the number of ions available for collection. Therefore, a 10 μsec pulse duration was adopted.

Now the appropriate working pressure should be selected to allow for maximum ion collection. Apparently this should be at high pressures. The limit for this high pressure can be estimated by comparing the sheath thickness to the ion mean free path, λ, at a given pressure. Therefore, from Figure 23 it is clear the ratio $\lambda/S > 1$ from low pressure up to pressure P, where $P < 4$ mTorr. As a result the working pressure P_w can be selected to be $0.1 < P_w < 2$ mTorr.

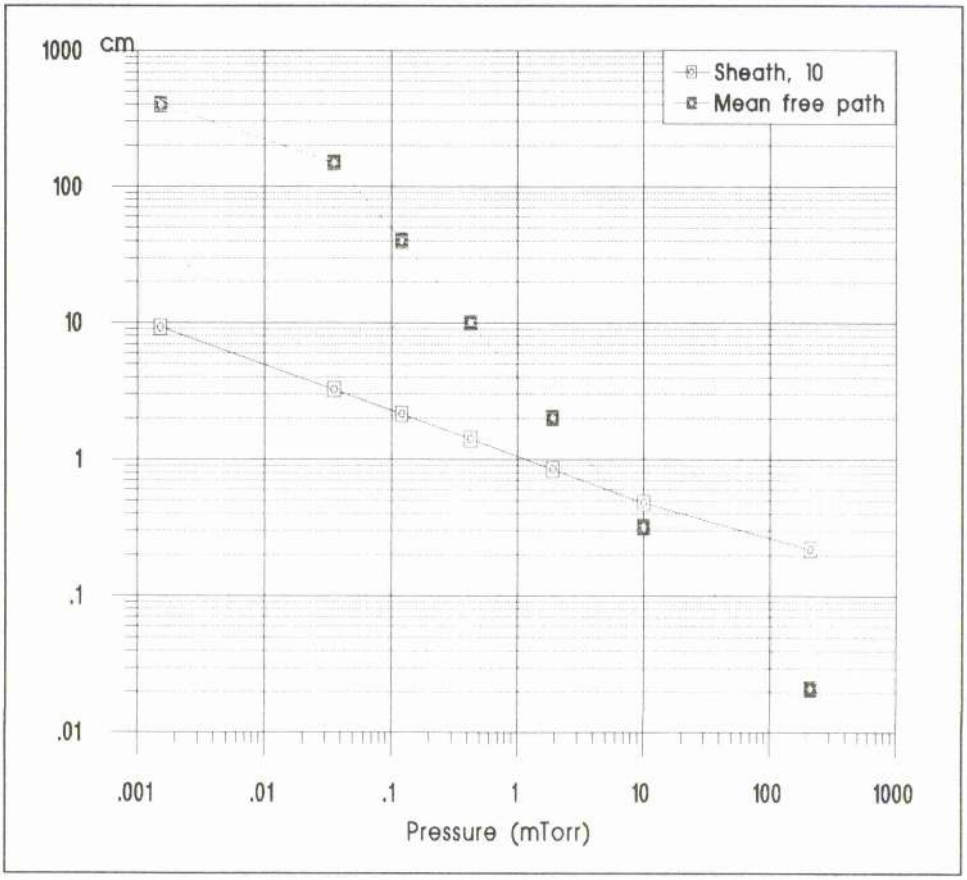

Figure 23. The comparison between the sheath thickness and the mean free paths at the different pressures.

This range of pressure does not show a significant difference in the number of ions available for collection between Case-I and Case-II (see Figure 24). The total number of ions within the sheath is found to be almost the same for the two cases except in the high pressure range.

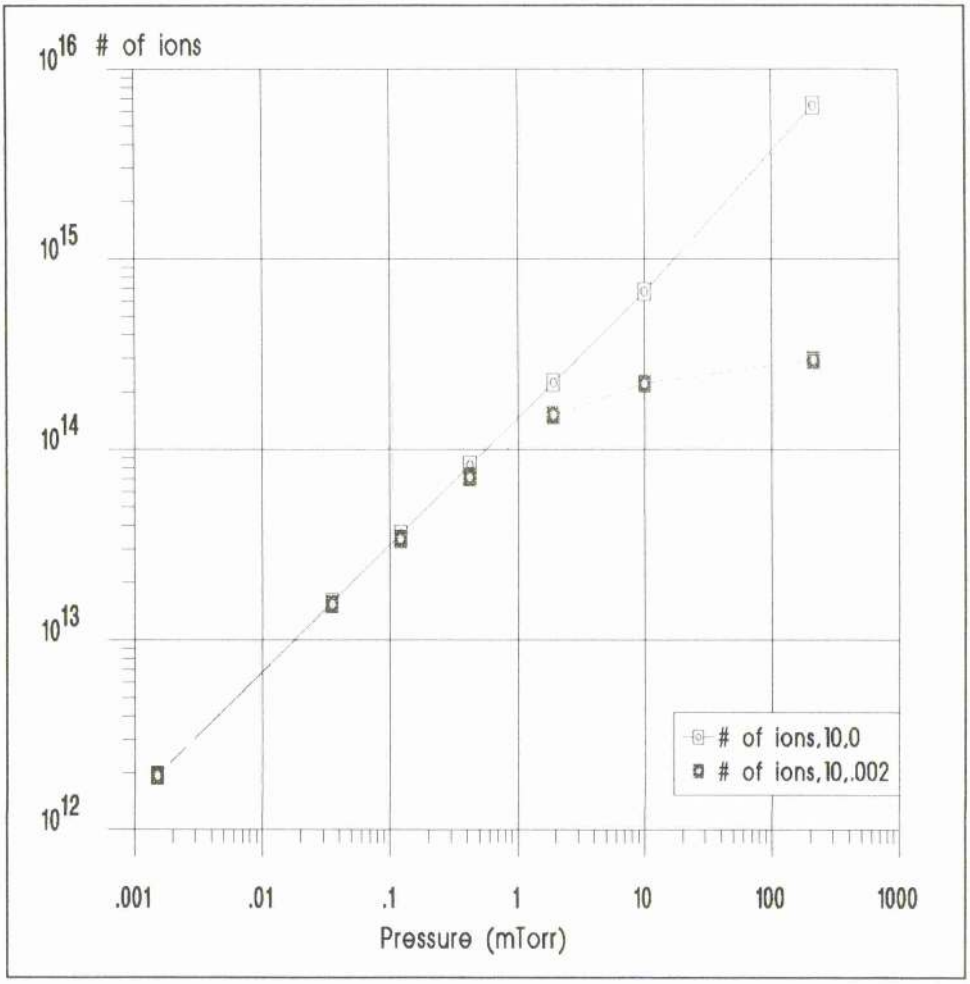

Figure 24. Comparison between Case-I and Case-II on the total number of ion available for collection.

The estimated time to collect 2.5 x 10^{19} ions, that is available per cm^3 of air, was calculated for the different pressures, for the two cases and for a high voltage pulse duration of 10 μsec. The time is shown in Figure 25. It is clear from that it would take between 1 to 10 minutes to collect 2.5 x 10^{19} ions depending on the working pressure (2-0.1 mTorr).

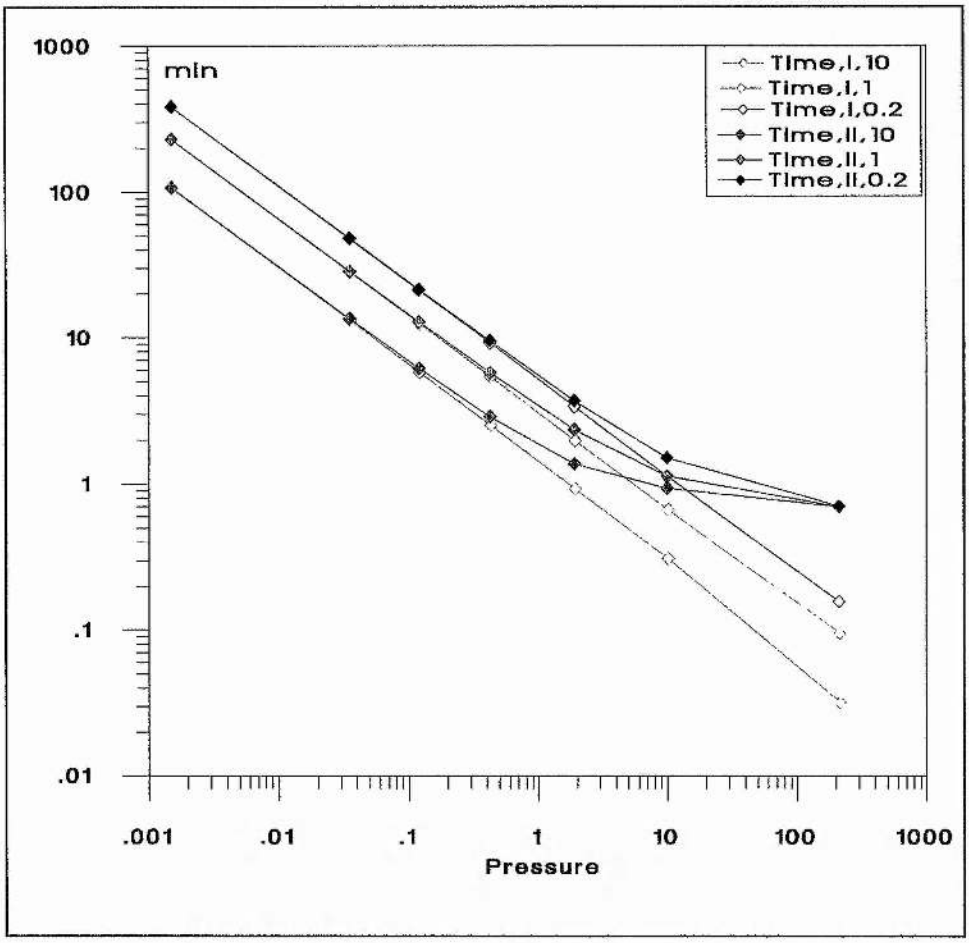

Figure 25. The estimated time to collect 2.5 x 10^{19} ions for cases I and II and for different pulse durations .2, 1, and 10 μsec.

The time required to implant a given tritium concentration into the plastic scentillator can be estimated. In Singh scintillation cell, presented in chapter 2, the total activity in the cell was 0.048 Bq and the total number of atoms is 0.048 (Bq)/1.7671x10^{-9} (sec^{-1})= 2.7x10^{7} atoms. This means that in order to similarly detect an alike concentration in the plastic scintillator target one should implant 2.7x10^{7} tritium atom in the target. For a 1.15 cm radius target the amount of tritium that is implanted equal 2.7x10^{7} / (1.15^{2} x π) = 6.5x10^{6} #/cm^{2} and for 4 and 6 cm targets 5.4x10^{5} and 2.4x10^{5} #/cm^{2} respectively. Now, for 1cm^{3} air samples containing tritium, HT, with different concentrations 0.3, 0.03, 0.003, and 0.0003 Bq/cm^{3}, which are equivalent to 100 %, 10%, 1% and 0.1% of

the DAC value for HTO respectively, or equivalent to $4x10^{-5}$, $4x10^{-6}$, and 4×10^{-7} of DAC value for HT respectively, the time required for implantation can be calculated using the program presented in Appendix III. Figure 26 shows the calculated implantation time of 2.5×10^{19} ions, available in a cm^{-3}, into different size targets at different pressures.

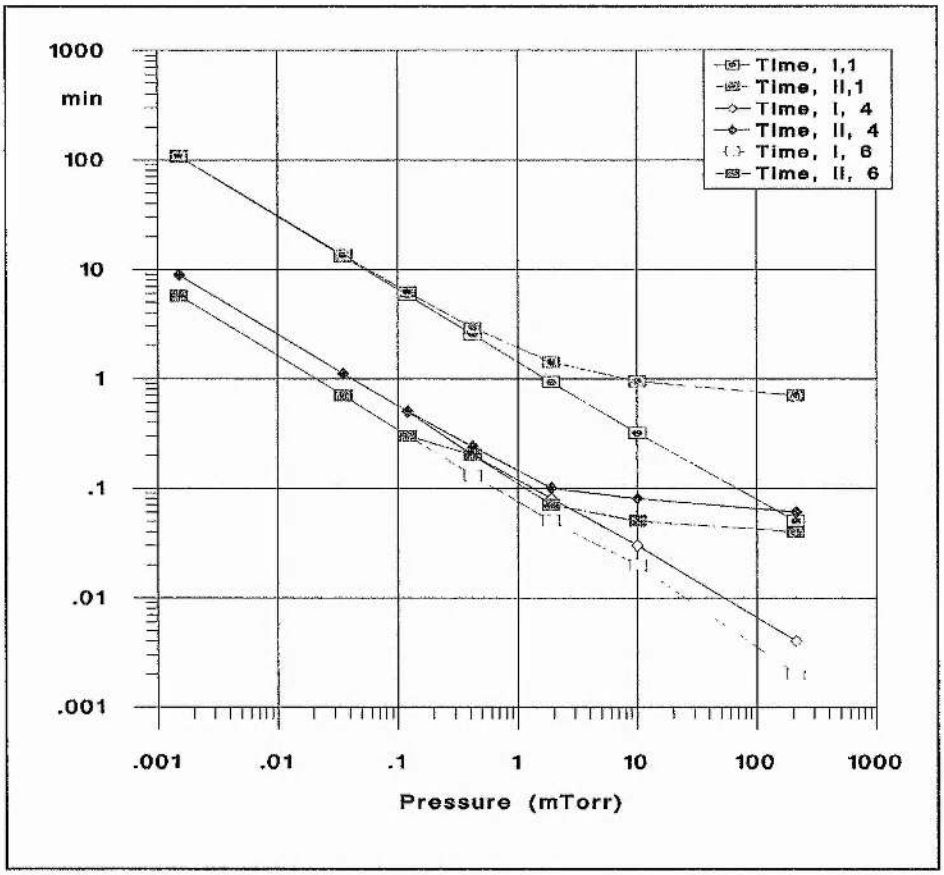

Figure 26. Estimated implantation time for samples of different initial tritium concentrations into targets with different radiuses. Legend(Time, case, radius of the target).

The estimated time to collect ions would be reduced when repeating the same calculations but for targets with larger radius. A sample with a given tritium concentration, Bq/cm^3, would take between 6-2 minutes to be collected under a pressure of .01-1 mTorr in a target with a radius of 1.15 cm. The same sample would only require 2 - 0.07 minutes to be collected onto a 6 cm radius target. This characteristic is

advantageous for utilizing the developed device to operate over a wide range of concentrations, to speed up urgent measurements and to operate at different levels of sensitivity.

Increasing the target cathode area would require the use of a high voltage power source of high power output. At this stage a high voltage power source of a maximum of 200 watt was used and the target radius was limited to 1.15 cm.

The PSII components

The PSII system consists of two parts; i) the implantation chamber and ii) the high voltage pulse modulator.

The implantation chamber

The implantation chamber is shown in

Figure 27. The chamber is a cylindrical stainless steel tube 9 cm long with a diameter of 9 cm. Connected to the chamber is the quartz tube of the surfatron into which a light guide and high voltage feed-through are inserted at the other end. The chamber is connected to the vacuum pumping system through a 1.225 cm (0.5 in) tube in the base of the chamber. The dimensions of the chamber were selected so that the maximum expansion of the sheath for a given pulse at the minimum pressure of .01 mTorr would not reach the walls of the chamber.

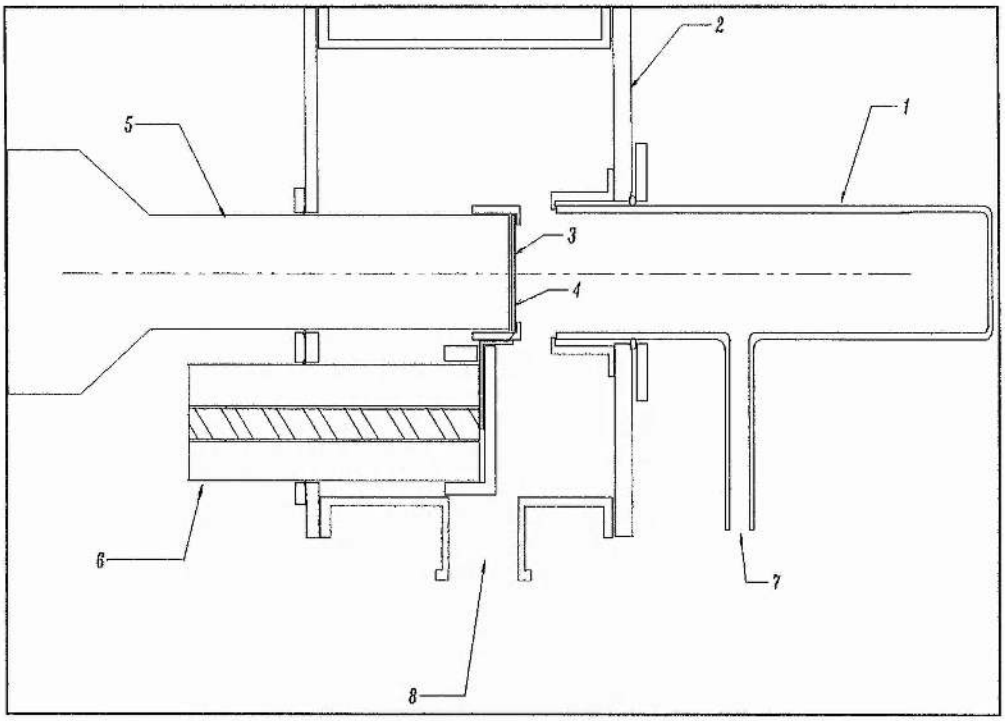

Figure 27. The implantation chamber assembly. 1) The quartz tube, 2) the chamber, 3) an Al foil, 4) the thin plastic scintillator, 5) the light guide, 6) the high voltage feed through, 7) air inlet and 8) vacuum pump connection.

High Voltage (HV) pulse modulator

The high voltage pulse modulator is the second part of the PSII. As a HV pulse modulator with the PSII specifications is not available commercially, it had to be designed and built by combining commercially available components with specially constructed components. The power source and pulse modulator are required to be compact in size and able to produce a series of negative HV pulses. The high voltage pulse modulator consists of a power supply, a high voltage switch, a compatible 0.1μF capacitor, a dump relay and interlock switches. The overall diagram of the HV modulator is shown in Figure 28.

For the high voltage power supply a compact Spellman EHT power supply unit model PTV 60N200/240/MCNP was selected. It provides very well regulated low ripple high

voltage in a compact design. The power supply is capable of providing -60 kV with a maximum DC current of 3.5 mA. The high voltage switch is a Behlke fast high voltage transistor switch model HTS 650/02. It is capable of generating precise high voltage pulses with amplitude up to 65 kV. The turn-on rise time varies between 70-135 nsec depending on the load impedance. The high voltage switch has an upper limit of repetition rate of 3 kHz for continuous frequency and 2 MHz for burst frequency. The high voltage switch, HTS 650/02 was chosen because it does not need a complex drive circuitry's or heating power as it is used for other conventional high voltage switches such as electron tubes and gas discharge tubes. Furthermore, being a solid state switch, the HTS 650/02 switch is supposed to have a life time typical of semiconductor devices. Also the switch is compact in size. The HTS switch requires a 5 VDC power and a TTL signal with an amplitude of 3-10 volts. The HTS switch is controlled by a TTL signal produced by a signal generator Thandar model TG105 which is capable of producing a continuous burst of single pulses with the desired pulse duration and pulse period starting form 5 Hz up to 5 MHz. The pulses produced by the signal generator have been chosen to have a fixed 10 μsec on-time. Details of these units are given in appendix II. The dump relay was introduced to dump the stored charge in the 0.1 μF. A number of interlock switches were introduced to secure safe operation of the whole PSII system. The importance of the production of a negative high voltage pulse with specific characteristics, which cover the pulse shape, duration, repetition rate and magnitude have already been described in the previous chapter.

The production of the desired negative high voltage pulses was fine tuned after experimenting with the pulse modulator by changing the value of the capacitance C_I, and the resistor R_S shown in Figure 28 and monitoring the changes in the pulse shape at

initially low and then relatively high voltages utilizing a high voltage probe and an oscilloscope. The details of the probe specifications are tabulated in Appendix II. Optimum values of the C_L and R_S were found to be 50 Ω and 96 pF respectively. By selecting the period of the triggering pulse at the signal generator and applying the gate mode, the production of the desired negative high voltage pulse was achieved. Figure 29 shows a sketch of a negative high voltage pulse.

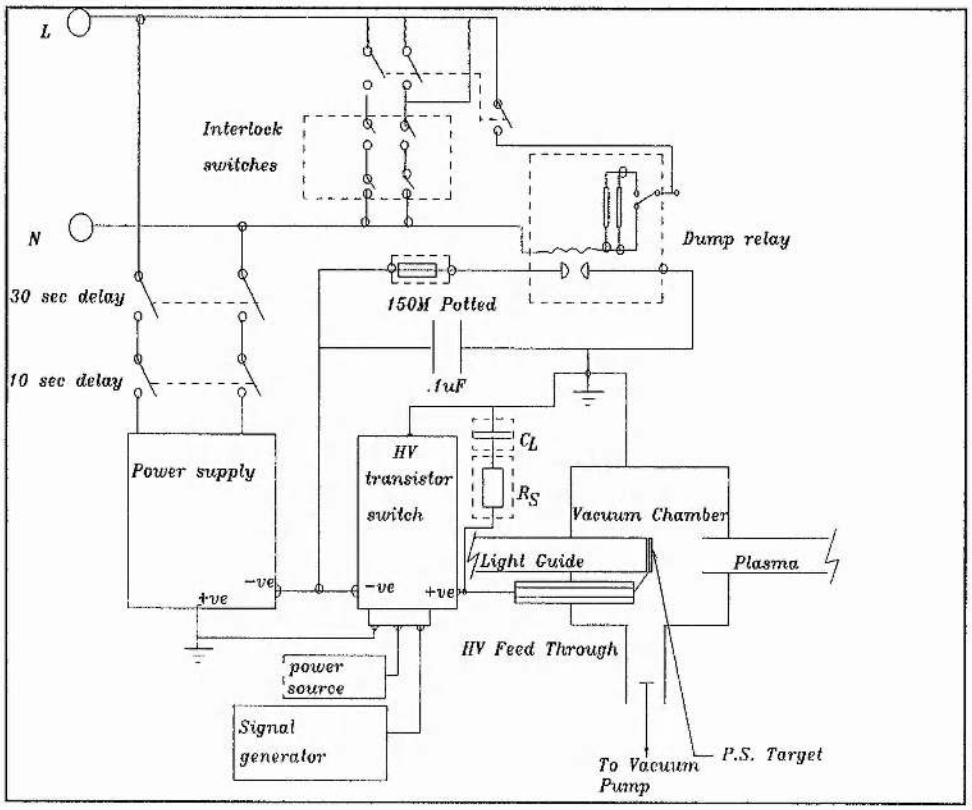

Figure 28. The plasma source ion implantation system.

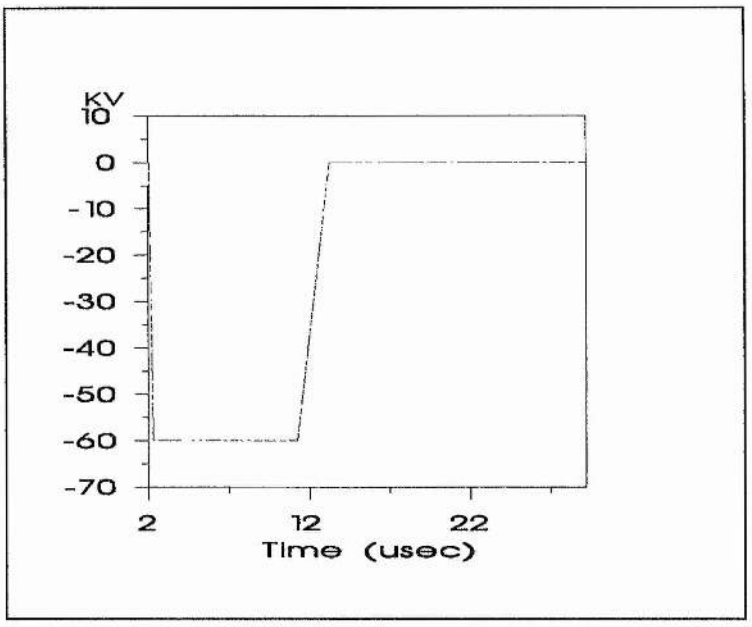

Figure 29. A sketch of a negative high voltage pulse.

The resulting pulse has a rise time of ≅ .1 μsec, a peak duration of 10 μsec and a pulse turn off time ≅ 2 μsec.

The pulse repetition rate was chosen to be ≈ < 2 kHz, that is to work within the maximum limitation of the chosen switch. The pulse on-time is 10 μsec and the off-time is 500 μsec. This will provide ample time for the ions to refill the depleted sheath volume.

The HV negative pulse magnitude was chosen to be 50 kV in order to minimize sputtering and allow for the implanted ions to pass through the aluminum foil.

The scintillation counting assembly

The scintillation counting assembly consists of the target assembly, the detection setup and the electronics.

The target assembly

The target assembly comprises of: i) the plastic scintillator target; ii) the high voltage cathode and iii) the light guide.

The plastic scintillator target

The plastic scintillator target is a layer 20 μm thick of polyvinyltoluene with added scintillation, commercially known as type NE 102. This thickness is readily available in the laboratory. Nevertheless, 20 μm thickness represents an optimum choice. Although a different thickness could be adopted however, the thicker the plastic scintillator the higher the effect of surface charging during plasma source ion implantation. This will result in lowering the energy of the accelerated ions, hence reducing the final thickness of the sheath. As a result the dose of implanted ions to the plastic scintillator is reduced. Figure 30 shows the effect of increasing the thickness of the plastic scintillator on the total number of ions available for collection at different pressures.

The minimum thickness required for actual implantation is estimated from the known ions ranges in the plastic scintillator. The ranges of different ions in water was taken to represent their range in plastic scintillator which have roughly the same electron density. The ranges of the different ions with different energies (Watt 1993) were plotted in Figure 31. The normalized ranges of these ions in water are illustrated in Figure 32.

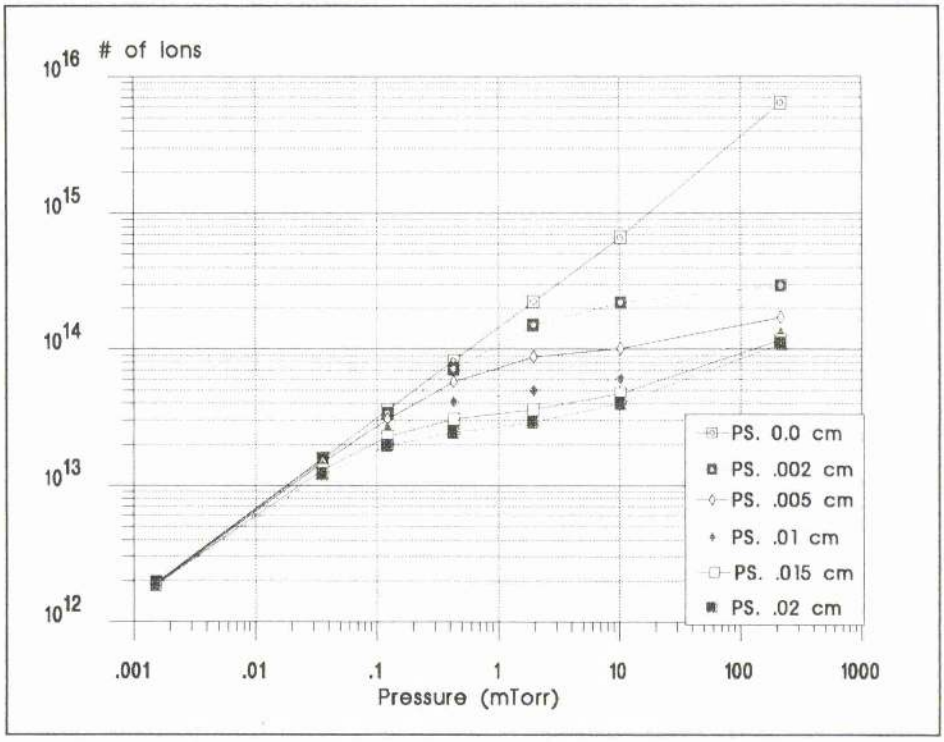

Figure 30. The effect of increasing the plastic scintillator thickness on the total number of ions available for collection at different pressures.

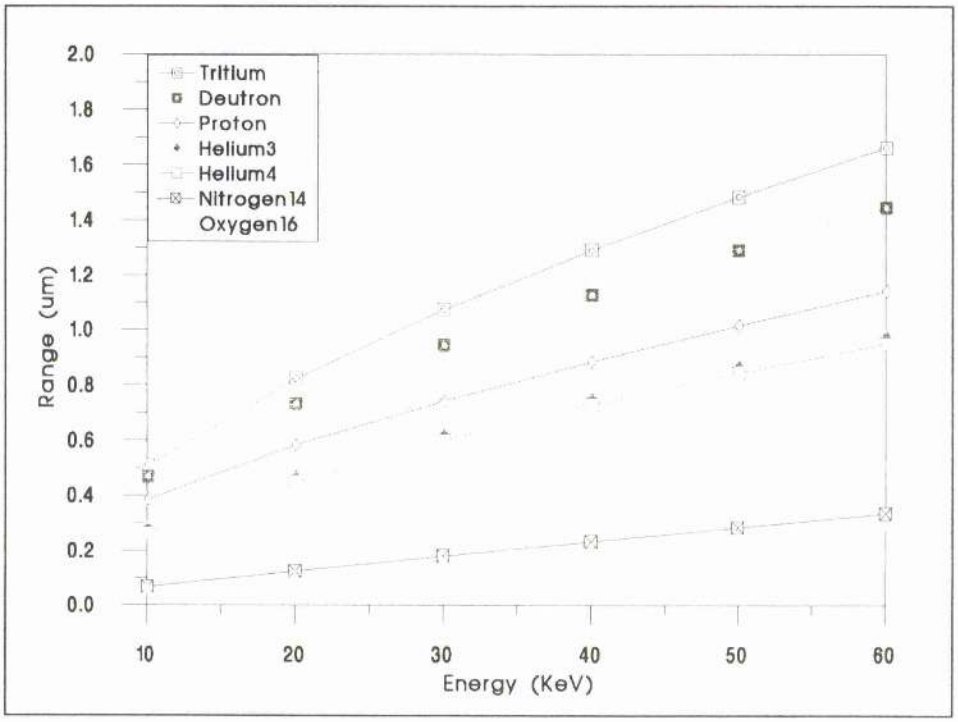

Figure 31. The range of different ions in water (Watt 1993).

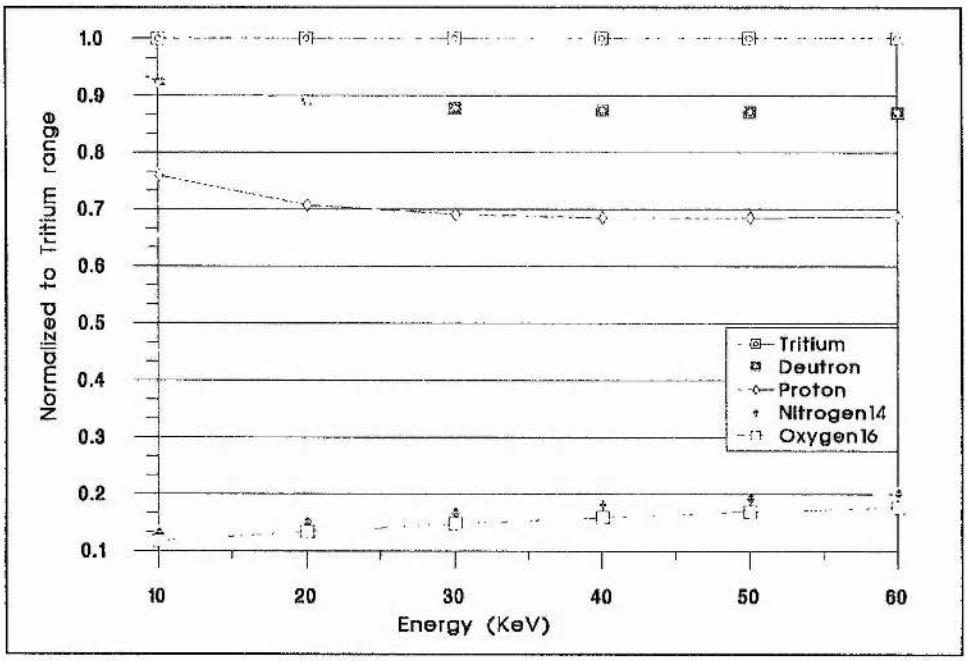

Figure 32. Normalized ranges of ions in water.

Nitrogen and oxygen ion ranges in water lie within the first 20 % of the tritium ion's range at the same energy. From Figure 31 nitrogen and oxygen ions with energies within a maximum of 60 keV would stop within 0.5 μm of a plastic scintillator material, while ions of hydrogen isotopes with energies ranging between 10-60 keV would penetrate to 0.5 - 1.7 μm. Therefore, the minimum thickness of the plastic scintillator can be chosen to be ten fold of this i.e. 17 μm.

The high voltage cathode

Two different cathodes were used: i) a 2.45 cm diameter and 0.15 μm thick Al-microfiol and ii) strips that forms a 2.45 cm diameter disc made out of Al-foil. Ideally in PSII when a non conducting material is to be implanted with ions it should be placed on top of the high voltage cathode. In our case the plastic scintillator is to be observed by a photomultiplier tube (PMT). Therefore, a clear line of sight should be made for the PMT. A number of ways can be adopted to position the high voltage cathode with respect to the plastic scintillator. The simplest two ways selected were, Case-I and

Case-II Figure 18. Case-I gives a clear line of sight for the PMT to observe any possible scintillations in the plastic scintillator. Also, the Al-microfoil acts both as a reflector and as an ion separator reducing the unnecessary heavy ion implantation into the plastic scintillator. Severe sputtering may occur and can destroy the Al-microfoil resulting in termination of the whole process. In Case-II the cathode is made out of strips, with spacing in between, in order not to block the line of sight to the PMT and to provide the field necessary to attract the ions. The geometry here allows for exposing the whole surface of the plastic scintillator to the ions and protects the cathode from sputtering.

Case-I and Case-II aims at maximum collection of the tritium ions and to separate or enrich the concentration of the collected tritium.

Tritium separation

It is difficult to separate and enrich the specific activity of tritium in an air sample in a rapid, easy way without complexities or without the use of extra instrumentation. However, the utilization of the fact that the depth distribution of the implanted ions is energy and mass dependent and different ions with equal kinetic energy have different implantation ranges in a given material facilitate the separation during deposition. During implantation the majority of the accelerated ions would be ions of gases other than tritium. Only a very small fraction is tritium ions. Light energetic ions will be deposited deeper inside the plastic scintillator than slow heavy ions. Tritium ions, in comparison to other heavier ions, will be distributed over a longer range inside the plastic scintillator material whereas the heavier ions are distributed in the first 20% of the tritium range. In order to prevent unnecessary implantation of air ions into the plastic scintillator, a very thin aluminum microfoil was selected to be placed on it. The detailed justification for the selection and the required thickness is discussed below. When the

implantation process is initiated, different ions will reside at different depths inside the aluminum microfoil that covers the plastic scintillator. Only tritium ions will be deposited in the plastic scintillator.

Optimizing the 'Al' microfoil thickness

The estimated ranges for proton, deuterium, tritium, helium, nitrogen, and oxygen ions in aluminum foil were calculated. First, the curve for the total stopping power of ions in aluminum (Andersern and Ziegler 1980) was extrapolated down to .01 MeV/amu (see Figure 33). Second, the stopping power for deuterium and tritium ions were extracted knowing that the abscissa in the curve is in MeV/amu and not in MeV. Third, the stopping power in keV/amu was calculated by multiplying by the factor 269.8 given in the previous reference. Finally, the range in μm was calculated for each ion at different energies. Figure 34 shows the above estimated ranges. Hydrogen projected ranges in aluminum of mass density 2.698 g/cm3 and for different energies were extracted from the curve for the range of hydrogen ions in Al(13) (Andersern and Ziegler 1980), and were added to the curve in Figure 34.

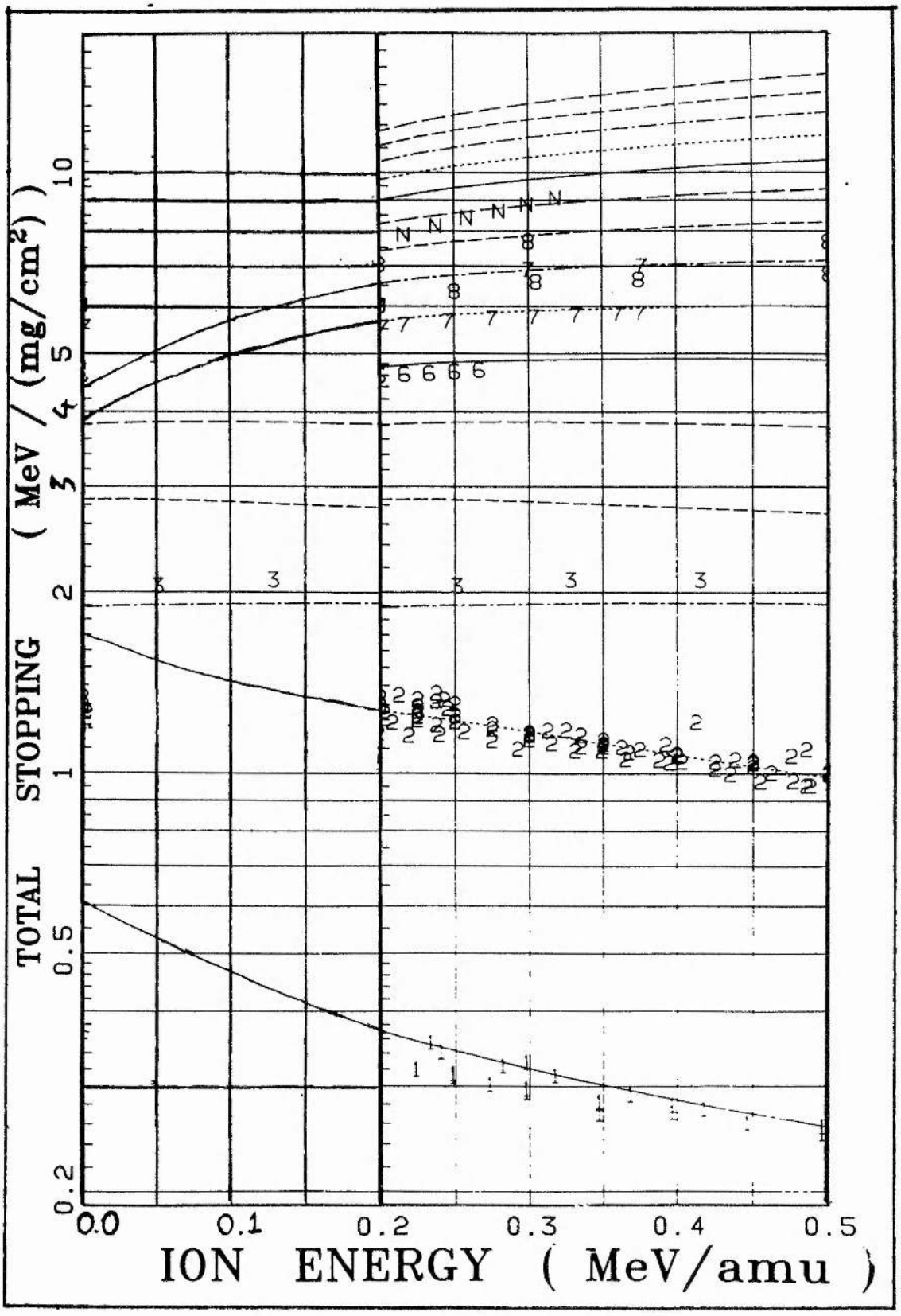

Figure 33. The total stopping power of ions in aluminum (Andersern and Ziegler 1980).

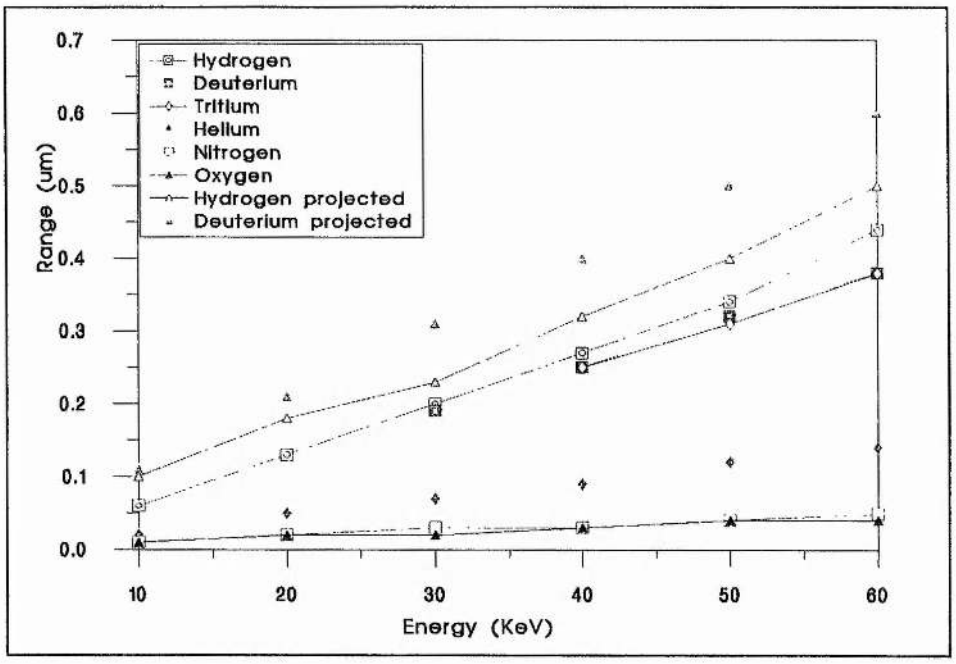

Figure 34. Ranges of the different ions in aluminum (13) calculated from (Ziegler 1980) and the projected ranges for hydrogen and deuterium in aluminum (2.698 g/cm3).

The normalized ranges of these ions in aluminum are illustrated in Figure 35.

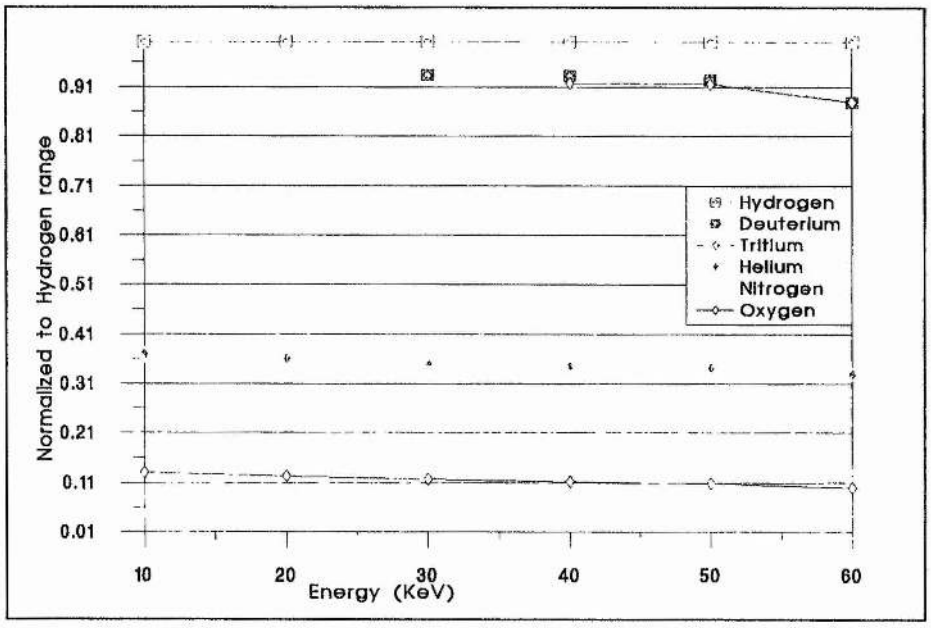

Figure 35. Normalized ranges of ions in aluminum foil.

Nitrogen and oxygen ion ranges in aluminum lie within the first 20% of the tritium ion range. From Figure 34, the use of aluminum foil 0.15 μm thick would be able to stop most if not all of the nitrogen and oxygen ions accelerated to a maximum energy of 60 keV. Hydrogen isotopes ions with energies above 25 keV would be expected to penetrate such a foil.

For Case-I all the collected ions will be subjected to separation by depositing heavy ions, nitrogen and oxygen, in Al -microfoil and depositing the tritium ions in the plastic scintillator. In Case-II all of the ions regardless of whether they are heavy or not will be deposited into the plastic scintillator. The lighter tritium ions will reside at a deeper range in the plastic scintillator away from quenching impurities implanted such as oxygen ions.

The light guide

The light guide was made out of acrylic material and was cut to the dimensions shown in Figure 36. The viewing ends were polished to minimize light losses due to reflection and scattering.

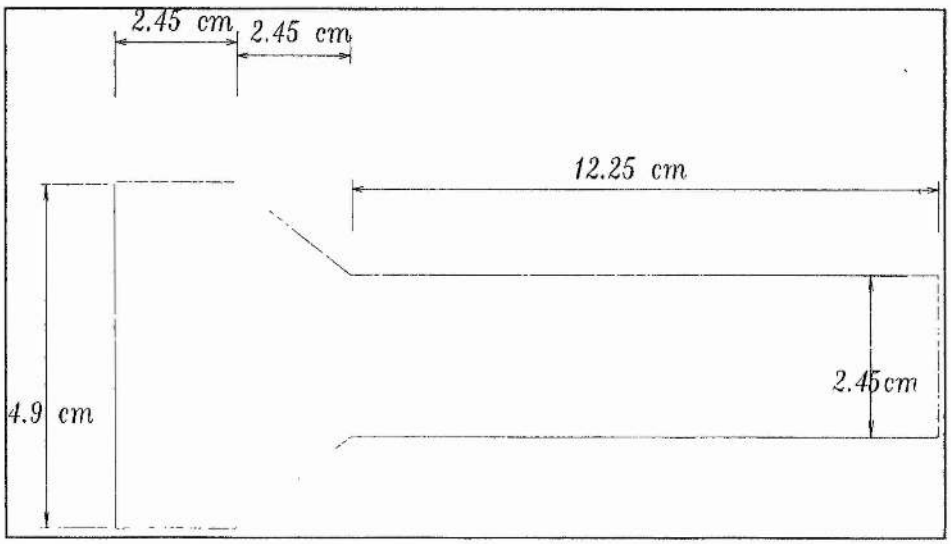

Figure 36. The light guide.

The light guide was connected to a photo multiplier tube 'PMT' as shown in Figure 37.

On the 2.45 cm diameter face the plastic scintillator was placed while on the other 4.9 cm diameter face the PMT was positioned. Silicon oil was used as an optical contact on both faces. The part of the light guide outside the PSII chamber was wrapped in several layers of black tape in order to exclude light. The whole chamber was made light tight.

The setup and electronics

The scintillation counting setup and assembly is shown in Figure 37. The PMT is a 2.0 in diameter EMI tube type 9656L shielded by a Mu-metal shield and enclosed into a tube housing which is grounded to minimize the noise effect. The PMT high voltage power is supplied by a J&P power supply, it provided the PMT with a positive 1200 V. The PMT output was fed into a EG&G preamplifier model 113. Which in turn is connected to a Tenelec TC243 main amplifier. The amplified signals where fed to a Norland multi-channel analyzer model 5300.

The test of the scintillation assembly

First the scintillation assembly was tested for light tightness. Potential sources of light were identified. These include the transparent high voltage lead-through, the quartz tube and the produced plasma. All of the light sources were covered with black tape. It would be ideal to shield the plasma light by a shutter, however it was found convenient at this stage to switch the PMT high voltage power supply off during plasma production and ion implantation. After the collection time the PMT can be energized for scintillation detection.

The scintillation assembly was then tested for the detection of β^- radiation of different maximum energies using C^{14} and Sr^{90} β^- sources. The maximum β^- energy of these isotopes are 156 keV and 540 keV respectively. The radioactive sources have an

activity of 330 kBq for C^{14} and 74 kBq for Sr^{90}. First the background was measured for 100, 600, 800, and 1600 sec. Then the radioactive sources were introduced in turn and were counted for the same counting times. The radioactive sources were positioned inside the PSII chamber almost touching the plastic scintillator target. Due to the size of the plastic scintillator it is essential to have the same geometry when counting the activity in the sources and when counting the background. Any change of the geometry will affect the results. Figure 38 and Figure 39 show the net count / channel for Sr^{90} and C^{14} respectively. It is evident that the use of a single PMT would not permit the detection of tritium weak β^- particles emitted.

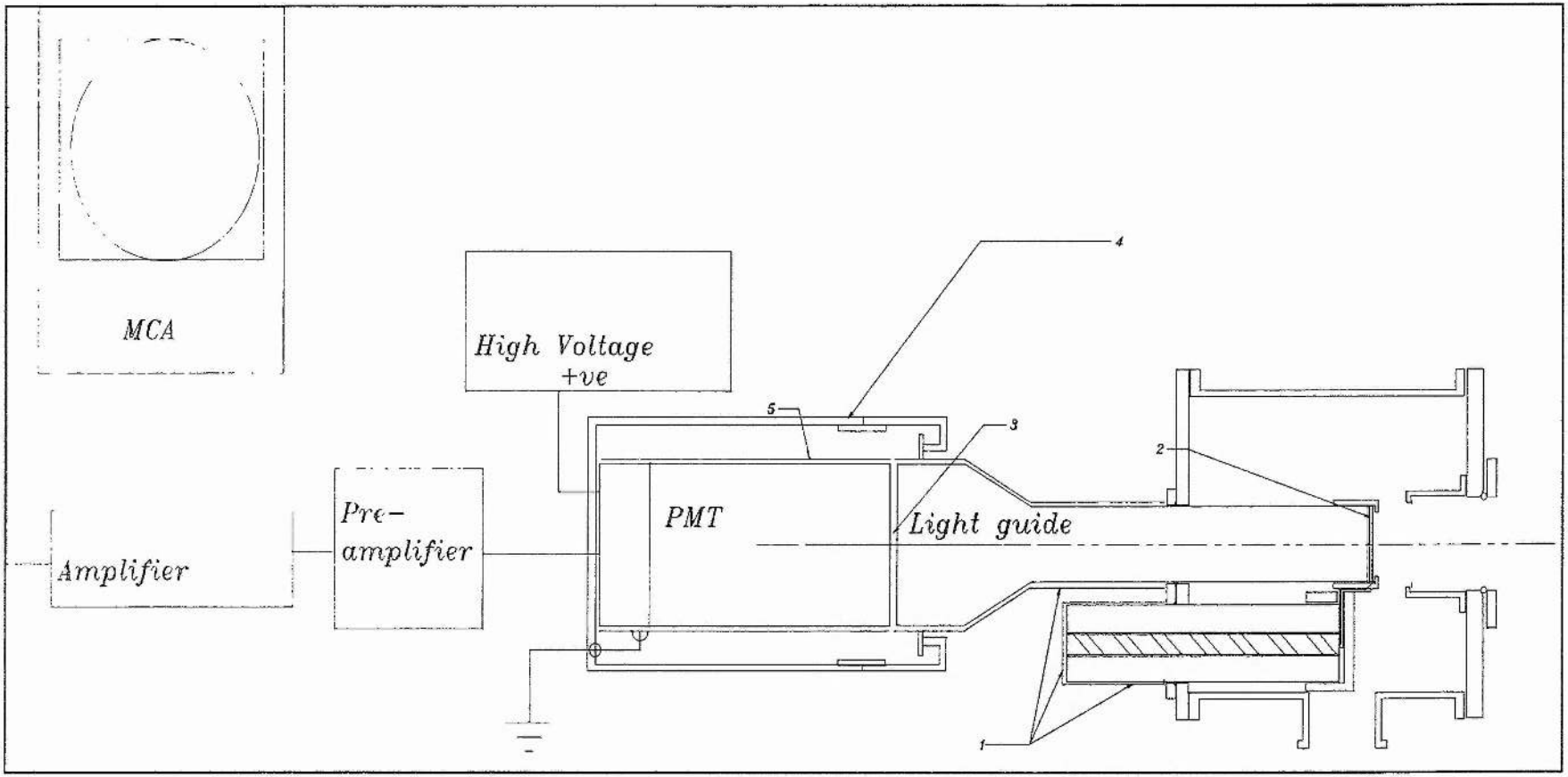

Figure 37. The scintillation counting assembly, 1) light tight black tape, 2) target assembly, 3) optical contact (silicon oil), 4)PMT housing and Mu-metal shield.

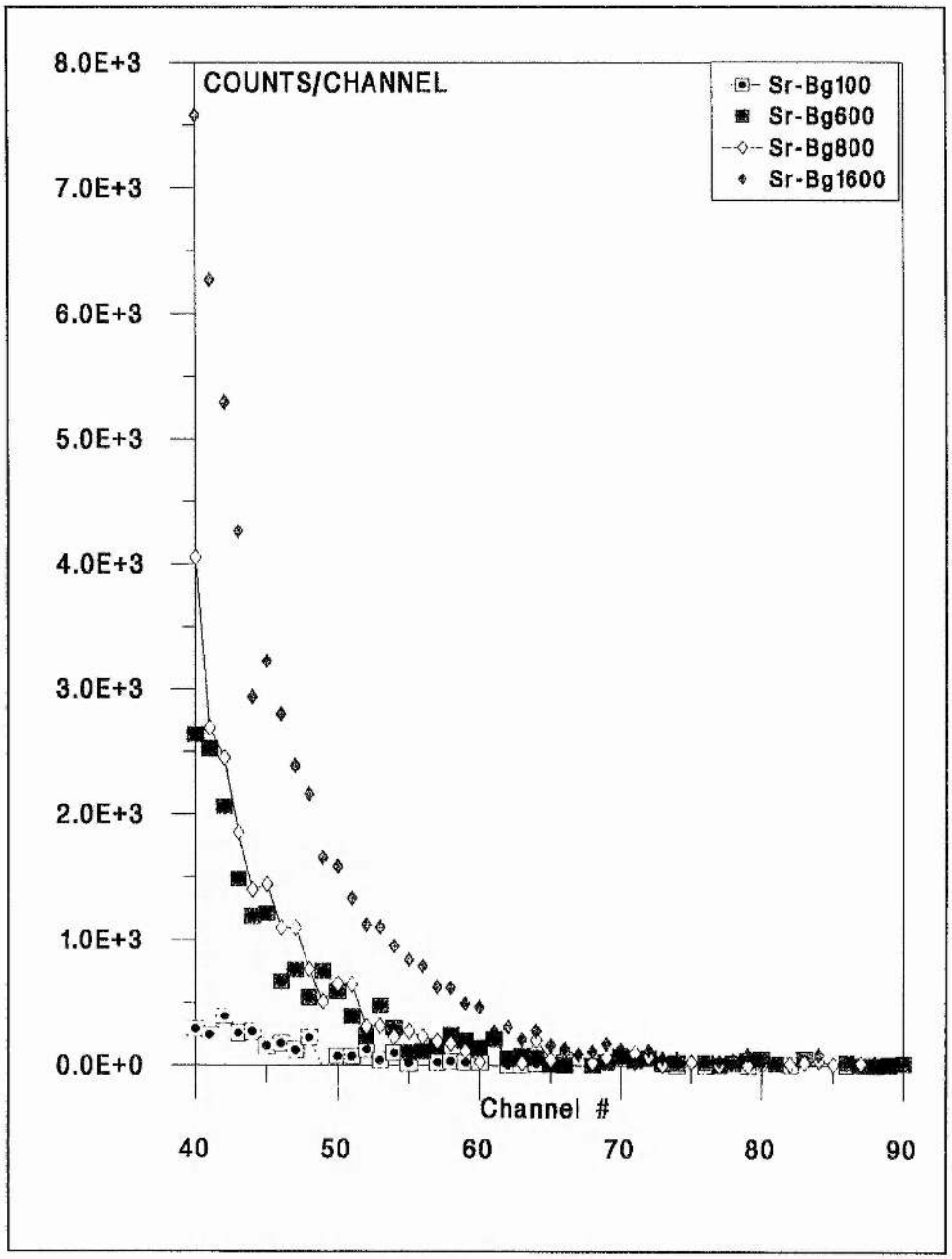

Figure 38. Counts · channel for a Sr^{90} source counted in the scintillation assembly for 100, 600, 800, and 1600 sec.

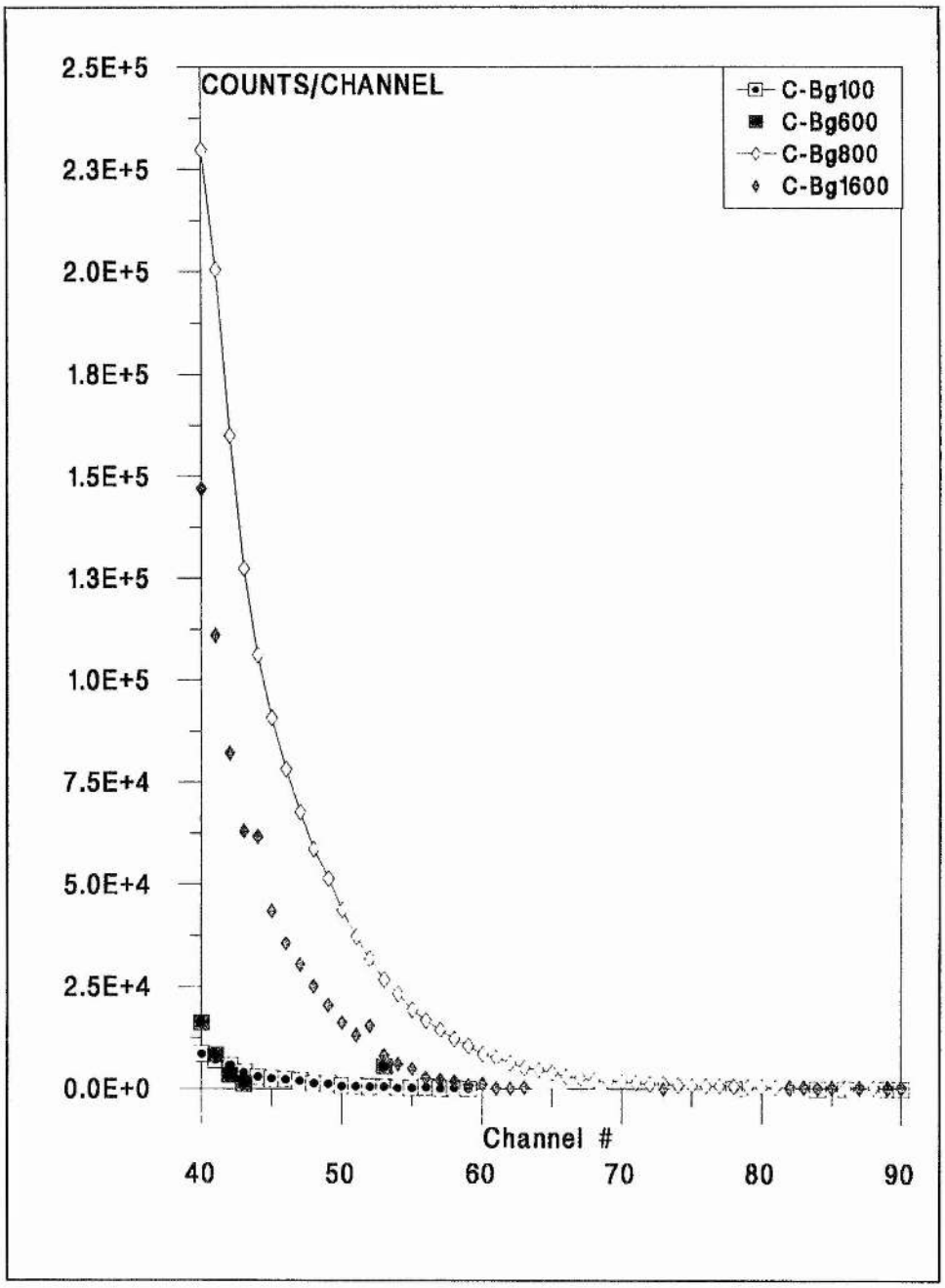

Figure 39. Counts / channel for a C^{14} source counted in the scintillation assembly for 100, 600, 800, and 1600 sec.

Chapter 5

Conclusion and Recommendations

Chapter 5

Conclusion and Recommendations

Conclusion

In radiological protection there is a requirement to monitor tritium concentrations in workplaces, such as tritium handling facilities, heavy water reactors and future fusion reactors. Tritium concentrations in air must be measurable down to fractions of the derived air concentrations, currently 8×10^3 Bq/cm^3 for HT and 0.3 Bq/ cm^3 for HTO. To achieve this objective, an innovative technique was proposed in which tritium ions produced in a plasma ion source are accelerated and detected via the T(d, He-4)n reaction or by implantation of the accelerated tritium ions into a scintillation detector for subsequent counting of the beta rays. The former method was estimated to be more sensitive but was not pursued because of difficulties in acquiring the essential 120 kV high voltage power source. Instead only a 60 kV power source was available. Consequently, effort was expended in producing a working prototype which had the capability to be minimized in size for portability. Therefore, the ion source volume, implantation chamber volume, high voltage power unit and high voltage pulse modulator were designed and selected to be small in size. The average total volume is within 0.2 m^3.

To obtain an optimum yield of tritium ions from the sampled air, the 'surfatron' type of plasma source was selected and merged into a non-line-of-sight 'plasma source ion implantation' unit. The surfatron was selected because of its capability to support a large size plasma over a wide range of gas pressure, from 4.0 to 0.1 mTorr, with ions of

low temperature. Plasma source ion implantation technique was chosen because of its high efficiency in extracting ions and directing them to the target. In contrast to the normal 'line-of-sight' technique the technique does not require beam focusing.

The version designed and constructed can collect up to 2.5 X 10^{19} ions in 1 to 10 minutes, depending on the working pressure (2-0.1 mTorr), for an acceleration voltage of 60 kV in 10 μsec pulses with a repetition rate of 2 kHz. By designing aluminum filters to give good discrimination of tritium ions against the unwanted background of nitrogen and oxygen ions, maximization of sensitivity was expected. Although the tests of the device are still on-going, the sensitivity was forecast, provided a coincident scintillation detection setup is used, to be comparable with the liquid scintillation technique, i.e. 0.4 mBq/cm^3 for a bubbler collected sample counted for 10 minutes.

The existence of the beam was confirmed by observation of sputtering from an Al cathode during lower energy implantation at 30 kV. Furthermore, the design had shown, at least by calculation, that it is capable of fast deposition and fast build-up of measurable tritium concentrations in the plastic scintillator. Also, the design calculation indicated that a plastic scintillator target can be loaded with sampled ions of air at a rate that is proportional to the target area. Unlike liquid scintillation counting, this new technique would permit fast and sensitive response thereby eliminating the need for time consuming sample collection and sample preparation for detection. And by incorporating targets of different sizes a wide-range of concentrations can be covered. Also, the developed technique would produce no liquid waste. Moreover, the implanted target can be stored for repeat assays should the need arise.

Recommendations for future work

There is room for modifications to the prototype device. For the surfatron the substitution of the magnetron with another RF signal generator that produces MHz signals would result in minimum if not zero power reflection from the surfatron coaxial structure, hence safer operation.

The plasma source ion implantation subsystem can be modified to optimize performance. Ion implantation can be increased by enlarging the target area and accelerating to a higher energies by using a higher current high-voltage generator. Modifying the high-voltage pulse modulator to produce square sub-nanosecond pulses would enrich the implantation current in tritium ions. The cathode and plastic scintillator arrangement could be modified to have a mesh like cathode embedded inside a thin plastic scintillator that let the two parts make one single disc that can be easily installed and removed from the top of the light guide.

The sensitivity of the scintillation detector could be improved dramatically by incorporating a coincidence counting technique to reduce random background noise. Also, the introduction of an optical shutter before the PMT would eliminate the need for switching the PMT power off and on during implantation and later during scintillation detection. This will result in a more stable operation of the PMT.

The problems encountered do warrant further investigation and testing in field conditions to obtain quantitative results for function and sensitivity after calibration with a standard gaseous tritium source.

Appendixes

Appendix I

Properties of tritium

The physical properties of tritium are almost identical to that of hydrogen. Chemically, tritium behaves like hydrogen so that reactions that occur with hydrogen also occur with tritium. Deviations in tritium interactions with materials from that of hydrogen occur because the tritium mass is three times that of hydrogen; it is radioactive emitting β^- particles and transmits to form helium-3. The mass difference will affect the rate of chemical reactions and the other differences can cause deviations in tritium interactions with materials.

Table 11: The following table gives some of the properties of tritium.

Property	***Value***	***Reference***
Half life	12.43±.05 year	(Taylor 1982)
Decay constant	1.7671×10^{-9} sec^{-1}	(Taylor 1982)
Decay product	^{3}He	
Characteristics of β^-	Beta (100%)	
Maximum energy (keV)	18.6	(NCRP 1985)
Average energy (keV)	5.685	(NCRP 1985)
Most probable β^- energy (keV)	2 to 3	(Kherani and Shmayda 1992)
Max. track length in air (cm)	0.5	
Half thickness in Al (mm)	0.1	(Miller and Holtslander 1984)
Max. track length in water (μm)	6.0	(Caresten 1979)
Aver. track length in water (μm)	0.56	(Caresten 1979)
β^- radiation above 17 keV	0.05 %	(Miller and Holtslander 1984)
Old Annual Limit of Intake (ALI)	3×10^{9} Bq	(ICRP 1978)
New Annual Limit of Intake, ALI	1×10^{9} Bq	(ICRP 1991)
Biological half life	9.7 d	(ICRP 1979)
Dissociation energy (T_2--> 2T)	4.59 eV	(Miller and Holtslander 1984)
Ionization energy (T-->$T^+ + e^-$)	13.55 eV	(Miller and Holtslander 1984)
Atomic weight (g)	3.016	(Miller and Holtslander 1984)
1 kg of T_2	0.359 EBq	

Appendix II

Equipment characteristics

Table 12: Semirigid cable characteristics.

Cable #	RG-402
Inner conductor O.D (in)	0.0362 ± 0.0007
Dielectric conductor material	SCW
Dielectric OD(in)	0.1175 ± 0.001
Dielectric material	PTFE Type F-1
Outer conductor OD (in)	0.141 ± 0.001
Outer conductor material	Copper
Safe bend radius (in)	.250
Max. Weight-ibs. /100 ft	3.44
Operating temp. range (c°)	-40 ; 100
Impedance and tolerance (ohms)	50 ± 1.0
Dielectric strength rating-KVRMS 60 Hz	5.0
Max. operating frequency (GHz)	20

Table 13 The technical specification of the EMI copper foil

Material	copper coated non-woven nylon fabric
Adhesive	cross-linked acrylic adhesive
Operating temp.	-20 to +80 C°
Surface conductivity	0.04 ohm/sq. typ.
Attenuation typ.	60db (1MHz to 10 GHz)

The major technical specifications of the high voltage power supply model 60N200/240/MCNP.

- Input: 115 ac ±10 % @4A max 50/60 Hz
- Output: 60 kV negative.
- Output control: Voltage and current are externally programmable over the entire range from zero to maximum rating via 0-10 VDC reference or potentiometer.

The major technical specifications of the high voltage transistor switch model HTS 650:

Specification		
Max. operating voltage	65	kVDC
Switch breakdown voltage	>72	kVDC
Isolation voltage	85	kVDC
Max. peak current	30	ADC
Static on-resistance	360	Ω
Max. off-state current	<15	μADC
Turn-on delay time	125	nsec
Turn-rise time	120	nsec
Typical turn-on jitter	100	psec
On-time	10	μm
Max. burst frequency	2	MHz
Max. continuous frequency	3	KHz
Continuous power dissipation	25	W
Natural switch capacitance	25	pF
Coupling capacitance	50	pF
Auxiliary supply voltage	5	VDC
Auxiliary supply current	400	mADC
Trigger signal voltage	2-10	VDC

Appendix III

Calculation of sheath expansion and ion implantation

This is the copy of the Mathcad program used for the calculation of the sheath expansion and ion implantation doses.

Initiation

$\varepsilon := 8.854187817 \cdot 10^{-12} \cdot \frac{farad}{m}$

$p_{atm} = 760\ Torr$

$\mu sec = 10^{-6} \cdot sec$

$mamp = 10^{-3} \cdot amp$

$mbar = Pa \cdot 100$

$r = 6 \cdot cm$ Target radius

$Area = r^2 \cdot \pi$

$Area = 113.097 \cdot cm^2$

$Ac := .3 \cdot Bq \cdot cm^{-3}$

$Vr := 60 \cdot KV$ Pulse HV

$Vo := 60 \cdot KV$

$\lambda 1 := 400 \cdot cm$ ~ P=.0015 mTorr

$\lambda 2 := 150 \cdot cm$ ~ P=.035 mTorr

$\lambda 3 = 40 \cdot cm$ ~ P=.12 mTorr

$\lambda 4 = 10 \cdot cm$ ~ P=.42 mTorr

$\lambda 5 = 2 \cdot cm$ ~ P=1.9 mTorr

$\lambda 6 = .32 \cdot cm$ ~ P=10 mTorr

$\lambda 7 := .021 \cdot cm$ ~ P=210 mTorr

$Bq := 1 \cdot sec^{-1}$

$Vr = 60 \cdot KV$ Pulse HV

$Vo := 60 \cdot KV$

$Mion := 14 \cdot 1.67 \cdot 10^{-27} \cdot kg$ Nitrogen mass

$q = 1.60217733 \cdot 10^{-19} \cdot coul$

$Con := 2.4 \cdot 10^{5}$ Desired implantation density

$d = (.00) \cdot cm$ PS thickness (>0 for PS on top of the cathode).

$ts := 10 \cdot \mu sec$

$\kappa = 3$ Dielectric constant of PS material.

The calculation of the density numbers at different working pressures (Ppi).

$p_{p0} = .0015 \cdot 10^{-3}$ $nno1 = \frac{p_{p0}}{p_{atm}} \cdot (2.55 \cdot 10^{19} \cdot cm^{-3})$ $nnto1 = \frac{p_{p0}}{p_{atm}} \cdot \left(\frac{Ac \cdot sec}{1.7671 \cdot 10^{-9}}\right)$

$p_{p0} = .035 \cdot 10^{-3}$ $nno2 = \frac{p_{p0}}{p_{atm}} \cdot (2.55 \cdot 10^{19} \cdot cm^{-3})$ $nnto2 = \frac{p_{p0}}{p_{atm}} \cdot \left(\frac{Ac \cdot sec}{1.7671 \cdot 10^{-9}}\right)$

$p_{p0} = .12 \cdot 10^{-3}$ $nno3 = \frac{p_{p0}}{p_{atm}} \cdot (2.55 \cdot 10^{19} \cdot cm^{-3})$ $nnto3 = \frac{p_{p0}}{p_{atm}} \cdot \left(\frac{Ac \cdot sec}{1.7671 \cdot 10^{-9}}\right)$

$p_{p0} = .42 \cdot 10^{-3}$ $nno4 = \frac{p_{p0}}{p_{atm}} \cdot (2.55 \cdot 10^{19} \cdot cm^{-3})$ $nnto4 = \frac{p_{p0}}{p_{atm}} \cdot \left(\frac{Ac \cdot sec}{1.7671 \cdot 10^{-9}}\right)$

$p_{p0} = 1.9 \cdot 10^{-3}$ $nno5 = \frac{p_{p0}}{p_{atm}} \cdot (2.55 \cdot 10^{19} \cdot cm^{-3})$ $nnto5 = \frac{p_{p0}}{p_{atm}} \cdot \left(\frac{Ac \cdot sec}{1.7671 \cdot 10^{-9}}\right)$

$p_{p0} = 10 \cdot 10^{-3}$ $nno6 = \frac{p_{p0}}{p_{atm}} \cdot (2.55 \cdot 10^{19} \cdot cm^{-3})$ $nnto6 = \frac{p_{p0}}{p_{atm}} \cdot \left(\frac{Ac \cdot sec}{1.7671 \cdot 10^{-9}}\right)$

$p_{p0} = 210 \cdot 10^{-3}$ $nno7 = \frac{p_{p0}}{p_{atm}} \cdot (2.55 \cdot 10^{19} \cdot cm^{-3})$ $nnto7 = \frac{p_{p0}}{p_{atm}} \cdot \left(\frac{Ac \cdot sec}{1.7671 \cdot 10^{-9}}\right)$

case I: $\lambda = \lambda 1$

$no = nno1$

$sr = \left(\frac{2 \cdot \varepsilon \cdot Vr}{no \cdot q}\right)^{.5}$ Initial sheath thickness

$\omega pi = \left(\frac{no \cdot q^2}{Mion \cdot \varepsilon}\right)^{.5}$ Plasma frequency

$sr1 = sr$

$\omega pi1 = \omega pi$

$so = sr$

$s = sr$

$T := \omega pi \cdot ts$ Normalized time

$T1 = T$

$Uo := \frac{Vo}{Vr}$ Normalized HV

$Tpulse := ts$

$Vo = Uo \cdot Vr$

$D = \frac{d}{sr}$ Normalized PS thickness

$\tau = 1 .. 150$

$d = D \cdot sr$

$i = 1$

$So := \frac{so}{sr}$ <- Normalized sheath thicknesses

$t_\tau := \frac{\tau}{\left(\frac{no \cdot q^2}{Mion \cdot \varepsilon}\right)^{.5}}$

$S := \frac{s}{sr}$ <- = = =

$sr = 0.011 \cdot m$

$S_0 = \frac{s}{sr}$ <- = = =

$Npt = 500$

$$DD1(T,S) = \frac{.222}{\left(S_0\right)^2 \cdot \left[1. + (.302) \cdot \frac{S_0}{\lambda} \cdot (sr)\right]^{.5}} \cdot \frac{\left[Uo - 2. \cdot D \cdot \frac{\left(S_0 - So\right)}{\kappa}\right]^{\left(\frac{3}{2}\right)}}{\left[1. + 1.33 \cdot \frac{D}{\left(S_0 \cdot \kappa\right)}\right]^{\left(\frac{3}{2}\right)}}$$

$S1 = rkfixed(S, 0, T, Npt, DD1)$ $i = 0 .. rows(S1) - 1$ $Tn = S1^{\langle 0 \rangle}$

$ss01 = S1_{Npt,1} \cdot so$

case Ii: $\lambda := \lambda 2$

$no := nno2$

$sr := \left(\frac{2\cdot\varepsilon\cdot Vr}{no\cdot q}\right)^{.5}$ Initial sheath thickness

$sr2 := sr$

$so := sr$

$s := sr$

$Uo := \frac{Vo}{Vr}$ Normalized HV

$Vo := Uo\cdot Vr$

$\tau := 1..150$

$i := 1$

$t_\tau := \frac{\tau}{\left(\frac{no\cdot q^2}{Mion\cdot\varepsilon}\right)^{.5}}$

$Npt := 500$

$\omega pi := \left(\frac{no\cdot q^2}{Mion\cdot\varepsilon}\right)^{.5}$ Plasma frequency

$\omega pi2 := \omega pi$

$T := \omega pi\cdot ts$ Normalized time

$T2 := T$

$Tpulse := ts$

$D := \frac{d}{sr}$ Normalized PS thickness

$d := D\cdot sr$

$So := \frac{so}{sr}$ <- Normalized sheath thicknesses

$S := \frac{s}{sr}$ <- = = = .

$S_0 := \frac{s}{sr}$ <- = = = .

$$DD2(T,S) := \frac{.222}{(S_0)^2\cdot\left[1. + (.302)\cdot\frac{S_0}{\lambda}\cdot(sr)\right]^{.5}}\cdot\frac{\left[Uo - 2.\cdot D\cdot\frac{(S_0 - So)}{\kappa}\right]^{\left(\frac{3}{2}\right)}}{\left[1. + 1.33\cdot\frac{D}{(S_0\cdot\kappa)}\right]^{\left(\frac{3}{2}\right)}}$$

$DD2(T,S) = 0.221947$

$S2 := rkfixed(S, 0, T, Npt, DD2)$ $i := 0..rows(S2) - 1$ $Tn := S2^{<0>}$

$ss02 := S2_{Npt,1}\cdot so$

case III: $\lambda = \lambda 3$

$no = nno3$

$sr = \left(\frac{2 \cdot \varepsilon \cdot Vr}{no \cdot q}\right)^{.5}$ Initial sheath thickness

$\omega pi = \left(\frac{no \cdot q^2}{Mion \cdot \varepsilon}\right)^{.5}$ Plasma frequency

$sr3 = sr$

$\omega pi3 = \omega pi$

$so := sr$

$s = sr$

$T := \omega pi \cdot ts$ Normalized time

$T3 := T$

$Uo := \frac{Vo}{Vr}$ Normalized HV

$Tpulse = ts$

$Vo = Uo \cdot Vr$

$D := \frac{d}{sr}$ Normalized PS thickness

$\tau = 1 .. 150$

$d = D \cdot sr$

$i = 1$

$So = \frac{so}{sr}$ <- Normalized sheath thicknesses

$t_\tau := \frac{\tau}{\left(\frac{no \cdot q^2}{Mion \cdot \varepsilon}\right)^{.5}}$

$S = \frac{s}{sr}$ <- = = =

$Npt = 500$

$S_0 := \frac{s}{sr}$ <- = = =

$$DD3(T,S) = \frac{.222}{\left(S_0\right)^2 \cdot \left[1. + (.302) \cdot \frac{S_0}{\lambda} \cdot (sr)\right]^{.5}} \cdot \frac{\left[Uo - 2. \cdot D \cdot \frac{\left(S_0 - So\right)}{\kappa}\right]^{\left(\frac{3}{2}\right)}}{\left[1. + 1.33 \cdot \frac{D}{\left(S_0 \cdot \kappa\right)}\right]^{\left(\frac{3}{2}\right)}}$$

$S3 = rkfixed(S, 0, T, Npt, DD3)$ $i = 0 .. rows(S3) - 1$ $Tn = S3^{\langle 0 \rangle}$

$ss03 = S3_{Npt,1} \cdot so$

case IV: $\lambda := \lambda 4$

$no := nno4$

$sr := \left(\frac{2 \cdot \varepsilon \cdot Vr}{no \cdot q}\right)^{.5}$ Initial sheath thickness

$\omega pi := \left(\frac{no \cdot q^2}{Mion \cdot \varepsilon}\right)^{.5}$ Plasma frequency

$sr4 := sr$

$\omega pi4 := \omega pi$

$so := sr$

$s := sr$

$T := \omega pi \cdot ts$ Normalized time

$T4 := T$

$Uo := \frac{Vo}{Vr}$ Normalized HV

$Tpulse := ts$

$Vo := Uo \cdot Vr$

$D := \frac{d}{sr}$ Normalized PS thickness

$\tau := 1 .. 150$

$d := D \cdot sr$

$i := 1$

$So := \frac{so}{sr}$ <- Normalized sheath thicknesses

$t_\tau := \frac{\tau}{\left(\frac{no \cdot q^2}{Mion \cdot \varepsilon}\right)^{.5}}$

$S := \frac{s}{sr}$ <- = = = .

$Npt := 500$

$S_0 := \frac{s}{sr}$ <- = = = .

$$DD4(T,S) := \frac{.222}{\left(S_0\right)^2 \cdot \left[1. + (.302) \cdot \frac{S_0}{\lambda} \cdot (sr)\right]^{.5}} \cdot \frac{\left[Uo - 2. \cdot D \cdot \frac{\left(S_0 - So\right)}{\kappa}\right]^{\left(\frac{3}{2}\right)}}{\left[1. + 1.33 \cdot \frac{D}{\left(S_0 \cdot \kappa\right)}\right]^{\left(\frac{3}{2}\right)}}$$

$S4 := rkfixed(S, 0, T, Npt, DD4)$ $i := 0 .. rows(S4) - 1$ $Tn := S4^{\langle 0 \rangle}$

$ss04 := S4_{Npt,1} \cdot so$

case V: $\lambda := \lambda 5$

$no := nno5$

$sr = \left(\frac{2 \cdot \varepsilon \cdot Vr}{no \cdot q}\right)^{.5}$ Initial sheath thickness

$\omega pi = \left(\frac{no \cdot q^2}{Mion \cdot \varepsilon}\right)^{.5}$ Plasma frequency

$sr5 := sr$

$so = sr$

$s = sr$

$\omega pi5 = \omega pi$

$T = \omega pi \cdot ts$ Normalized time

$T5 = T$

$Uo := \frac{Vo}{Vr}$ Normalized HV

$Tpulse = ts$

$Vo = Uo \cdot Vr$

$D = \frac{d}{sr}$ Normalized PS thickness

$\tau = 1 .. 150$

$d = D \cdot sr$

$i := 1$

$So = \frac{so}{sr}$ <- Normalized sheath thicknesses

$t_\tau = \frac{\tau}{\left(\frac{no \cdot q^2}{Mion \cdot \varepsilon}\right)^{.5}}$

$S := \frac{s}{sr}$ <- = = =

$Npt = 500$

$S_0 := \frac{s}{sr}$ <- = = =

$$DD5(T,S) = \frac{.222}{\left[S_0^{\,2} \cdot \left(1. + (.302) \cdot \frac{S_0}{\lambda} \cdot (sr)\right)\right]^{.5}} \cdot \frac{\left[Uo - 2. \cdot D \cdot \frac{(S_0 - So)}{\kappa}\right]^{\left(\frac{3}{2}\right)}}{\left[1. + 1.33 \cdot \frac{D}{(S_0 \cdot \kappa)}\right]^{\left(\frac{3}{2}\right)}}$$

$S5 = rkfixed(S, 0, T, Npt, DD5)$ $i = 0 .. rows(S5) - 1$ $Tn := S5^{\langle 0 \rangle}$

$ss05 = S5_{Npt,1} \cdot so$

case VI: $\lambda := \lambda 6$

==========

$no := nno6$

$sr := \left(\frac{2\cdot\varepsilon\cdot Vr}{no\cdot q}\right)^{.5}$ Initial sheath thickness

$\omega pi := \left(\frac{no\cdot q^2}{Mion\cdot\varepsilon}\right)^{.5}$ Plasma frequency

$sr6 := sr$

$\omega pi6 := \omega pi$

$so := sr$

$s := sr$

$T := \omega pi\cdot ts$ Normalized time

$T6 := T$

$Uo := \frac{Vo}{Vr}$ Normalized HV

$Tpulse := ts$

$Vo := Uo\cdot Vr$

$D := \frac{d}{sr}$ Normalized PS thickness

$\tau := 1..150$

$d := D\cdot sr$

$i := 1$

$So := \frac{so}{sr}$ <- Normalized sheath thicknesses

$t_\tau := \frac{\tau}{\left(\frac{no\cdot q^2}{Mion\cdot\varepsilon}\right)^{.5}}$

$S := \frac{s}{sr}$ <- = = =

$Npt := 500$

$S_0 := \frac{s}{sr}$ <- = = =

$$DD6(T,S) := \frac{.222}{(S_0)^2\cdot\left[1. + (.302)\cdot\frac{S_0}{\lambda}\cdot(sr)\right]^{.5}}\cdot\frac{\left[Uo - 2.\cdot D\cdot\frac{(S_0 - So)}{\kappa}\right]^{\left(\frac{3}{2}\right)}}{\left[1. + 1.33\cdot\frac{D}{(S_0\cdot\kappa)}\right]^{\left(\frac{3}{2}\right)}}$$

$S6 := rkfixed(S, 0, T, Npt, DD6)$ $i := 0..rows(S6) - 1$ $Tn := S6^{\langle 0\rangle}$

$ss06 := S6_{Npt,1}\cdot so$

case VII: $\lambda := \lambda 7$

$no = nno7$

$sr = \left(\frac{2 \cdot \varepsilon \cdot Vr}{no \cdot q}\right)^{.5}$ Initial sheath thickness

$\omega pi := \left(\frac{no \cdot q^2}{Mion \cdot \varepsilon}\right)^{.5}$ Plasma frequency

$sr7 = sr$

$\omega pi7 = \omega pi$

$so := sr$

$s := sr$

$T = \omega pi \cdot ts$ Normalized time

$T7 := T$

$Uo = \frac{Vo}{Vr}$ Normalized HV

$Tpulse := ts$

$Vo := Uo \cdot Vr$

$D = \frac{d}{sr}$ Normalized PS thickness

$\tau := 1 .. 150$

$d := D \cdot sr$

$i := 1$

$So = \frac{so}{sr}$ <- Normalized sheath thicknesses

$t_\tau := \frac{\tau}{\left(\frac{no \cdot q^2}{Mion \cdot \varepsilon}\right)^{.5}}$

$S = \frac{s}{sr}$ <- = = =

$Npt = 500$

$S_0 = \frac{s}{sr}$ <- = = =

$$DD7(T,S) = \frac{.222}{\left(S_0\right)^2 \cdot \left[1. + (.302) \cdot \frac{S_0}{\lambda} \cdot (sr)\right]^{.5}} \cdot \frac{\left[Uo - 2. \cdot D \cdot \frac{\left(S_0 - So\right)}{\kappa}\right]^{\left(\frac{3}{2}\right)}}{\left[1. + 1.33 \cdot \frac{D}{\left(S_0 \cdot \kappa\right)}\right]^{\left(\frac{3}{2}\right)}}$$

$S7 = rkfixed(S, 0, T, Npt, DD7)$ $i = 0 .. rows(S7) - 1$ $Tn = S7^{\langle 0 \rangle}$

$ss07 := S7_{Npt,1} \cdot so$

Pressure (mTorr)	The mean free path	Number density	Plasma frequency	Time scale
0.0015	$\lambda 1 = 400 \cdot cm$	$nno1 = 5.03 \cdot 10^{10} \cdot cm^{-3}$	$\omega pi1 = 7.9 \cdot 10^{7} \cdot sec^{-1}$	$\frac{1}{\omega pi1} = 0.013 \cdot \mu sec$
0.035	$\lambda 2 = 150 \cdot cm$	$nno2 = 1.17 \cdot 10^{12} \cdot cm^{-3}$	$\omega pi2 = 3.8 \cdot 10^{8} \cdot sec^{-1}$	$\frac{1}{\omega pi2} = 0.003 \cdot \mu sec$
0.12	$\lambda 3 = 40 \cdot cm$	$nno3 = 4.03 \cdot 10^{12} \cdot cm^{-3}$	$\omega pi3 = 7.1 \cdot 10^{8} \cdot sec^{-1}$	$\frac{1}{\omega pi3} = 0.001 \cdot \mu sec$
0.42	$\lambda 4 = 10 \cdot cm$	$nno4 = 1.41 \cdot 10^{13} \cdot cm^{-3}$	$\omega pi4 = 1.3 \cdot 10^{9} \cdot sec^{-1}$	$\frac{1}{\omega pi4} = 7.6 \cdot 10^{-4} \cdot \mu sec$
1.0	$\lambda 5 = 2 \cdot cm$	$nno5 = 6.38 \cdot 10^{13} \cdot cm^{-3}$	$\omega pi5 = 2.8 \cdot 10^{9} \cdot sec^{-1}$	$\frac{1}{\omega pi5} = 3.6 \cdot 10^{-4} \cdot \mu sec$
10	$\lambda 6 = 0.32 \cdot cm$	$nno6 = 3.36 \cdot 10^{14} \cdot cm^{-3}$	$\omega pi6 = 6.5 \cdot 10^{9} \cdot sec^{-1}$	$\frac{1}{\omega pi6} = 1.6 \cdot 10^{-4} \cdot \mu sec$
210	$\lambda 7 = 0.021 \cdot cm$	$nno7 = 7.05 \cdot 10^{15} \cdot cm^{-3}$	$\omega pi7 = 3 \cdot 10^{10} \cdot sec^{-1}$	$\frac{1}{\omega pi7} = 3.4 \cdot 10^{-5} \cdot \mu sec$

Initial sheath extent at the commence of the pulse	Sheath thickness at the end of the pulse
	1- Numerical results from the modified D. Wang model eq. 25.
$sr1 = 1.148 \cdot cm$	$ss01 = 9.265 \cdot cm$
$sr2 = 0.238 \cdot cm$	$ss02 = 3.241 \cdot cm$
$sr3 = 0.128 \cdot cm$	$ss03 = 2.147 \cdot cm$
$sr4 = 0.069 \cdot cm$	$ss04 = 1.41 \cdot cm$
$sr5 = 0.032 \cdot cm$	$ss05 = 0.847 \cdot cm$
$sr6 = 0.014 \cdot cm$	$ss06 = 0.48 \cdot cm$
$sr7 = 0.003 \cdot cm$	$ss07 = 0.22 \cdot cm$

The number of ions within the modified D. Wang model sheath volume

P. (mTorr)

tritium ions in the volume

0.0015	$\phi 1 = nno1 \cdot (ss01 \cdot Area)$	$\phi t1 = nnto1 \cdot (ss01 \cdot Area)$
0.035	$\phi 2 = nno2 \cdot (ss02 \cdot Area)$	$\phi t2 = nnto2 \cdot (ss02 \cdot Area)$
0.12	$\phi 3 = nno3 \cdot (ss03 \cdot Area)$	$\phi t3 = nnto3 \cdot (ss03 \cdot Area)$
0.42	$\phi 4 = nno4 \cdot (ss04 \cdot Area)$	$\phi t4 = nnto4 \cdot (ss04 \cdot Area)$
1.9	$\phi 5 = nno5 \cdot (ss05 \cdot Area)$	$\phi t5 = nnto5 \cdot (ss05 \cdot Area)$
10	$\phi 6 = nno6 \cdot (ss06 \cdot Area)$	$\phi t6 = nnto6 \cdot (ss06 \cdot Area)$
210	$\phi 7 = nno7 \cdot (ss07 \cdot Area)$	$\phi t7 = nnto7 \cdot (ss07 \cdot Area)$

$f = 2000 \cdot Hz$

Calculating the number of pulses required to accumulate

2.5x10 ^{19} #/cm ^{2} Air

$Con = 2.4 \cdot 10^5$ *#/cm ^{2} Tritium*

$$No1_{pulses} = \frac{2.5 \cdot 10^{19}}{\phi 1} \qquad Not1_{pulses} = \frac{Con}{\phi t1}$$

$$No2_{pulses} = \frac{2.5 \cdot 10^{19}}{\phi 2} \qquad Not2_{pulses} = \frac{Con}{\phi t2}$$

$$No3_{pulses} = \frac{2.5 \cdot 10^{19}}{\phi 3} \qquad Not3_{pulses} = \frac{Con}{\phi t3}$$

$$No4_{pulses} = \frac{2.5 \cdot 10^{19}}{\phi 4} \qquad Not4_{pulses} = \frac{Con}{\phi t4}$$

$$No5_{pulses} = \frac{2.5 \cdot 10^{19}}{\phi 5} \qquad Not5_{pulses} = \frac{Con}{\phi t5}$$

$$No6_{pulses} = \frac{2.5 \cdot 10^{19}}{\phi 6} \qquad Not6_{pulses} = \frac{Con}{\phi t6}$$

$$No7_{pulses} = \frac{2.5 \cdot 10^{19}}{\phi 7} \qquad Not7_{pulses} = \frac{Con}{\phi t7}$$

Calculating the time required to accumulate

2.5x10 ^{19} #/cm ^{2} Air

The maximum frequency for the HV switch ***and Tritium***

$$Colect_{t1} = \frac{No1_{pulses}}{f} \qquad Colect_{tt1} = \frac{Not1_{pulses}}{f}$$

$$Colect_{t2} = \frac{No2_{pulses}}{f} \qquad Colect_{tt2} = \frac{Not2_{pulses}}{f}$$

$$Colect_{t3} = \frac{No3_{pulses}}{f} \qquad Colect_{tt3} = \frac{Not3_{pulses}}{f}$$

$$Colect_{t4} = \frac{No4_{pulses}}{f} \qquad Colect_{tt4} = \frac{Not4_{pulses}}{f}$$

$$Colect_{t5} = \frac{No5_{pulses}}{f} \qquad Colect_{tt5} = \frac{Not5_{pulses}}{f}$$

$$Colect_{t6} = \frac{No6_{pulses}}{f} \qquad Colect_{tt6} = \frac{Not6_{pulses}}{f}$$

$$Colect_{t7} = \frac{No7_{pulses}}{f} \qquad Colect_{tt7} = \frac{Not7_{pulses}}{f}$$

$r = 6 \cdot cm$

$Ac = 0.3 \cdot sec^{-1} \cdot cm^{-3}$ $d = 0 \cdot cm$ $Area = 113.097 \cdot cm^2$ $Con = 2.4 \cdot 10^5$

The time required to accumulate

Pressure (mTorr)	***2.5x10 [19] #/cm [2] Air***	$Con = 2.4 \cdot 10^5$ ***# /cm [2] Tritium***
0.0015	$Colect_{t1} = 3.951 \cdot min$	$Colect_{tt1} = 0.006 \cdot min$
0.035	$Colect_{t2} = 0.484 \cdot min$	$Colect_{tt2} = 6.979 \cdot 10^{-4} \cdot min$
0.12	$Colect_{t3} = 0.213 \cdot min$	$Colect_{tt3} = 3.073 \cdot 10^{-4} \cdot min$
0.42	$Colect_{t4} = 0.093 \cdot min$	$Colect_{tt4} = 1.336 \cdot 10^{-4} \cdot min$
1.9	$Colect_{t5} = 0.034 \cdot min$	$Colect_{tt5} = 4.919 \cdot 10^{-5} \cdot min$
10	$Colect_{t6} = 0.011 \cdot min$	$Colect_{tt6} = 1.65 \cdot 10^{-5} \cdot min$
210	$Colect_{t7} = 0.071 \cdot sec$	$Colect_{tt7} = 1.03 \cdot 10^{-4} \cdot sec$

References

Anders, A. (1990). A formulary for plasma physics, Akademie-Verlag Berlin.

Andersern, and Ziegler, J. F. (1980). Hydrogen stopping powers and ranges in all elements, Pergamon press, NewYork.

Aoyama, T. (1990). "A Tritium-In-Air monitor with compensation and additional recording of α–, β–, and γ– backgrounds." *IEEE TRANSACTIONS ON NUCLEAR SCIENCE, VOL.37,NO,APRIL 1990*, 37(2), 885-891.

Aoyama, T., Sugiura, H., and Watanabe, T. (1987). "Application of air proportional counters to a tritium-in-air monitor." *Nuclear instruments and methods in physics research A*, 254, 620-626.

Aoyama, T., and Watanabe, T. (1985). "A new type of ^{3}H surface-contamination monitor." *Health physics*, 48(6), 773-779.

Aoyama, T., and Watanabe, T. (1989). "A new type of tritium-in-air monitor for fusion reactors." *Fusion Engineering and Design*, 10, 423-427.

Ballance, P. E., Richards, A., and Thomas, R. N. (1992). *Tritium: Radiation protection in the laboratory*, Association of University radiation protection officers, Leeds.

Beach, L., and Hoots, S. S. (1980). "A real-time tritium monitor with an MPC proportional response to airborne mixtures of TH and THO." *Nuclear instruments and methods*, 175, 369-377.

Beneking, C., and Anderer, P. (1992). "Radiation efficiency of hg-ar surface-wave discharges." *Journal Of Physics D-Applied Physics*, 25, 1470-1482.

Brolley, D., and al, e. (1960). *Monoenergetic neutron sources reaction with light nuclei*, .

Brown, I. G. (1989). *The physics and technology of ion sources*, John Wiley & Sons.

Brown, R. M. (1984). "Tritium in the environment." *CRNL-2739-4*, CFFTP (Canadian Fusion Fuel Technology Project), Toronto, Canada.

Brown, R. M., and Workman, W. (1986). "Experiments on the measurement of tritium in environmental materials." *CRNL-2739-7*, Chalk river nuclear laboratories, Chalk River, Ontario.

Budnitz, R. J. (1975). "Tritium instrumentation for environmental and occupational monitoring-A review." *Health physics*, 26, 165-178.

Caresten, A. L. (1979). "Tritium in the environment." *Adv. Radiat. Biol*, 8, 419-458.

Caterini, M. (1986). "Tritium profiling in solids using T(d,α)n reaction." *G-68040*, CFFTP.

Chen, J., Conrad, J. R., and Dodd, R. A. (1993). "Dose and dose-rate effects on the structure of methane plasma source ion-implanted 304 stainless-steel." *Materials Science And Engineering A-Structural Materials Properties Microstructure And Processing*, 161, 97-103.

Chiles, M. M. (1987). "Evaluation of a thin Caf_2(Eu) scintillator for detecting tritium." *IEEE Transactions On Nuclear Science*, 34, 386-388.

Collins, G. A., and Tendys, J. (1994). "Measurements of potentials and sheath formation in plasma immersion ion-implantation." *Journal Of Vacuum Science & Technology B*, 12, 875-879.

Conrad, J. R. (1987). "Sheath thickness and potential profiles of ion-matrix sheaths for cylindrical and spherical electrodes." *Journal of applied physics*, 62, 777-779.

Cowper, G., and Osborne, R. "Measurement of tritium in air in the presence of gamma radiation." *1st International congress of radiation protection*, Rome, 285-293.

CRC. (1964-1965). *Handbook of chemistry and physics*, , Cleveland, Ohaio.

CRC. (1987). *Handbook of fast neutron generation*, CRC press.

Davey, E. C., and Faught, R. T. (1986). "A discriminating tritium monitor engineered for tritium handling facility application." *fusion technology*, 10, 1349-1356.

Deb, D., Siambis, J., and Symons, R. (1994). "Plasma ion-implantation technology for broad industrial application." *Journal Of Vacuum Science & Technology B*, 12, 828-832.

Emmert, G. A. (1994). "Model for expanding sheaths and surface charging at dielectric surfaces during plasma source ion-implantation." *Journal Of Vacuum Science & Technology B*, 12, 880-883.

Francou, M., Danel, J. S., and Peccoud, L. (1995). "Deep and fast plasma-etching for silicon micromachining." *Sensors And Actuators A-Physical*, 46, 17-21.

Franklyn, C. B., and Nothnagel, G. (1994). "Nitrogen profiles of high-dose, high-temperature plasma source ion- implantation treated austenitic stainless-steel." *Journal Of Vacuum Science & Technology B*, 12, 923-926.

Frenzel, L. E. (1994). *Communication electronics*, McGraw-Hill, Singapore.

Fukui, M. (1993). "Development of a convenient monitoring method for tritiated water vapor in air using small water dishes as passive samplers." *Radiation protection dosimetry*, 48(2), 169-178.

GlaGola, B. G., Phillips, G. W., Marlow, K. W., and Myers, L. T. (1984). "Low level tritium detection using accelerator mass spectrometry." *Nuclear instruments and methods in physics B*, 5, 221-225.

Goebel, D. M. (1994). "High-power modulator for plasma ion-implantation." *Journal Of Vacuum Science & Technology B*, 12, 838-842.

Gunzel, R., Wieser, E., Richter, E., and Steffen, J. (1994). "Plasma source ion-implantation of oxygen and nitrogen in aluminum." *Journal Of Vacuum Science & Technology B*, 12, 927-930.

Hahn, S. J., and Lee, J. K. (1992). "Kinetic simulation of the transient sheath in plasma ion-implantation." *Japanese Journal Of Applied Physics Part 1-Regular Papers Short Notes & Review Papers*, 31, 2570-2579.

Hans, K., Reinhard, K., and Rolf, H. (1992). "Tritium inventory measurements using calorimetry." *Fusion technology*, 21, 412-418.

Hastie, R. J. (1993). "Plasma particle dynamics." Plasma physics an introductory course, R. Dendy, ed., Cambridge University Press, Cambridge, 1-28.

Hofstetter, K. J., and Wilson, H. T. (1991). "A rapid method for air born tritium analysis." *Trans amer nuclear society (USA)*, 64, 90-91.

Housiadas, C., and Douglas, K. (1995). "Experimental and modeling studies on the exposure of wall surfaces to tritium gas in ambient room conditions." *Fusion Technology*, 28, 871-876.

ICRP. (1978). "Limits for intakes of radionuclides by workers." *ICRP-30*, International Commission on Radiological Protection, New York.

ICRP. (1979). "Limits for intakes of radionuclides by workers." *ICRP-30*, International Commission on Radiological Protection, New York.

ICRP. (1991). "Annual limits on intake of radionuclide by workers based on the 1990 recommendations." *ICRP-60*, International Commission on Radiological Protection, New York.

Jalbert, R. A. (1985). "A new tritium monitor for the Tokamak fusion test reactor." *Fusion technology*, 8, 2077-2081.

Jalbert, R. A., and Hiebert, R. D. (1971). "Gamma insensitive air monitor for radioactive gases." *Nuclear instruments and methods*, 96, 61-66.

Johnson, J. R., and Myers, D. K. (1984). "Biological hazards and Dosimetry of tritium." *CRNL-2739-3*, CFFTP, Chalk river-Ontario.

Johnson, P. C. (1993). "Industrial plasmas." Plasma physics an introductory course, R. Dendy, ed., Cambridge University Press, Cambridge, 339-367.

Jones, E. C., En, W., Ogawa, S., Fraser, D. B., and Cheung, N. W. (1994). "Anomalous behavior of shallow bf3 plasma immersion ion-implantation." *Journal Of Vacuum Science & Technology B*, 12, 956-961.

Kato, T. (1979). "Measurement of tritium in air by adsorbent." *Nuclear instruments and methods*, 163, 463-465.

Kaufman, S., and Libby, W., F.,. (1954). "The natural distribution of tritium." *Physical review*, 93, 1337-1344.

Kherani, N. P., and Shmayda, W. T. (1992). "Tritium-materials interaction." *CFFTP I-9219*, CFFTP, Toronto.

Kherani, N. P., and Shmayda, W. T. (1995). "Ionization surface activity monitor for tritium." *Fusion technology*, 28, 893-898.

Knoll, G. F. (1979). *Radiation detection and measurement*, John Wiley & Sons, Inc.

Lasser, R. (1989). *Tritium and helium-3 in metals*, Sporinger-Verlag, Berlin.

Lieberman, M. A. (1989). "Model of plasma immersion ion-implantation." *Journal Of Applied Physics*, 66, 2926-2929.

MacDonald, A. D. (1966). *Microwave breakdown in gases*, John Wiley & Sons, NewYork.

Malaczynski, G. W., Elmoursi, A. A., Hamdi, A. H., and Qiu, X. H. (1993). "High-voltage implantation facility at gm research." *Nuclear Instruments & Methods In Physics Research Section B-Beam Interactions With Materials And Atoms*, 74, 13-17.

Margot-Chaker, J., Moisan, M., Chaker, M., Glaude, V. M. M., Lauque, P., Paraszczak, J., and Sauve, G. (1989). "Tube diameter and wave frequency limitations when using the electromagnetic surface wave in the m=1 (dipolar) mode to sustain a plasma column." *Journal of Applied physics*, 66(9), 4134-4148.

Mason, A. S., and Ostlund, H. G. "Atmospheric HT and HTO: V. distribution and large-scale circulation." *Int. Symp. on the behavior of tritium in the environment*, San Francisco, USA.

Mason, J. A., and Vassallo, G. (1992). "Tritium measurement by isothermal calorimetry." *Fusion technology*, 21, 425-429.

Matossian, J. N. (1994). "Plasma ion-implantation technology at hughes-research-laboratories." *Journal Of Vacuum Science & Technology B*, 12, 850-853.

McElroy, R. G. C. (1984). "Tritium monitoring." *CRNL-2739-1*, CFFTP, Toronto, Canada.

McElroy, R. G. C., and Johnson, J. R. (1988). "A review of the need for species specific tritium monitors." *Fusion technology*, 14(2B), 1021-1025.

McElroy, R. G. C., Osborne, R. V., and Surette, R. A. (1982). "A monitor for the separate detection of HT and HTO." *IEEE transactions on nuclear science*, NS-29(1), 816-818.

McElroy, R. G. C., Wood, M. J., and Surette, R. A. (1985). "A modulated flow tritiated water vapor monitor." *Fusion technology*, 8, 2103-2107.

McGann, W. J., Entine, G., Farrell, R. F., Clapp, A., and Squillante, M. R. (1988). "Solid-state nuclear detectors for monitoring low levels of tritium." *Fusion technology*, 14(2), 1041-1046.

Mclain, M., and Lee, P. J. T. (1987). "Direct measurement of airborne tritiated water by liquid scintillation counting of desiccant." *Radiation protection management*, 4(4), 39-44.

Mihai, A., Hascaal, M., and Hanrahan, R. (1984). "A new portable tritium monitor." *Health physics*, 46(3), 719.

Miller, J. M., and Holtslander, W. J. (1984). "Recovery and packaging tritium." *CRNL-2739-2*, Chalk River Nuclear Laboratories, Chalk River, Ontario.

Moghissi, A. A., Kelley, H. L., Phillips, C. R., and Renier, J. E. (1969). "A tritium monitor based on scintillation." *Nuclear instruments and methods*, 68, 159.

Moisan, M., Beaudry, C., and Leprince, P. (1974). "A new device for the production of long plasma columns at a high electron density." *Physics letters*, 50A(2), 125-126.

Moisan, M., Beaudry, C., and Leprince, P. (1975). "A small microwave plasma source for long column production without magnetic field." *IEEE transactions on plasma science*, PS-3(2), 55-59.

Moisan, M., Shivarova, A., and Trivelpiece, A. W. (1982). "Review article experimental investigations of the propagation of surface waves along a plasma column." *Plasma physics*, 24(11), 1331-1400.

Moisan, M., and Zakrzewski, Z. (1986). "Plasma sustained by surface waves at microwave and RF frequencies: experimental investigation and application." , 381-430.

Moisan, M., and Zakrzewski, Z. (1991). "Plasma sources based on the propagation of electromagnetic surface- waves." *Journal Of Physics D-Applied Physics*, 24, 1025-1048.

Moisan, M., Zakrzewski, Z., and Pantel, R. (1979). "The theory and characteristics of an efficient surface wave launcher (surfatron) producing long plasma columns." *Journal of applied physics*, 12, 219-237.

Nagowala, S., and al, e. (1973). *Activation analysis with neutron generator*, John Wiley.

Nasser, E. (1971). *Fundamentals of gaseous ionization and plasma electronics*, John Wiley & Sons Inc.

NCRP. (1976). "Tritium measurement technique." *#47*, National council on radiation protection and measurements, Washington D.C.,USA.

NCRP. (1985). "A handbook of radioactivity measurements procedures." *58*, National council on radiation protection and measurements, Bethesda,MD.

Nickerson, S. B. (1982). "A recommended program of tritium monitoring research and development." *F-82004*, CFFTP (Canadian Fusion Fuel Technology Project).

Okada, S., and Momoshima, N. (1993). "Overview of tritium - characteristics, sources, and problems." *Health Physics*, 65, 595-609.

Osborne, R. V. (1970). "Detector for tritium in water." *Nuclear instruments and methods*, 77, 170-172.

Osborne, R. V. (1975). "Central tritium monitor for CANDU nuclear power stations." *IEEE transactions on nuclear science*, NS-22, 676-680.

Otlet, R. L., Walker, A. J., and Caldwell-Nichols, C. J. (1992). "Practical environmental, working area and stack discharge samplers, passive and dynamic, for measurement of tritium as HTO and HT." *Fusion technology*, 21, 550-555.

Peterson, J. H. T., and Baker, D. A. (1985). "Tritium production, releases and population doses at nuclear power reactors." *Fusion technology*, 8(2), 2544-2550.

Pixley, R. E., and Stussi, H. (1987). "A simple method for measuring tritium surface contamination." *Nuclear instruments and methods in physics research A*, 261, 600.

Pomathiod, L., Michau, J. L., and Hamelin, M. (1988). "Design and characteristics of SIPPI, an ion source for long-distance SIMS analysis of the Phobo surface." *Rev.sci.instrum.*, 59(11), 2409-2417.

Purghel, L., and Vylcov, N. (1995). "Tritium discrimination in a mixed radiation fueled using an ionization chamber." *Fusion technology*, 28, 930-933.

Qin, S., and Chan, C. (1992). "The response of a microwave multipolar bucket plasma to a high-voltage pulse with finite rise time." *IEEE Transactions On Plasma Science*, 20, 569-571.

Qin, S., and Chan, C. (1994a). "An evaluation of contamination from plasma immersion ion-implantation on silicon device characteristics." *Journal Of Electronic Materials*, 23, 337-340.

Qin, S., and Chan, C. (1994b). "Plasma immersion ion-implantation doping experiments for microelectronics." *Journal Of Vacuum Science & Technology B*, 12, 962-968.

Qin, S., Chan, C., Mcgruer, N. E., Browning, J., and Warner, K. (1991). "The response of a microwave multipolar bucket plasma to a high-voltage pulse." *IEEE Transactions On Plasma Science*, 19, 1272-1278.

Rahman, M. M., and Solntzev, G. S. (1995a). "Evaluation of energy and studying the gas heating effect on surface- wave sustained plasma columns." *Indian Journal Of Pure & Applied Physics*, 32, 857-862.

Rahman, M. M., and Solntzev, G. S. (1995b). "Minimization of axial electron-density gradient of surface-wave produced plasma columns." *Indian Journal Of Pure & Applied Physics*, 33, 260-264.

Rodrigo, L., Miller, J. M., Bokwa, S. R., Johnson, R. E., MacDonald, B. M., and Senohrabek, J. (1992). "Tritium measurement and monitoring in experimental and process systems with ionization chambers." *fusion technology*, 21, 629-6635.

Samandi, M., Shedden, B. A., Bell, T., Collins, G. A., Hutchings, R., and Tendys, J. (1994). "Significance of nitrogen mass-transfer mechanisms on the nitriding behavior of austenitic stainless-steel." *Journal Of Vacuum Science & Technology B*, 12, 935-939.

Sawicki, J. (1988). "Depth profiling of tritium in materials for fusion technology." *Fusion technology*, 14(2), 884.

Scheuer, J. T., Shamim, M., and Conrad, J. R. (1990). "Model of plasma source ion-implantation in planar, cylindrical, and spherical geometries." *Journal Of Applied Physics*, 67, 1241-1245.

Shamim, M., Scheuer, J. T., and Conrad, J. R. (1991a). "Measurements of spatial and temporal sheath evolution for spherical and cylindrical geometries in plasma source ion-implantation." *Journal Of Applied Physics*, 69, 2904-2908.

Shamim, M. M., Scheuer, J. T., Fetherston, R. P., and Conrad, J. R. (1991b). "Measurement of electron-emission due to energetic ion-bombardment in plasma source ion-implantation." *Journal Of Applied Physics*, 70, 4756-4759.

Sheng, T., Felch, S. B., and Cooper, C. B. (1994). "Characteristics of a plasma doping system for semiconductor device fabrication." *Journal Of Vacuum Science & Technology B*, 12, 969-972.

Shmayda, W. T. (1984). "Tritium interactions with materials." , CFFTP.

Singh, A. N., and Kadwani, M. G. (1974). "A sensitive detector system for the continuous monitoring of tritium in the air." *IEEE transactions on nuclear science*, NS-21, 188-193.

Singh, A. N., Nair, C. K. G., Rathnakaran, M., and Patel, M. D. (1995). "A fast responding tritium in air monitor for use in operational areas of heavy-water power-reactors." *Nuclear Instruments & Methods In Physics Research Section A- Accelerators Spectrometers Detectors And Associated Equipment*, 357, 601-604.

Singh, A. N., Rathnakaran, M., and Vohra, K. G. (1985). "An on-line tritium-in-water monitor." *Nuclear instruments and methods in physics research A*, 236, 159-164.

Smith, P. P., Buchanan, R. A., Roth, J. R., and Kamath, S. G. (1994). "Enhanced pitting corrosion-resistance of 304l stainless-steel by plasma ion-implantation." *Journal Of Vacuum Science & Technology B*, 12, 940-944.

Soete, D., and al, e. (1973). *Neutron activation analysis*, Wiley-Interscience.

Songsheng, J., Ansun, Y., Yunfeng, C., Zuying, Z., Dexing, L., and Qian, L. (1984). "Determination of tritium using a small Van de graaff accelerator." *Nuclear instruments and methods in physics B*, 5, 226-229.

Speth, R. R., Emmert, G. A., and Goeckner, M. J. (1994). "Influence of the high-voltage pulse-shape on the plasma source ion- implantation process." *Applied Physics Letters*, 65, 2272-2274.

Stephenson, J. (1984). "A diffusion sampler for tritiated water vapor." *Health physics*, 46(3), 718.

Stewart, R. A., and Lieberman, M. A. (1991). "Model of plasma immersion ion-implantation for voltage pulses with finite rise and fall times." *Journal Of Applied Physics*, 70, 3481-3487.

Surette, R. A., and Wood, M. J. (1993). "Evaluation of electric ion chamber for tritium measurement." *Health physics*, 65(4), 418-421.

Tang, B. Y., Fetherston, R. P., Shamim, M., Breun, R. A., Chen, A., and Conrad, J. R. (1993). "Measurement of ion species ratio in the plasma source ion-implantation process." *Journal Of Applied Physics*, 73, 4176-4180.

Taylor, C. B. (1982). "A uniform scale for reporting low level tritium measurement in water." *Int.J.Appl.Rad.Isoto.*, 33, 337.

Taylor, C. B. (1994). "The relationship between electrolytic deuterium and tritium separation factors, and attainment of improved accuracy in radiometric low-level tritium measurement." *Applied Radiation And Isotopes*, 45, 683-692.

Thomas, K., Alport, M. J., and Sheridan, T. E. (1994). "2 ion fluid model for plasma source ion-implantation." *Journal Of Vacuum Science & Technology B*, 12, 901-904.

Trivelpiece, A. W., and Gould, R. W. (1959). *Journal of applied physics*, 30, 1784.

Tuszewski, M., Scheuer, J. T., Campbell, I. H., and Laurich, B. K. (1994). "Plasma immersion ion-implantation for semiconductor thin-film growth." *Journal Of Vacuum Science & Technology B*, 12, 973-976.

Uhm, H. S., and Lee, W. M. (1991a). "High-concentration of deuterium in palladium from plasma ion-implantation." *Physics Of Fluids B-Plasma Physics*, 3, 3188-3193.

Uhm, H. S., and Lee, W. M. (1991b). "High-dose neutron generation from plasma ion-implantation." *Journal Of Applied Physics*, 69, 8056-8063.

UNSCEAR, U. N. S. C. o. t. E. o. A. R. (1982). "Ionizing radiation: sources and biological effects." , United Nations, New York.

UNSCEAR, U. N. S. C. o. t. E. o. A. R. (1988). "Ionizing radiation: sources and biological effects." , United Nations.

Vahedi, V., Lieberman, M. A., Alves, M. V., Verboncoeur, J. P., and Birdsall, C. K. (1991). "A one-dimensional collisional model for plasma-immersion ion-implantation." *Journal Of Applied Physics*, 69, 2008-2014.

Vajo, J. J., Williams, J. D., Wei, R. H., Wilson, R. G., and Matossian, J. N. (1994). "Plasma ion-implantation of nitrogen into silicon -characterization of the depth profiles of implanted ions." *Journal Of Applied Physics*, 76, 5666-5675.

Valyi, L. (1979). *Atom and ion sources*, John Wiley & Sons.

Walter, K. C. (1994). "Nitrogen plasma source ion-implantation of aluminum." *Journal Of Vacuum Science & Technology B*, 12, 945-950.

Wang, D. Z., Ma, T. C., and Deng, X. L. (1993a). "Model of collisional sheath evolution in plasma source ion-implantation." *Journal Of Applied Physics*, 74, 2986-2988.

Wang, D. Z., Ma, T. C., and Deng, X. L. (1994a). "Energy and angle distributions of ions striking a spherical target in plasma source ion-implantation." *Journal Of Applied Physics*, 75, 1335-1339.

Wang, D. Z., Ma, T. C., and Gong, Y. (1993b). "A monte-carlo simulation-model for plasma source ion-implantation." *Journal Of Applied Physics*, 73, 4171-4175.

Wang, H. S., Cheng, K. Q., Li, J. Q., Geng, M., Zheng, X. C., Xing, D. Z., and Shang, Z. K. (1994b). "Interaction between the plasma the workpiece surface in the process of plasma source ion-implantation." *Surface & Coatings Technology*, 66, 525-528.

Watt, D. E. (1993). "Track structure data for ionizing radiations in liquid water." *BIOPHYS/1/93*, University of St.Andrews, St.Andrews.

Wong, K. Y., Lamberger, P. H., Jalbert, R. A., and Shmayda, W. T. (1988). "Safe handling of tritium." IAEA safety series procedures and data document, IAEA.

Wood, B. P. (1993). "Displacement current and multiple-pulse effects in plasma source ion- implantation." *Journal Of Applied Physics*, 73, 4770-4778.

Wood, M. J., Mcelroy, R. G. C., Surette, R. A., and Brown, R. M. (1993). "Tritium sampling and measurement." *Health Physics*, 65, 610-627.

Wood, M. J., and Workman, W. J. G. (1992). "Environmental monitoring of tritium in air with passive diffusion samplers." *Fusion technology*, 21, 529-535.

Yamamoto, I., Kaba, A., and Kanagawa, A. (1988). "Attachment of membrane separator for removal of radon to ionization chamber installed for tritium stack monitor." *Journal of nuclear science and technology*, 25(3), 289-294.

Zakrzewski, Z. (1983). "Conditions of existence and axial structure of long microwave discharges sustained by traveling waves." *Journal of physics D: Applied physics*, 16, 171-180.

Zhang, L., Shohet, J. L., Dallmann, D., Booske, J. H., Speth, R. R., Shenai, K., Goeckner, M. J., Kruger, J. B., Rissman, P., Turner, J. E., Perezalbuerne, E., Lee, S., and Meyyappan, N. (1994). "Low-energy separation by implantation of oxygen structures via plasma source ion-implantation." *Applied Physics Letters*, 65, 962-964.

Zhao, G., Wu, S., Ren, Y., Zhou, Z., Song,L.,, Wang, J., Shi, L., and Kong, L. (1986). "Determination of the concentrations of tritium and helium in titanium tritide targets." *Nuclear instruments and methods in physics B*, 17, 56-61.

Ziegler, J. F. (1980). Stopping cross-sections for energetic ions in all elements, Pergamon press, NewYork.